Max-Planck-Institut
für Meteorologie

MAX-PLANCK-GESELLSCHAFT

International Max Planck Research School
on Earth System Modelling

Variability of Arctic sea ice

Nikolay Vladimirovich Koldunov

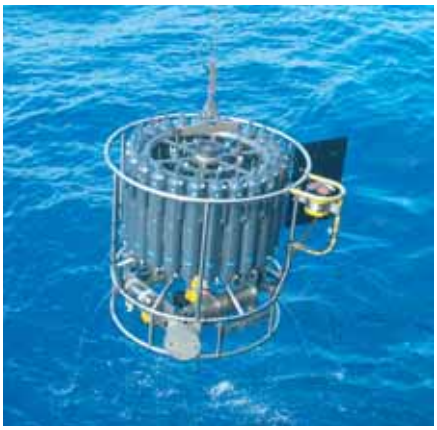

Berichte zur Erdsystemforschung 79/2010

Reports on Earth System Science

Hinweis

Die Berichte zur Erdsystemforschung werden vom Max-Planck-Institut für Meteorologie in Hamburg in unregelmäßiger Abfolge herausgegeben.

Sie enthalten wissenschaftliche und technische Beiträge, inklusive Dissertationen.

Die Beiträge geben nicht notwendigerweise die Auffassung des Instituts wieder.

Die "Berichte zur Erdsystemforschung" führen die vorherigen Reihen "Reports" und "Examensarbeiten" weiter.

Notice

The Reports on Earth System Science are published by the Max Planck Institute for Meteorology in Hamburg. They appear in irregular intervals.

They contain scientific and technical contributions, including Ph. D. theses.

The Reports do not necessarily reflect the opinion of the Institute.

The "Reports on Earth System Science" continue the former "Reports" and "Examensarbeiten" of the Max Planck Institute.

Anschrift / Address

Max-Planck-Institut für Meteorologie
Bundesstrasse 53
20146 Hamburg
Deutschland

Tel.: +49-(0)40-4 11 73-0
Fax: +49-(0)40-4 11 73-298
Web: www.mpimet.mpg.de

Layout:

Bettina Diallo, PR & Grafik

Titelfotos:
vorne:
Christian Klepp - Jochem Marotzke - Christian Klepp
hinten:
Clotilde Dubois - Christian Klepp - Katsumasa Tanaka

Berichte zur Erdsystemforschung 79/2010

Variability of Arctic sea ice

Nikolay Vladimirovich Koldunov

aus Sankt Petersburg, Russland

Hamburg 2010

Reports on Earth System Science 79/2010

ISSN 1614-1199

Nikolay Vladimirovich Koldunov
Max-Planck-Institut für Meteorologie
Bundesstrasse 53
20146 Hamburg
Germany

Als Dissertation angenommen
vom Department Geowissenschaften der Universität Hamburg

auf Grund der Gutachten von
Prof. Dr. Detlef Stammer
und
Prof. Dr. Jochem Marotzke

Hamburg, den 23. April 2010
Prof. Dr. Jürgen Oßenbrügge
Leiter des Departments für Geowissenschaften

ISSN 1614-1199

Variability of Arctic sea ice

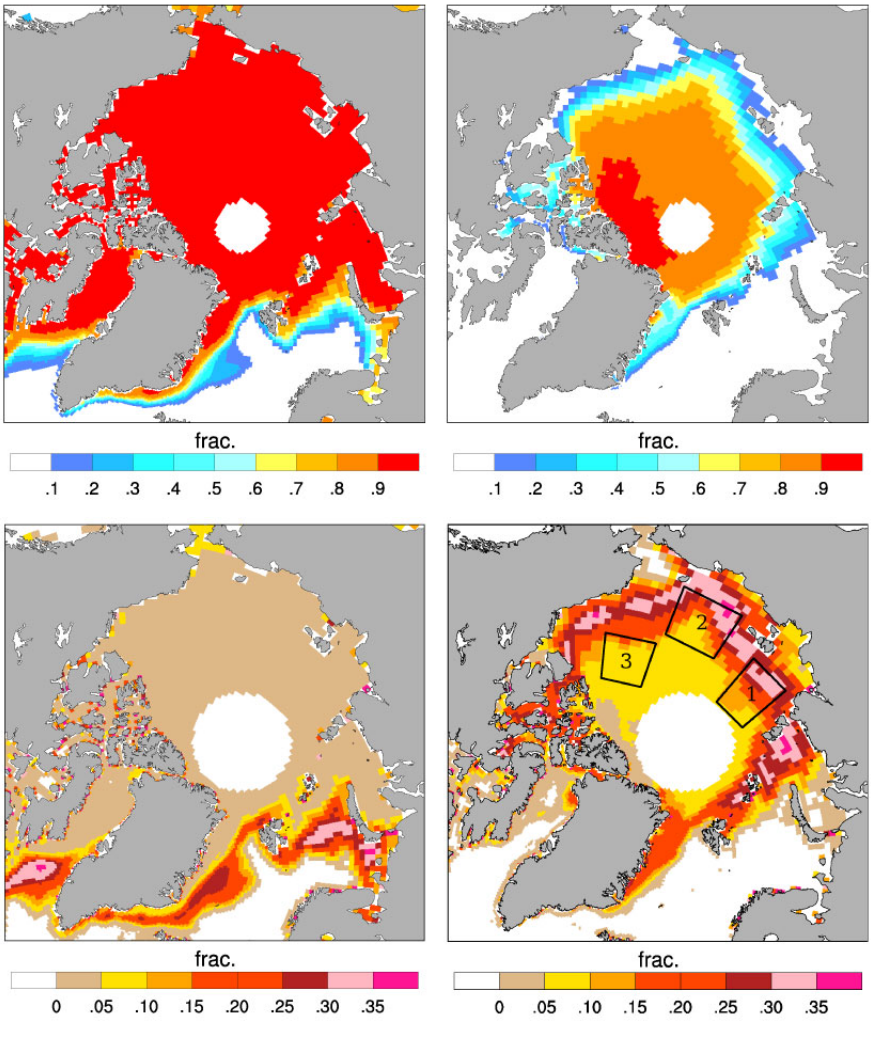

Nikolay Vladimirovich Koldunov

Hamburg 2010

Cover picture

Upper panel: Mean sea ice concentration analyzed from the GSFC satellite data over the period 1980-1999 for (left) March and (right) September. Lower panel: Standard deviation of monthly mean sea ice concentrations analyzed from the GSFC satellite data over the period 1980-1999 for (left) March and (right) September. Rectangles indicate geographic locations for which time series of sea ice concentrations are shown in Fig. 2.9

Contents

List of Figures

List of Tables

Dedication

to my grandfather,
Nikolay Fedorovich Koldunov

Acknowledgement

First and foremost, I would like to thank my scientific adviser Prof. Dr. Detlef Stammer for his enormous patience, genuine interest in my work, understanding, continual scientific and mental support. I also wish to thank my co-adviser Prof. Dr. Jochem Marotzke for his encouragement, many useful discussions and for teaching me how to be a good scientist. Thanks to Prof. Dr. Hartmut Grassl for chairing my advisory panel and his support in the extension of my funding period.

Many thanks to my wife Lena for her love and for having so much patience with me. She always believed in me and did not let me give up.

I would like to thank Dr. Armin Köhl for his help with the MITgcm model, for sharing knowledge about adjoint simulations and for the many useful discussions and suggestions. I also wish to thank Dr. Nuno Serra for his passion for oceanography and many useful scripts that made my life much easier.

I would like to thank IMPRS-ESM for financial support and for giving me the opportunity to expand my knowledge about the Earth System. A very special thanks goes to Dr. Antje Weitz and Cornelia Kampmann for their advice and for always having the right words to cheer me up.

I thank Dr. Helmuth Haak and Dr. Johann Jungclaus from MPI-M for making the model results available and for many helpful discussions. I thank also Carl Wunsch for helpful comments on the second chapter. Two anonymous reviewers helped improve the second chapter significantly during the review process for the Journal of Climate. All model simulations were made in the Deutsches Klimarechenzentrum (DKRZ).

I would like to thank all my colleagues from the Institut für Meereskunde and the Max Planck Institute for Meteorology for always having the doors open and for their willingness to help. Special thanks to Dr. Dirk Notz, Jun.-Prof. Dr. Lars Kaleschke, Dr. Stefan Kern and Dr. Gunnar Spreen for many interesting discussions about sea ice.

I wish to thank my mother Nina, my father Vladimir and my brothers Aleksey and Viktor for their love and support of my decisions that, sometimes, seemed very odd to them.

I also would like to thank all the people who have helped me to fall in love with the Arctic Ocean. Many thanks to Dr. Igor Dmitrenko, Dr. Sergey Kirillov, Prof. Dr. Sc. Leo Timokhov, Dr. Heidemarie Kassens and Dr. Jens Hölemann.

Many thanks to my friends, Anna Akimova, Ismael Núñez-Riboni, Ksenia Glushak, Michail Itkin and Nidia Martinez who make my stay in Hamburg even more pleasant.

Abstract

Arctic sea ice is considered to be an important climate change indicator due to its large sensitivity to a changing climate. At the same time changing arctic sea ice has a large feedback potential on the climate. Understanding the relation between changes in sea ice (especially the summer sea ice distribution and thickness as monitored typically by September values) and changes in the ocean or atmosphere is therefore important for understanding future sea ice and climate variations. In this thesis Arctic sea ice parameters are being analyzed in observations and climate models, and the sensitivity of sea ice changes over the Arctic to atmospheric forcing fields are analyzed using an adjoint modeling framework.

The work is divided in two parts. In the first part the primary focus is on concentrations, thickness and transports of Arctic sea ice, as simulated by the Max-Planck-Institute for Meteorology (MPI-M) coupled model for the period 1980 to 1999, and as observed simultaneously during field programs and by satellites. The comparison of model results with observations is based on two model realizations: (1) a fully coupled ECHAM5/MPI-OM run forced by 20^{th} century CO_2 concentrations and (2) an ocean-ice MPI-OM run forced by the NCEP atmospheric reanalysis-1. Results of the fully-coupled run show significant discrepancies to observations with respect to the spatial distribution of the ice concentration and ice thickness during summer months. The coupled model tends to overestimate the ice concentration in the Siberian shelf seas and near the Canadian coast, likely because of deficits in the model's Beaufort Gyre and Transpolar Drift. Moreover, the coupled run essentially lacks interannual variability in ice and ocean parameters that is simulated when using NCEP surface forcing. Causes for such big discrepancies arise from errors in the ECHAM5/MPI-OM atmosphere and associated errors in surface forcing fields (especially wind stress); potentially they could arise also from insufficient atmospheric variability in the ECHAM model, e.g., associated with AO/NAO. As can be expected, the NCEP-forced run shows much increased skill in its ice and ocean circulation parameters; nevertheless it still lacks many details present in the ice observations. Common to both model runs is too strong an ice export through Fram Straight and too much heat content in the interior of the Arctic Ocean, both of which may affect sea ice budgets and decadal to centennial projections of sea ice in the Arctic.

In the second part of the thesis we investigate spatial and temporal distribution of adjoint-based sensitivities of the mean September sea ice area (AREA) and volume (VOLUME) to surface atmospheric temperature and wind in the regional Arctic Ocean setup of the Massachusetts Institute of Technology global circulation model (MITgcm) for the period 1980 to 2007. The adjoint-based sensitivities allows us to document influences of the atmosphere (as well as the ocean) on sea ice and follow those influences throughout the year. We show that during October-May atmospheric forcing fields have a minor effect on the September sea ice characteristics, while after the onset of the spring melting until the end of September atmospheric

forcing influence September sea ice characteristics considerably. The AREA is highly sensitive to temperature changes during June-July over the regions close to the ice edge in the Arctic seas. The VOLUME is highly sensitive to temperature changes over the central parts of the Arctic Ocean, also during June-July. The export of thicker ice from the central parts of the Arctic Ocean to the Siberian Shelf seas on average increases the AREA, but decreases the VOLUME. The sensitivities of AREA and VOLUME to thermodynamical and dynamical atmospheric forcing are mainly controlled by the background distribution of sea ice concentration (SIC) and sea ice thickness (SIT).

A comparison of the sea ice conditions during the periods 1980-1989, 1990-1999 and 2000-2007 reveals that during 2000-2007, due to dramatic decline of SIC and SIT, sea ice sensitivities to atmospheric forcing increase, suggesting that a comparable atmospheric forcing led to a stronger sea ice response compared to the two other periods. Both AREA and VOLUME sensitivities demonstrate that some influence of the atmospheric conditions extends at least four years into the future. Strength of the sensitivities gradually increase from year to year and show the same seasonal cycle as one-year sensitivities. We believe that SIT is the primary agent that carries atmospheric influence through the years.

Chapter 1

Introduction

The Arctic Ocean is the smallest and shallowest ocean on the Earth (Fig. 1.1). It is located in the polar region of the Northern Hemisphere and is almost completely surrounded by Eurasia and North America. The Arctic Ocean is now an important sea route that provides supplies for North Russia. It is a great source of mineral resources that are located mostly on its vast shelf areas and yet they do not experience intensive exploration, due to the harsh environmental conditions. A notable feature of the Arctic Ocean that is greatly responsible for the difficulties in its exploration is the relatively thin layer of sea ice that covers central parts of the ocean throughout the year and seasonally appears along the ocean margins.

Arctic sea ice is not only an important component of the climate system, it also provides habitat for living organisms. Arctic indigenous people rely on sea ice for transportation and hunting. During recent decades the state of the Arctic sea ice has experienced dramatic changes and we need to have high quality observational systems and numerical models to monitor the present state of the sea ice and to be able to predict the future changes that will affect the Arctic region and the Earth System as a whole.

Scientific exploration of the Arctic sea ice was started by Fridtjof Nansen at the end of the 19^{th} century during his drift on the "Fram" vessel. He proved Henrik Mohn's theory that the main ice drift in the Arctic is from the seas of East Siberia through the North Pole towards the Fram Strait (Nansen, 1897). His observations of wind-sea ice interactions led to development of Ekman theory of wind-driven surface currents (Ekman, 1905). Arctic explorer A. Kolchak, on the basis of his own observations during an expedition on polar ship "Zarya" and analysis of the information about ice movement and wind directions from other polar expeditions, proposed the existence of anticyclonic movement of the sea ice in the Canadian sector of the Arctic Ocean, later named the Beaufort Gyre (Kolchak, 1909, 1928). The first detailed overview of sea ice's geophysical properties was based on observations during the Norwegian North Polar expedition with the "Maud", which were published by Malmgren (1928).

Airplanes were the most efficient platform to observe sea ice characteristics over large areas in the first half of the 20^{th} century. Regular airborne reconnaissance

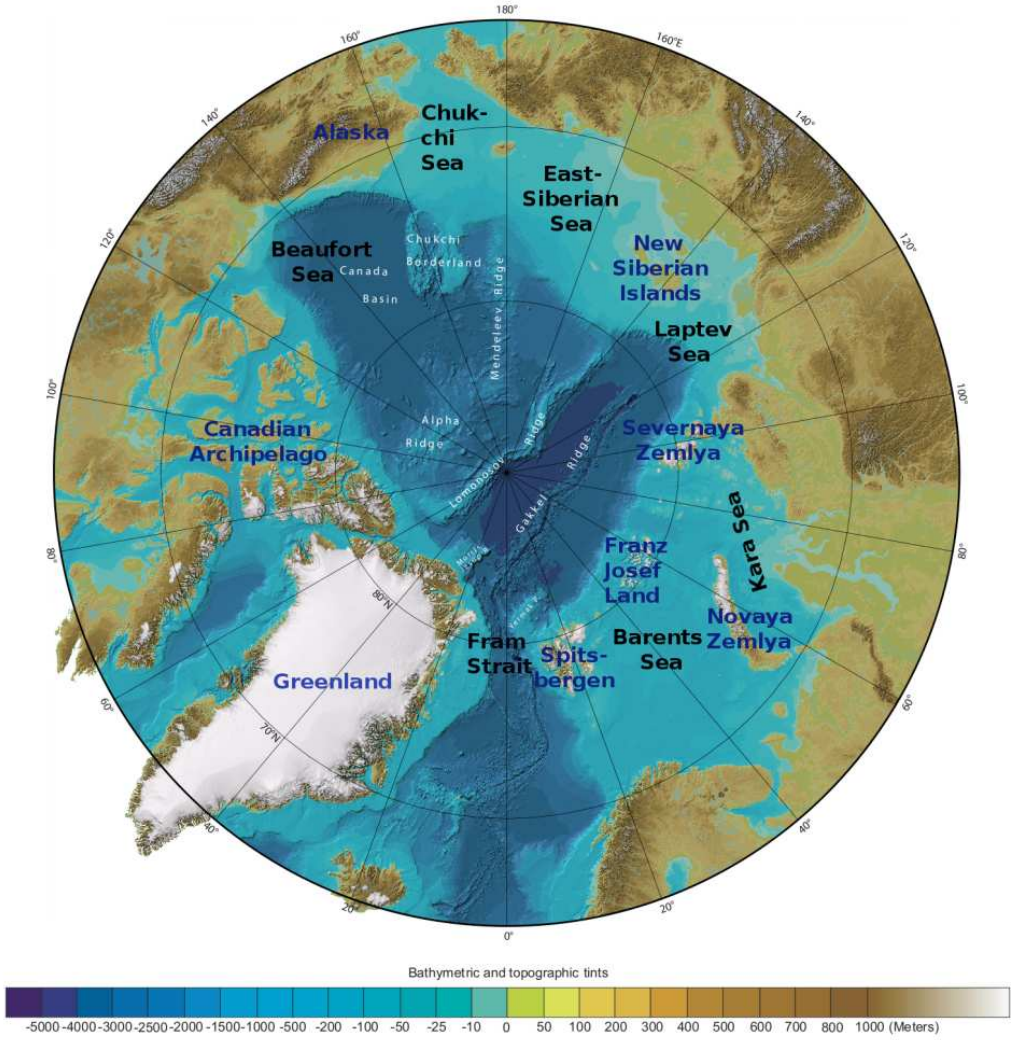

Figure 1.1— Arctic Ocean including geographical place names. The Amerasian Basin, mentioned in the text, includes the region from the Lomonosov Ridge towards the Pacific Ocean. The Eurasian Basin includes regions from the Lomonosov Ridge towards the Atlantic Ocean. Based on a map produced by the International Bathymetric Chart of the Arctic Ocean (IBCAO), Jakobsson et al. (2008).

flights began in the middle of the 1930s in order to provide sea ice information for Soviet Union activities along the Northern Sea Route (Borodachev and Shilnikov, 2002). Observers estimated sea ice total concentration, partial concentrations and forms of the encountered stages of ice development, plus additional sea ice parameters significant for ice navigation (hummocks, ridges, openings, stages of melting, etc.). Advances in aviation since the middle of the 1950s also made it possible to

establish drifting stations on the ice floes so that long-term observations of sea ice physical properties in the central Arctic become possible (e.g. "North Pole" stations, T-3 iceberg stations).

The launch of the first satellites equipped with microwave instruments led to a breakthrough in large-scale sea ice observations. They allowed estimates of sea ice concentration and sea ice transport, regardless of weather conditions and presence of light. From 1978 to the present time, the longest and first regular time series of global sea ice data has been provided by the microwave instruments on board Nimbus-7 and the Defense Meteorological Satellite Program (DMSP) satellites ((Parkinson and Cavalieri, 2008).

The first submarine trans-Arctic cruise under the ice was carried out in August 1958 by the US nuclear submarine "Nautilus". Later, since the 1970s, submarine sonar measurements have become one of the important sources of information about sea ice thickness. Other sources include direct observations during ship and airborne polar expeditions, by visual estimation of the ice thickness turned by the icebreaker, or by drilling holes in the ice (Romanov, 1995); indirect geophysical methods include electromagnetic sounding (Haas, 2004). There were several attempts to use satellites to obtain sea ice thickness data by directly measuring sea ice free board (Laxon et al., 2003; Spreen, 2008), and by using ice age information (Maslanik et al., 2007b). Nevertheless, only with the launch of the CryoSat-2 satellite does the scientific community expect to receive sea ice thickness data with sufficient spatial and temporal resolution.

Data obtained during polar expeditions, and later by satellite missions, lay the foundation for developing of sea ice models. The first person who mathematically describe thermodynamic sea ice growth was Stefan (1891). Later there were attempts to describe sea ice growth by empirical relationships (e.g. Zubov (1945)) or to find those that will have analytical solutions (e.g. Kolesnikov (1946); Doronin (1959)). When faster computers come into play it become possible to create models that can be solved numerically reasonably quickly. Very detailed one-dimensional thermodynamic model were solved by Maykut and Untersteiner (1971), but it was too expensive in terms of computer time and a simplified version that can be used in climate simulations was developed by Semtner (1976). Currently most climate models use variations of the Semtner (1976) model or develop their own on the basis of the Maykut and Untersteiner model (see, e.g., Bitz and Lipscomb (1999)).

Models of sea ice dynamics were developed alongside thermodynamic models. Earlier works consider sea ice as a flat, infinite plate with spatially constant wind and water stresses applied to it along with the Coriolis force (e.g. Sverdrup (1928); Shuleikin (1938)). Later works consider sea ice as a fluid continuum but with complex constructive behavior that might be elastic-plastic (Coon et al., 1974) or viscous-plastic (Hibler, 1979). Finally dynamic and thermodynamic models were combined together by Hibler, who developed a fully coupled dynamic-thermodynamic model suitable for long-term climate simulations (Hibler, 1980). Now modifications of this sea ice model are included in most of the climate models.

Both observations and models help us to understand the role and importance of the Arctic sea ice for the climate system. Sea ice is a relatively thin layer on the top of the sea, but it affects the climate system considerably. As a barrier with high conductivity between the ocean and the atmosphere it complicates the ocean-atmosphere heat exchange. Sea ice also controls most of the atmosphere-ocean momentum and matter transfers.

Due to its high albedo (about 0.5-0.7), sea ice reflects a significant amount of the short-wave solar radiation and reduces the amount of the energy absorbed at the Earths surface. Conversely, open water has low albedo (about 0.06) and absorbs most of the incoming short-wave radiation. As a result of such big albedo differences, a decrease in the sea ice area leads to an increase in the amount of energy absorbed by the ocean. Absorbed energy will increase the surface ocean temperature, and consequently prevent formation of the new sea ice, leading to further reduction in the sea ice cover. This mechanism is called positive sea ice-albedo feedback and it is an important, while probably not dominating, contributor to the observed Arctic surface atmospheric temperature amplification (Winton, 2006; Graversen and Wang, 2009).

During winter, when there is no incoming solar short-wave radiation in the Arctic, emission of the long-wave radiation cools the snow and ice surfaces. This leads to extraction of heat from the atmosphere. Cooling of the atmosphere over the sea ice stabilizes its stratification. Convection is suppressed in the stratified atmosphere, and therefore a cooler local climate is sustained. A good review of recent papers that describe the possible influence of Arctic sea ice on global atmospheric circulation can be found in Budikova (2009).

Freezing and melting of the sea ice changes the salinity of the surface water. Those changes may influence North Atlantic Deep Water formation, which in turn may affect global Thermohaline Circulation. This probably happened in the 1970s, when increased transport of the sea ice through the Fram Strait caused the "Great Salinity Anomaly" in the North Atlantic (Dickson et al., 1988).

During the last decade, the Arctic sea ice has been experiencing dramatic changes that may have consequences not only for the Arctic region, but for the whole Earth System. Satellite observations indicate continuous shrinking of the sea ice since the beginning of the record in 1978. For the years 1978-1996, the rate of decline in sea ice extent stood at -2.2% per decade, while for the years 1996-2007 it increased to -10.1% per decade (Comiso et al., 2008). A record minimum sea ice extent was reached on 14 September 2007 at 4.1×10^6 km^2. Such a sharp decline had not been projected by any of the IPCC climate models (Stroeve et al., 2007). The IPCC models develop fast, as do observations, and we believe that a continuous evaluation of individual IPCC models against available observations is necessary to improve their skill. This evaluation is usually performed for multi-model ensembles and pays less attention to the details of the individual models or explores only one sea ice component. We think that one should study all three main sea ice components together with forcing from the atmosphere and the ocean to have a chance of evaluating the sea ice model's skill

in the Arctic in a more complex and complete way than has been done in previous studies.

It is likely that the atmospheric forcing is dominating sea ice changes, at least on the annual time scale. But details of the atmospheric influence on sea ice are still unclear. Sea ice is a mobile medium and sometimes it is hard to estimate how, for example, temperature change at a certain point will affect sea ice characteristics several months after. Where will extreme forcing lead to significant changes for the whole body of the Arctic sea ice, and where will the responses only be local? What will the signs of these changes be? What difference will it make if extreme atmospheric events happen one month earlier or later? Answers to these questions might be given by the sensitivity analysis, but the classical way of doing so properly for the whole Arctic Ocean would require multiple ensemble runs and take a lot of time. Here we use a relatively novel approach to investigate how dynamical and thermodynamical atmospheric forcing in different regions and during different months may affect September sea ice characteristics.

1.1 Goals of the thesis

The thesis investigates two major questions. The first part aims to identify problems that led to the discrepancies between Arctic sea ice observations and simulations done by the latest MPI-M model. The main objectives of the first part are:

- to evaluate the skill of ECHAM5/MPI-OM model in simulating climatological sea ice characteristics and climate variability,
- to investigate how atmospheric forcing influences sea ice characteristics in this specific model, and how uncertainties in the atmospheric model influence sea ice simulations,
- to estimate how the ocean state in the model influence the simulated sea ice distribution.

In the second part we will explore Arctic sea ice sensitivities to atmospheric forcing calculated with the adjoint method in the regional setup of the MITgcm model, to identify spatial and temporal variability of atmospheric influence on sea ice. The main objectives of the second part are:

- to investigate which physical processes are involved during the year in shaping mean September sea ice area and volume,
- to investigate how sensitivities of the mean September sea ice area and volume to atmospheric forcing change on interannual time scale as represented here by three different periods,
- to explore whether sensitivities in the mean September sea ice area and volume to atmospheric forcing extend further back in time for more than one year.

1.2 Structure

The thesis consists of two main parts (Chapters 2 and 3) and overall conclusion and an outlook (Chapter 4). Each of the main chapters includes an introduction, a description of the data and methods, results, and concluding remarks.

Chapter 2 provides an evaluation of the ECHAM5/MPI-OM model simulation of sea ice for the period 1980-1999 with respect to available observational data. In particular we compare model results with satellite observations of sea ice concentration and sea ice transport and also with climatological sea ice thickness data. We analyze forcing fields that are relevant for the sea ice simulation, namely sea level pressure, surface atmospheric temperature, and ocean temperature.

Chapter 3 provides an analysis of mean September sea ice area and volume sensitivities to atmospheric forcing. First we make a brief comparison of the MITgcm regional setup with sea ice observational data. Then the spatial variability of adjoint sensitivities for the whole period of simulations and for three separate periods is described. Finally we take a closer look at the evolution of sensitivities in different regions and describe sensitivities that exist on time scales of more than a year.

Chapter 2 of this thesis has been published in the Journal of Climate as: Koldunov, N. V., Stammer, D., Marotzke, J., May 2010. Present-day arctic sea ice variability in the coupled ECHAM5/MPI-OM model. *Journal of Climate* 23 (10), 2520-2543.

Chapter 2

Present-day Arctic Sea Ice Variability in the Coupled ECHAM5/MPI-OM Model[1]

2.1 Introduction

The projection of sea ice provided by the Intergovernmental Panel on Climate Change (IPCC) suggests a dramatic decline of Arctic summer sea ice extent (SIE) over the next 50 to 100 years. Yet, an analysis of the full ensemble of all IPCC climate projections of Arctic summer sea ice under increasing CO_2 conditions shows a considerable spread of individual simulations (Stroeve et al., 2007) and reveals that only 50% of all solutions suggest an extinction of Arctic summer sea ice by 2100 (Serreze et al., 2007) in response to enhanced atmospheric CO_2 concentrations. This points to substantial uncertainties in projected climate indices, among them summer sea ice parameters. At the same time it underlines the need to carefully test the skill of coupled climate models to improve them, and to increase the confidence in the IPCC climate projections of important climate parameters.

With respect to testing sea ice simulations of models participating in the IPCC Fourth Assessment Report (AR4), several studies were performed previously. As an example, Parkinson et al. (2006) compared sea ice extent in 11 GCMs participating in IPCC AR4 (including ECHAM/MPI-OM) with satellite data. They found that, based on a subset of 11 models, on average they overestimated the mean sea ice extent in the northern hemisphere throughout the year with a maximum difference of 14.1% in concentration reached during September. Similar results were obtained by Zhang and Walsh (2006), Kattsov et al. (2007), Arzel et al. (2006), who used different subsets of IPCC AR4 models. Hu et al. (2004) noted significant differences in multi-model annual mean ice thickness from IPCC AR4 models with the climatology of Bourke and Garrett (1987) in that the maximum ice thickness was shifted

[1]Koldunov, N. V., Stammer, D., Marotzke, J., May 2010. Present-day arctic sea ice variability in the coupled ECHAM5/MPI-OM model. *Journal of Climate* 23 (10), 2520-2543

to the center of the Arctic Basin instead of north of Canadian Archipelago and too thick ice in the region from the Kara Sea to the Barents Sea. Gerdes and Köberle (2007) compared Arctic sea ice thickness variability in IPCC AR4 simulations of the 20th century climate and in ocean-sea ice hindcasts. The authors documented the significant spread in sea ice simulations and identified a few models with apparently better quality than others relative to observations. Most of the above studies agree in that proper atmospheric forcing fields are critical for obtaining reasonable simulations of the sea ice characteristics (Walsh and Crane, 1992; Bitz et al., 2002), more so than details of underlying sea ice models (Flato et al., 2004). Chapman and Walsh (2007) showed that, relative to ERA-40, IPCC AR4 models tend to have colder surface air temperatures (by 1-2°C) and higher sea level pressure (SLP) over the Eurasian sector of the Arctic Ocean. Cassano et al. (2006) analyze Arctic circulation patterns in ten IPCC AR4 models (excluding ECHAM5/MPI-OM) and found that high-pressure circulation patterns over the central Arctic are usually overestimated and that low-pressure patterns, such as the Islandic low, are underestimated.

In contrast to previous ensemble investigations, the goal of this chapter is to perform a detailed analysis of the MPI-M coupled ocean-ice model results. Specifically, the analysis aims at identifying the quality and potential causes of errors in the model's present day simulations of sea ice concentration and thickness distribution as well as ice transports. Testing the hindcast of coupled climate models against the existing climate data record provides a stringent test of the model's skill in simulating present day climate and its variability. However, performing a detailed model evaluation against observations is difficult in a multi-model inter-comparison context and usually takes an in-depth analysis of an individual simulation. The coupled ECHAM5/MPI-OM model was chosen here because it was identified before as one of the best in simulating sea ice parameters (Parkinson et al., 2006). Any deficit identified below is therefore likely to hold also for all other IPCC type models.

The model evaluation will be performed based on two simulations of the identical ocean-ice coupled model. One of the simulations is a 20^{th} century simulation of the fully coupled ECHAM5/MPI-OM model. The second run is driven by the NCEP/NCAR reanalysis. The two runs were identified because the first run represents a typical present-day climate simulation of an IPCC type coupled model while the second run represents an ocean-sea ice simulation containing a more realistic atmosphere, thus quantifying in detail the impact of the atmosphere on the MPI-OM sea ice simulations. A comparison of model results will focus on the 20-year period 1980-1999 which represents a typical sea ice "climatology" period that is used by most of the above mentioned model/observation comparison studies. We will see below that substantial problems exist with coupled climate models simulating the present day Arctic ice climate. We therefore left out the recent extreme years which are being studied separately in several individual investigations (e.g., Kauker et al. (2009), Lindsay et al. (2009), Zhang et al. (2008)).

The objectives of this study are in detail:

- to evaluate the skill of ECHAM5/MPI-OM model in simulating climatological

sea ice characteristics,

- to evaluate the skill of ECHAM5/MPI-OM model in simulating Arctic climate variability,
- to estimate how atmospheric forcing influences sea ice characteristics in this specific model,
- to estimate how different ocean states in the model may affect the simulated sea ice distribution.

The structure of the remaining chapter is as follows: in Section 2 we describe the approach and datasets used in this study as well as their uncertainties. In Section 3 we discuss simulations of the sea ice concentrations and thickness and compare them with observations. Section 4 concentrates on ice transports. Section 5 describes atmospheric and ocean forcing fields. Section 6 provides a discussion and concluding remarks.

2.2 Methodology

Our study is based on output of the Max-Planck-Institute for Meteorology Hamburg Primitive Equation Ocean Model (MPI-OM) which will be compared here with available satellite and in situ observations of sea ice concentration (SIC), sea ice thickness (SIT) and sea ice drift. In the following we will describe first the underlying numerical experiments, before summarizing the observations.

2.2.1 MPI-OM model

All numerical experiments are based on the coupled ocean-ice MPI-OM model. Technical details of the ocean module and the embedded sea ice module are provided by Marsland et al. (2003) and Jungclaus et al. (2006). The ocean model is based on the primitive equations for a hydrostatic Boussinesq fluid and is formulated with a free surface on an Arakawa C grid. It is run here with 1.5° horizontal resolution and with 40 unevenly spaced vertical levels. The model uses an along-isopycnal diffusion following Redi (1982) and Griffies (1998), and isopycnal tracer mixing by unresolved eddies is parameterized following Gent et al. (1995). The embedded sea ice module is a Hibler type dynamic-thermodynamic sea ice model with viscous-plastic rheology and snow (Hibler, 1979). Thermodynamic growth of sea ice is described by the zero-layer formulation of Semtner (1976). The sea ice coverage is fractional within grid cells and related to the thickness according to sub-grid scale parameterization of lateral versus vertical ablation and accretion following Stössel and Owens (1992). Haak (2004) provided a detailed description of the ice model.

Jungclaus et al. (2006) investigated the general quality of the 300 year control integration of the ECHAM/MPI-OM model and found that over much of the ocean sea surface temperature (SST) in the model deviated from the observations for less

than 1 K. But there is some greater regional difference, for example North Atlantic Current transports an excessive amount of heat to the Barents sea region leading to higher than observed SST there. Nevertheless global-scale transports of heat and freshwater are in the good agreement with observations, some temperature and salinity deviations from observations in intermediate and deep oceans are not large enough to seriously influence large-scale circulations and the North Atlantic overturning circulation is stable. The authors also made a rough examination of Arctic sea ice characteristics in the model and point to the lack of summer ice melting over Siberian and Canadian shelf and shifted sea ice circulation, issues that will be addressed here in detail.

The following two runs are analyzed during this study:

1. A 20^{th} century ECHAM5/MPI-OM run with observed anthropogenic forcing (CO_2, CH_4, N_2O, CFCs, O_3 and sulfate) which does not include any CO_2 increase after the year 2000. In the following this run will be called ECHAM.

2. A run of the MPI-OM model forced by the NCEP/NCAR reanalysis (NCEP-RA1) surface forcing. In the following this run will be called FNCEP.

Because those two runs differ only in their atmospheric component and respective forcing fields, differences in the resulting sea ice characteristics and ocean conditions will shed light on the impact of the uncertainties of the atmosphere of the fully coupled climate model on the simulations of sea ice. We note that feedback processes over sea ice are included only in the ECHAM run. The NCEP atmosphere has feedbacks included to the extent that they are represented in observations that were assimilated, and since fluxes between the atmosphere and the ocean are calculated using the bulk formula, those feedbaks, at least to some extent, will be active here as well.

The ECHAM run

The ECHAM5/MPI-OM model is a coupled ocean-atmosphere-ice model, with the ocean-ice component represented by the MPI-OM model. For details of the ECHAM5 atmosphere model see Roeckner et al. (2003); it is based on version 5.2 of the ECHAM model and was run at a T63 spatial resolution, equivalent to a 1.875° resolution in latitude and longitude, with 31 vertical levels. Atmosphere, ice and ocean are coupled by means of the Ocean-Atmosphere-Sea Ice-Soil (OASIS) coupler (Valcke et al., 2003), which performs the interpolation between ocean and atmosphere grids. From the atmosphere to the ocean it transfers fluxes of momentum, heat and freshwater; from the ocean to the atmosphere it transfers sea surface temperature, sea ice thickness and concentration, snow thickness and surface velocity. The coupled model includes a river runoff scheme (Hagemann and Dümenil, 1997; Hagemann and Gates, 2003) which treats river runoff and glacier calving interactively in the atmosphere model, and the respective freshwater fluxes are passed to the ocean as part of the atmospheric freshwater flux field.

For this study we use a simulation of the 20^{th} century driven by observed concentrations of climate relevant gases and aerosols (20C3M). Three realizations of the 20^{th} century have been performed in this configuration, which started from three different initial conditions of a preindustrial control integration. However, instead of using an ensemble average of all three runs, we analyze only one individual run, following the recognition (e.g., Gerdes and Köberle (2007)) that ensemble means contain less model-generated intrinsic variability than individual realizations which is the focus of this chapter.

The NCEP forced run

To investigate the sensitivity of the simulated SIE and the Arctic circulation and transport properties to the atmospheric forcing, we use the output available from a second experiment in which the ocean-ice component of the ECHAM/MPI-OM model was forced by the NCEP-RA1 reanalysis (Kalnay et al., 1996) with otherwise the same general set-up, as described by Haak et al. (2003). The NCEP-RA1 forcing fields consist of a downward short wave radiation, wind speed at 10 m, total cloud cover, dew point temperature, precipitation, air temperature at 2 m, wind stress and mean river runoff. A global scaling factor of 0.89 was applied to the NCEP-RA1 downward short wave radiation to correct for systematic bias between estimates of ERBE and ECMWF (Haak et al., 2003). The model is initialized from Levitus et al. (1998) climatological temperature and salinity, and integrated 11 times (in a cyclic manner) using daily NCEP-RA1 reanalysis atmosphere forcing fields computed through bulk formulae for the time period 1948-2001, thus performing a 550 year-long run. In ice-free regions, salinity in the surface layer (0-12 m) is restored towards the Levitus climatology, with a time constant of 180 days. Heat fluxes are parameterized through bulk formulae following Oberhuber (1993). As a consequence, the ocean's model upper layer temperature or the sea ice/snow layer skin temperature react to changes in the air temperature very quickly. As in the case of ECHAM, we use also only a single run out of an ensemble of available FNCEP runs. Sea ice concentrations between FNCEP runs were compared previously by Haak (2004), who found that differences between runs are negligible (see, e.g., Fig. 6.2 of Haak (2004)).

2.2.2 Satellite observations

Satellite data, used here for a test of the model results, were obtained from the National Snow and Ice Data Center (NSIDC) database and consist of sea ice concentrations (SIC) inferred from Nimbus-7 Scanning Multichannel Microwave Radiometer (SMMR) and from channel 8, 11 and 13 radiance of the Special Sensor Microwave/Imager (SSM/I) on board the Defense Meteorological Satellite Program (DMSP) at a grid cell size of 25×25 km as described by Cavalieri et al. (1996). The SIC fields were generated from the measured radiances, using the NASA Team (NT) algorithm developed by the Oceans and Ice Branch, Laboratory for Hydrospheric

Processes at NASA Goddard Space Flight Center (GSFC).

In the following we will use satellite-derived SIC primarily from March and September, representing periods of highest and lowest sea ice concentration, respectively, and compare those with model results. Respective satellite fields are interpolated onto the ocean model grid by using distance-weighted averaging. In essence, the code searches for four nearest neighbors of the destination grid point and calculates the mean of source grid points weighted by the distance from the destination grid point. Below we will refer to this data set as "GSFC".

Fig. 2.1 shows the time-mean GSFC SIC for March and September, both averaged over the period 1980 to 1999. While the March field reveals an entirely ice covered Arctic, the September field shows a substantially reduced ice cover around the rim of the basin, leaving maximum SIC to the north of Greenland. Shown in the lower row of the figure are associated standard deviation (STD) fields resulting for both months from monthly mean fields over the same 20-year period. We show STD values only in areas where time series of satellite SIC observations last more than 20 years, essentially covering the period after 1987 (leaving out some fraction of the central Arctic). The March fields show a fairly uniform ice distribution with close to 100% concentration over most of the Arctic. Noticeable interannual variability in March SIC exists only along the edges toward the Nordic Seas and in the Labrador Sea. We also note that the time-mean and STD ice concentration fields hint toward the impact of ocean transports on the ice edge and ice distribution, notably the ice concentration along the Greenland shelf and East Greenland Current as well as variations of the ice edge in the Barents Sea. During September we find a variability around 10% of SIC over large parts of the central Arctic. However, a large interannual September SIC variability exists around the entire ice edge, especially on the Siberia shelf region.

In addition to satellite GSFC SIC fields, we use sea ice motion fields as provided by the Polar Pathfinder program on a daily basis and with a 25 km spatial resolution (Fowler, 2003). This dataset, covering the period from 1980 to 1999, was computed from Advanced Very High Resolution Radiometer (AVHRR), Scanning Multichannel Microwave Radiometer (SMMR), Special Sensor Microwave/Imager (SSM/I), and International Arctic Buoy Program (IABP) buoy data. Daily gridded fields combine data from all sensors.

While comparing models with satellite data, one needs to address also the observational uncertainties. A comparison with sea ice concentration fields obtained from AVHRR, Landsat and SAR (Synthetic Aperture Radar) data (Comiso et al., 1997) showed that GSFC dataset tends to overestimate the sea ice concentration in regions with relatively low concentration (up to +50% in some cases) and to underestimate this parameter in regions with relatively high ice concentration (up to -20% in some cases). Moreover, Meier (2005) suggested that the NT algorithm underestimates ice concentrations (relative to AVHRR results) by 10.5% in summer and 8.4% during winter months. According to the data documentation in general, the accuracy of total sea ice concentrations is within +/- 5% of the actual sea ice concentration in

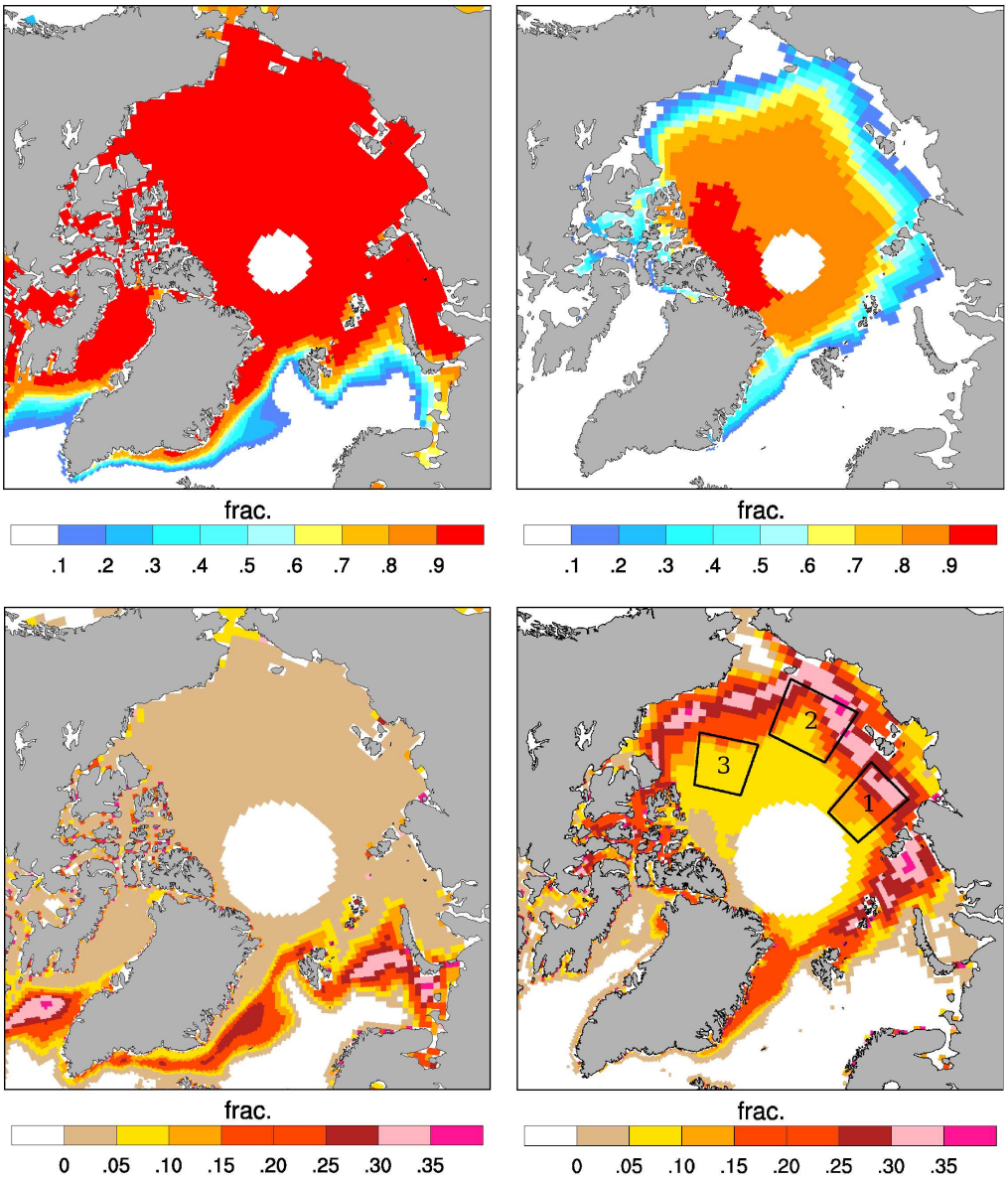

Figure 2.1— Upper panel: Mean sea ice concentration analyzed from the GSFC satellite data over the period 1980-1999 for (left) March and (right) September. Lower panel: Standard deviation of monthly mean sea ice concentrations analyzed from the GSFC satellite data over the period 1980-1999 for (left) March and (right) September. Rectangles indicate geographic locations for which time series of sea ice concentrations are shown in Fig. 2.9

winter, and +/- 15% in the Arctic during summer when melt ponds are present on the sea ice. Johnson et al. (2007) compared satellite based observations of Arc-

tic Ocean SIC with those simulated by nine models as part of the AOMIP project (Proshutinsky and Kowalik, 2007). The authors showed that all models seem to agree reasonably well during winter months. During summer months, however, SIC estimates vary less between observational datasets than between models, suggesting a substantially larger uncertainty in summer sea ice simulations by climate models than uncertainties present in the observational database.

2.2.3 In situ data

Due to the lack of sea ice thickness (SIT) observations, it is not straightforward to test the quality of sea ice thickness simulations of climate models. However, sea ice draft data collected by submarines in the Arctic Ocean represent an relatively extensive dataset in time and space from which ice thickness can be derived. Unfortunately, only respective data from the central Arctic Ocean have been unclassified by U.S. Navy and Royal Navy, while we find the highest model-data discrepancies in the Siberian seas.

The sea ice morphometric collected during Soviet Union's "Sever" (Konstantinov and Grachev, 2000) airborne expeditions and "North Pole" drifting station programs and other Russian sources were summarized by Romanov (1995) in form of hand drawn contour maps. The data in the central basin were obtained mostly in the 1970s, while the data in Siberian Shelf Seas have good spatial coverage also during the 1980s. Part of the data used for the creation of those maps are available at the NSIDC web site (`http://nsidc.org`), where among other things, maps of spatial data distributions are available as well. We will use this data as SIT climatology. The other source of climatological thickness distribution are maps that cover the whole Arctic including marginal seas is the article by Bourke and Garrett (1987). They used 17 submarine cruises during 1960-1982 and some additional data to construct maps of seasonal thickness distribution. But unfortunately in Bourke and Garrett (1987) no submarine measurements are available in Kara Sea and East Siberian Sea (compare Table 1) and ice draft measurements from only two submarine cruises are available in the Northern Laptev Sea from 1960 and 1962.

We compare the maps from Romanov (1995) with the mean estimate of the ice draft field obtained from 25 years (1975-2000) of submarine ice draft observations in the central Arctic Ocean (Rothrock et al., 2008). The two datasets show good agreement in the Canadian and Alaskian sectors, but Romanov (1995) demonstrates lower values (up to 90 cm) than Rothrock et al. (2008) in the area near the North Pole. The differences might be due either to climate variability since the datasets cover two different periods, or to sampling problems in both datasets. Polyakov et al. (2003) estimated ice thickness of fast ice on the basis of Russian observations on coastal stations in four Arctic marginal seas since 1936 through 2000 and found that sea ice thickness trends are small (about 1 cm/decade) and generally statistically insignificant. Also, maximum April-May fast-ice thickness measurements from Polyakov et al. (2003) and the map of sea ice thickness in April from Romanov (1995) show very good agreement. In summary, the comparison with Rothrock et al. (2008)

and Polyakov et al. (2003) gives us a reason to assume that the maps of Romanov (1995) can be used as climatology for the 1980-1999 period.

2.3 Sea ice concentration and thickness

We will start the analysis of SIC by comparing simulated SIC fields with observations. The comparison will be performed in terms of seasonal and interannual SIC variations. The analysis of sea ice transports (SIT), of differences in the atmospheric forcing and in the underlying ocean simulations will follow in the next sections.

2.3.1 Seasonal distribution of sea ice concentration

Fig. 2.2 shows that simulated SIC from the model runs ECHAM and FNCEP for March are in good agreement with satellite data (compare Fig. 2.1). In both cases the fields show concentrations near unity, and the locations of the ice edge agree with observations almost everywhere. The largest discrepancy appears in the reproduction of the ice tongue along the Greenland shelf, associated with the East Odden, where the model realizations tend to overestimate the observed SIC in this region. The ECHAM run shows somewhat better results than FNCEP near Greenland, but underestimates SIC in the region between Spitsbergen and Novaya Zemlya islands. In contrast, FNCEP simulates too much ice near Greenland and closer to observations in the region between Spitsbergen and Novaya Zemlya islands. Nevertheless, we can conclude that the model runs satisfactorily reproduce the wintertime sea ice extent and concentration.

The situation is substantially different during September (Fig. 2.3) when the simulated sea ice concentrations show significant discrepancies with respect to observations, even after taking into account errors in satellite data. Most noticeable, both model runs overestimate SIC in the Laptev and East Siberian Seas, near the Canadian coast and in the Canadian Archipelago. Positive biases reach concentration values of 0.4-0.6 in the Canadian Archipelago and 0.8 along the East Siberian coast. Satellite data suggest that the latter region is ice-free during summer months, or at least has low ice concentration, while both models show high SIC for this region. This holds especially for the ECHAM run, which shows further positive biases near Spitsbergen, Franz Josef Land and east of Greenland. In contrast, negative biases of about 0.4-0.5 are present in the FNCEP run to the north of the Kara Sea and further to the center of the Arctic Basin.

By showing the summer sea ice extent between 1900 and 2008 as simulated for 20^{th} century conditions by the ECHAM and FNCEP runs together with the observed Arctic summer sea ice extent for the satellite era, Fig. 2.4 illustrates the (by now well known) decline of the summer SIC over the entire observational record (see also the recent discussion by Parkinson and Cavalieri (2008)). SIC also declines in the 20^{th} century ECHAM run, but more slowly than observed. In contrast, the FNCEP run visually comes much closer to observed sea ice conditions in terms

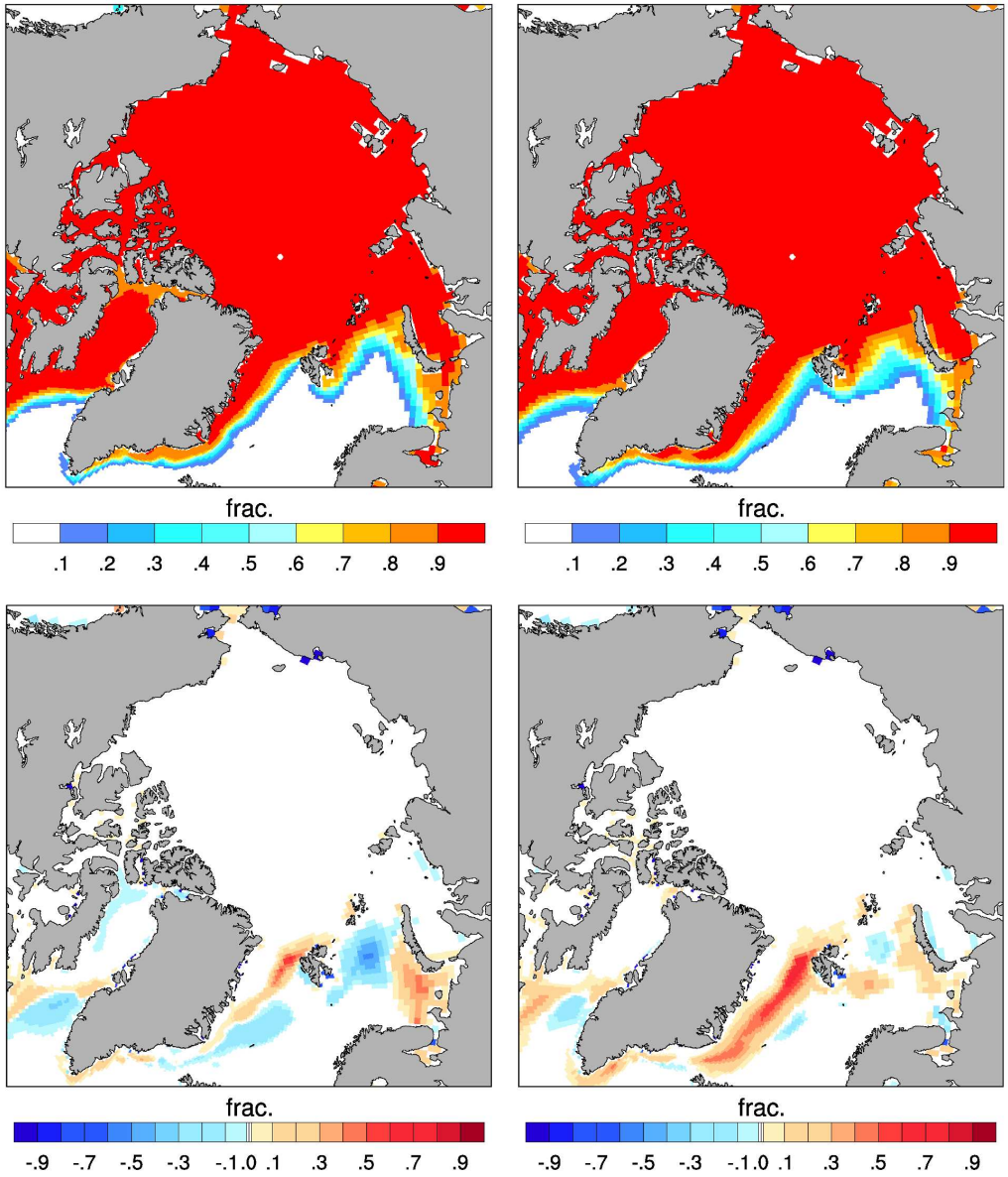

Figure 2.2— Upper panel: March mean sea ice concentrations (1980-1999) simulated by (left) the ECHAM run and (right) the FNCEP run. Lower panel: Differences in March mean (1980-1999) sea ice concentrations of (left) ECHAM minus GSFC and (right) FNCEP minus GSFC.

of the general level of SIE, its decline rate, but also in terms of its interannual variability; however decline rate does not withstand a formal significance test. A comparison of the ECHAM and FNCEP results suggests a large sensitivity of the detailed characteristics of sea ice simulations to the details of the atmospheric forcing.

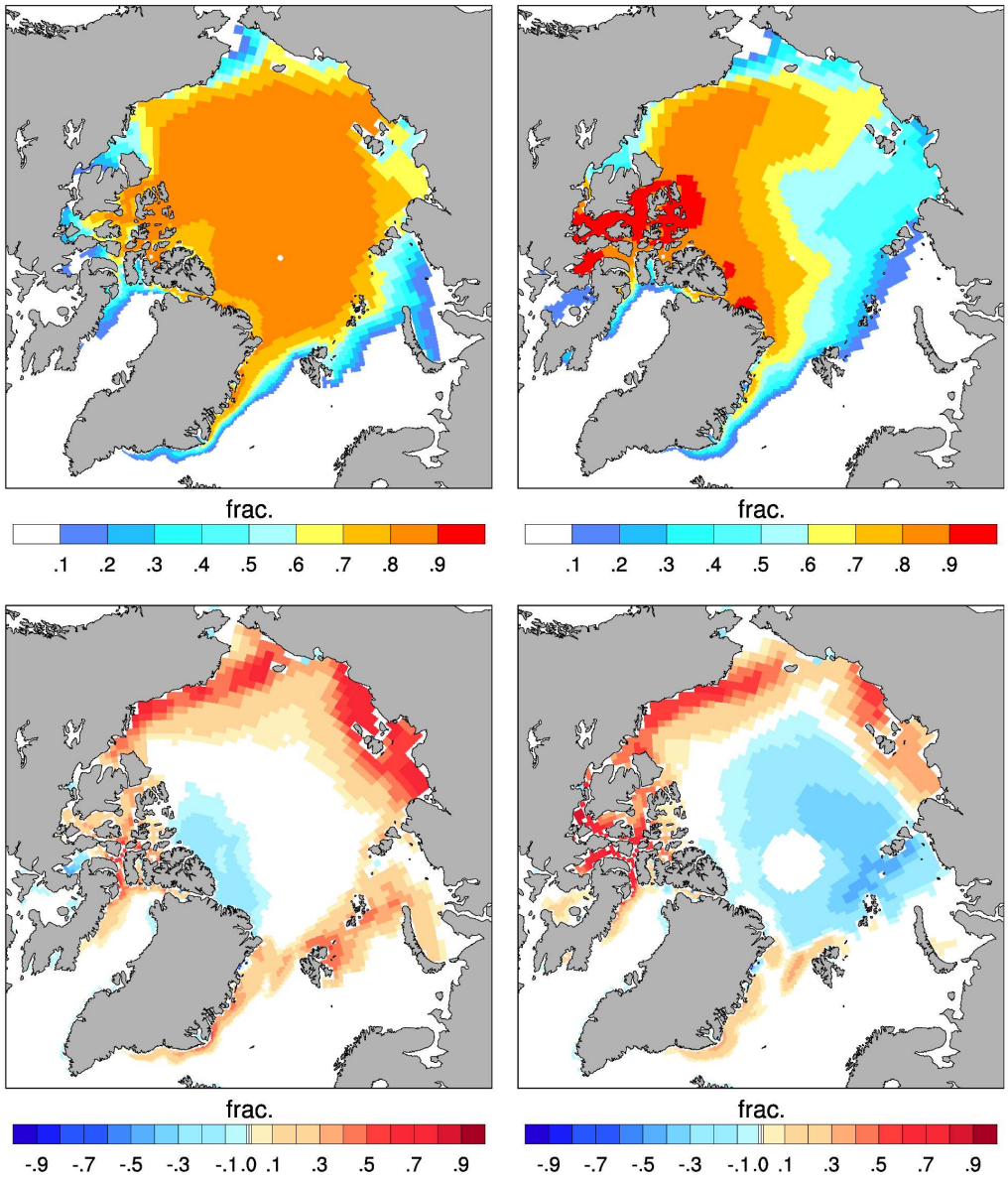

Figure 2.3— Upper panel: September mean sea ice concentrations (1980-1999) simulated by (left) the ECHAM run and (right) the FNCEP run. Lower panel: Differences in September mean (1980-1999) sea ice concentrations of (left) ECHAM minus GSFC and (right) FNCEP minus GSFC.

Anticipating results which are presented below, Fig. 2.4 thus already suggests that much of the deficits in the sea ice simulation of the coupled ECHAM model arise to a large extent (and maybe more than anything else) from problems in the model's atmosphere. This is consistent with results of previous studies, based on the earlier generations of climate models (Walsh and Crane, 1992; Bitz et al., 2002; Flato et al.,

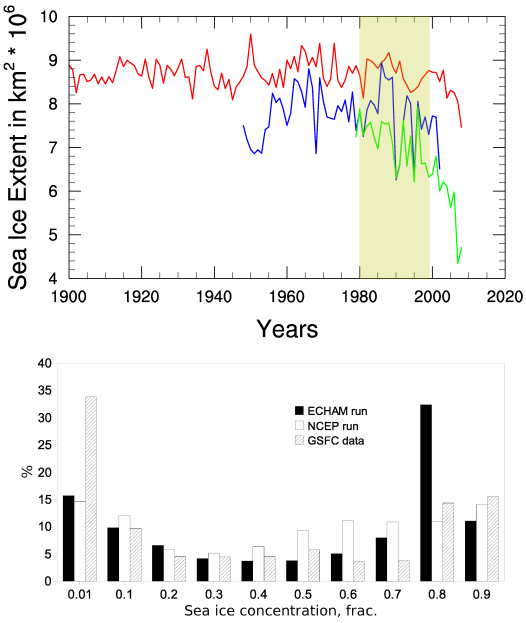

Figure 2.4— Top panel: September Arctic Sea ice extent (in km^2 10^6) as observed over the last 30 years (through 2008; green curve) and as simulated by the MPI-OM ECHAM run (red curve) and the FNCEP run (blue curve). The period used in this analysis marked by rectangle. Bottom panel: Distribution of Northern Hemisphere sea ice concentration (bin width 0.1 frac., beginning at 0.01 frac.) for September (1980-1999), as simulated by the two model runs and as observed by satellites.

2004) and there is not much improvement to report in this respect (Chapman and Walsh, 2007). Eisenman et al. (2007) discussed recently the impact of errors in the cloudiness over the Arctic on equilibrium sea ice solutions.

Fig. 2.4 in its lower panel shows histograms of September SIC as they follow from GSFC data and from the two model runs. In the case of GSFC, the distribution peaks near concentrations of zero and unity and thus has a shape not unlike that of the probability distribution of a harmonic function. The most significant differences to this observed distribution appears to exist in the ECHAM run, which peaks around unity, suggesting that the simulation of summer sea ice by this model is by far too compact as compared to observations, but also as compared to the FNCEP run. In contrast, histograms from all three datasets agree for March (not shown), again suggesting that the biggest problems exist in the summer sea ice concentrations of the ECHAM climate model. Our findings are in agreement with conclusions drawn by Deweaver and Bitz (2006), who identified the absence of typical atmospheric summertime features in the atmospheric circulation to be a primary problem of the CCSM3 sea ice simulation. The consistency of both conclusions might indicate that this is a more general problem in climate models.

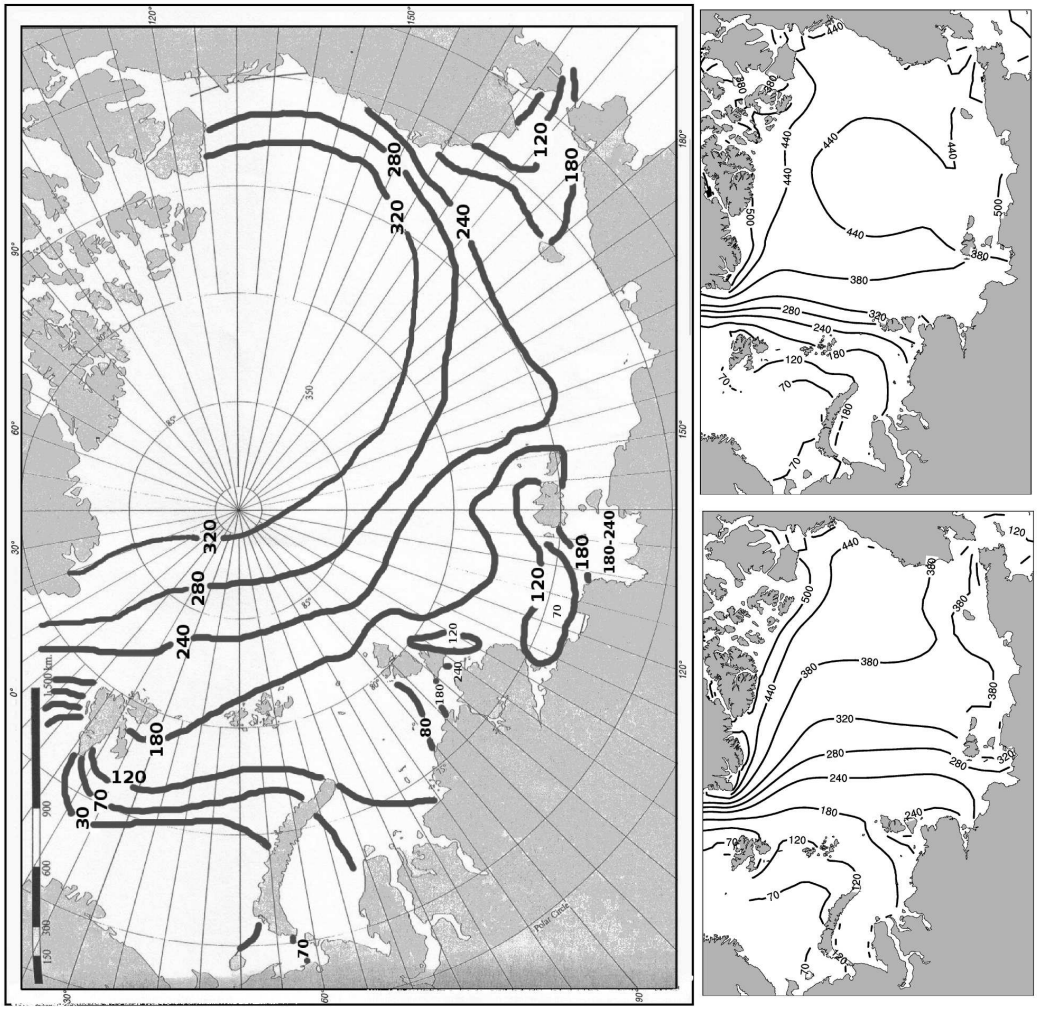

Figure 2.5— Left: Climatological April mean thickness of observed sea ice, adapted from Romanov (1995). Right column: mean April sea ice thickness for (top) ECHAM and (bottom) FNCEP.

2.3.2 Seasonal sea ice thickness

In Figs. 2.5 and 2.6 we compare simulated and observed SIT fields. For that purpose climatological SIT maps were adapted from Romanov (1995) for April and August-September (a March SIT climatology was not available). During April (Fig. 2.5), the climatological SIT is continuously decreasing in space from the north of Greenland and the Canadian Archipelago towards the Siberian Shelf seas and the coast of Alaska. Compared to Romanov (1995), the SIT in the ECHAM run is by far too thick (with mean values of 4-5 m) in the central Arctic Ocean, north of Greenland, off the Canadian coast, and in the Chukchi and East Siberian Seas. There are two areas where SIT maxima of 5 m are reached in ECHAM, one to the north of Greenland and another near the coast of the East Siberian Sea. Nevertheless, the ECHAM

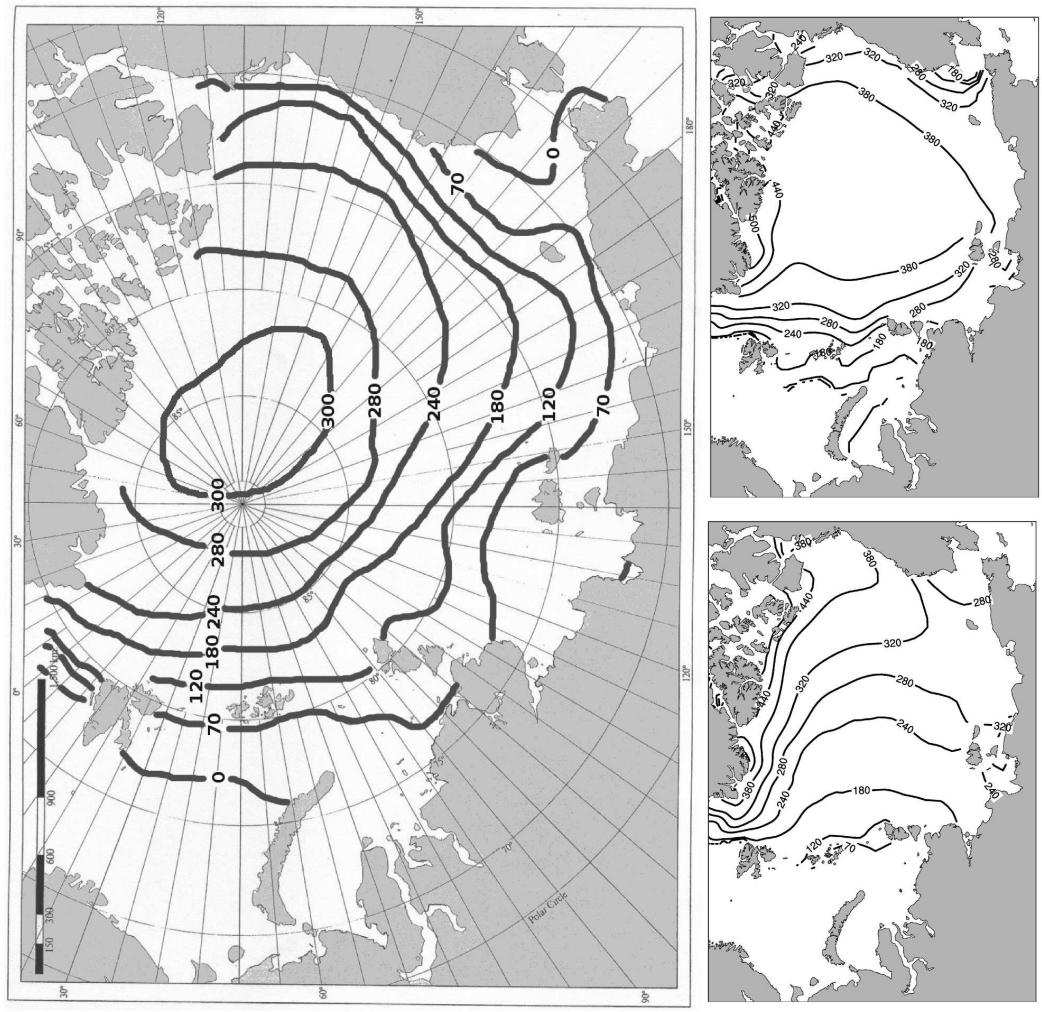

Figure 2.6— Left: Climatological August-September mean thickness of observed sea ice, adapted from Romanov (1995). Right column: mean August-September sea ice thickness for (top) ECHAM and (bottom) FNCEP.

simulated SIT continuously decreases toward the western part of the Arctic. For FNCEP, SIT is overall reduced relative to the ECHAM run, but still exceeds the values from Romanov (1995). Thick sea ice (3-4 m) occupies the center of the Arctic Ocean, the coast of Alaska, and the Chukchi and East Siberian Seas. There is only one SIT maximum to the north of Greenland, but ice accumulated near the East Siberian and Chukchi Sea coast is thicker than in the areas offshore. Continuous decrease of SIT towards the western part of the Arctic is also present but starts much closer to the center of the Arctic Ocean than in ECHAM and Romanov (1995).

The observed SIT distribution in August-September (Fig. 2.6) is characterized by a maximum (about 3 m) in the Canadian basin with SIT values declining below 70 cm toward the Siberian Shelf and toward zero in the Kara Sea. In contrast, the

SIT maximum in the ECHAM run is shifted laterally toward the North Pole, and from there SIT decreases steadily towards the Beaufort Sea, the coast of Alaska and the Chukchi Sea on one side, and the Laptev, Kara and Barents Seas on the other side. Sea ice thicker than observed is simulated in the East Siberian Sea (especially the western part), the Canadian Archipelago and Greenland, where the sea ice reaches its thickness maximum. In the FNCEP run, maximum SIT is located near the Canadian Archipelago, with a tongue of thick ice shifted to the Beaufort Sea and coast of Alaska, and further propagates towards the East Siberian Sea. As in winter, SIT is overestimated also during summer months by both model runs. Potentially more troublesome might be the fact that the model simulates wrong spatial structures of the summer sea ice thickness.

The above-mentioned SIT values are summarized in Table 2.1 for April and for September. From the table it is obvious that the spatial distribution of SIT is not well represented in the models, but also that differences between model runs are significant. While the FNCEP run tends to be closer to the climatological numbers, one has to be careful in this comparison, in that the climatological thickness distributions are also very uncertain (much more so than previously discussed satellite SIC observations).

Table 2.1— Sea ice thickness for April and August-September. The label "Atlas" refers to Romanov (1995).

	April			August-September		
Location	Atlas	ECHAM	NCEP	Atlas	ECHAM	NCEP
Central Arctic	2.4-3.2	4-4.5	2.8-4	1.8-3	3.5-4	1.8-3.3
Canadian Archipelago	3.2	4-5	4.5-5	2.8-3	4-5	4-5
Beaufort Sea	2.4-3.2	4.4	4-5	1.2-2.4	3.5-4	3.2-4
coast of Alaska	1.8-1.2	4.5	3-4	0-0.7	0-3.2	0-2.8
Chukchi Sea	1.8-1.2	4.5-5	3.8-4	0-0.7	0-3.2	0-2.5
East-Siberian Sea	1.8-2.4	4.5-5	3.5-4	0.7-1.8	3.2-3.8	2-2.5
Laptev Sea	$\leq$1.8	3.2-3.8	2.5-3	0-1.2	2.8-3.5	1.2-2.4
Kara Sea E	1-1.7	1.8-2.8	1.5-2	0-1.2	0-1.8	0
Kara sea W	1.3	1-2	1-1.5	0	0.7	0

A summary of simulated SIT is provided in Fig. 2.7 in form of a histogram of SIT simulated in the ECHAM and FNCEP runs (since observations are present only in form of hand drawn maps, it is impossible to include them into the figure): both model runs show roughly the same bimodal distribution during March; however, during September, the ECHAM run shows a peak in the distribution for 4 m thick sea ice, which is absent in the FNCEP run. Not only does the ECHAM run simulates too compact ice (compare Fig. 2.4), it actually also produces too thick summer ice as compared to the FNCEP run and presumably also as compared to the few available

observations.

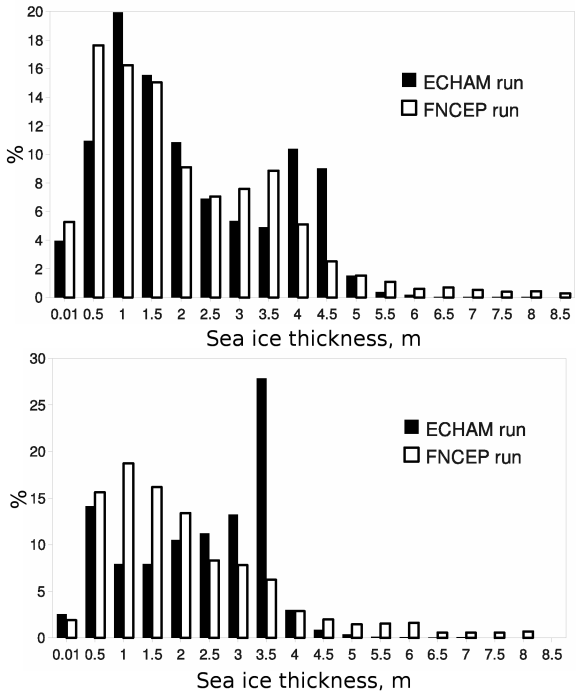

Figure 2.7— Distribution of sea ice thickness (bin width 0.5 m, beginning at 0.01 m) as simulated by the ECHAM and FNCEP model runs.

2.3.3 Interannual variations of sea ice concentration

Fields of the STD of observed SIC (Fig. 2.1, lower panels) suggest a substantial interannual variability in September SIC over the continental slope and shelf areas of the Eurasian sector. For comparison, Fig. 2.8 shows the respective fields of September SIC, but now from the ECHAM and FNCEP runs. The figure reveals that significant variability in SIC occurs only at the ice edges of the ECHAM run, notably on the Siberian shelf and toward the Barents Sea. However, hardly any variability in the simulated sea ice is present in the central Arctic. In contrast, observations indicate a further retreat of summer sea ice and much more variability in the central Arctic. We note that, unlike ECHAM, the FNCEP run shows a high degree of interannual SIC variability over a large fraction of the Siberian sector of the Arctic and to the east of the Lomonosov Ridge.

For a quantitative comparison of the model's interannual SIC variability with observations, we show in Fig. 2.9 time series of observed and simulated monthly-mean September SIC from three representative areas (see Figs. 2.1 and 2.8 for the geographic positions of these areas). It is obvious that the ECHAM run shows very little interannual variability, while the FNCEP run matches better the observed interannual variability, albeit often with different amplitude. The top panel represents

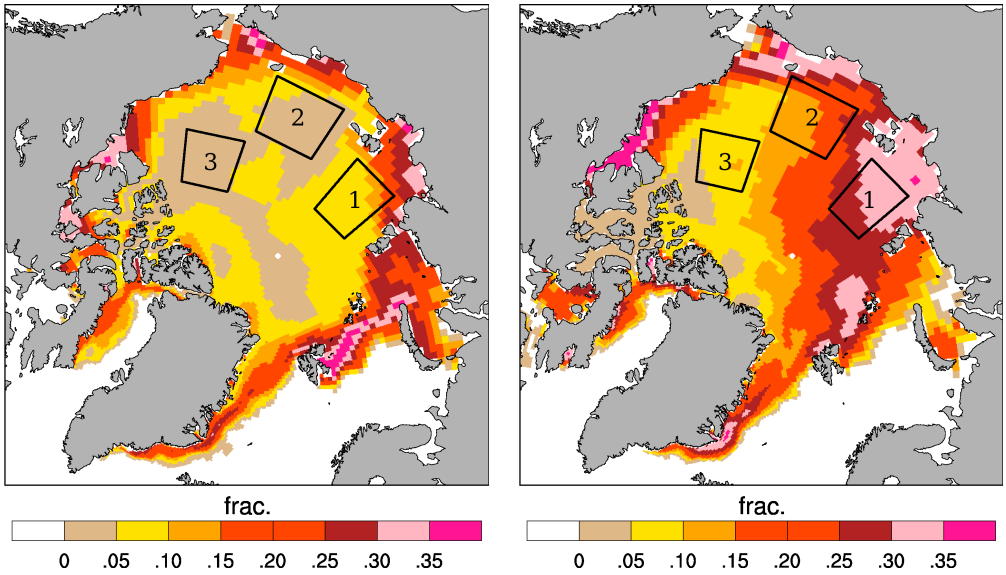

Figure 2.8— Standard deviation of monthly mean sea ice concentrations for September (1980-1999) (left) in the ECHAM run and (right) in the FNCEP run. Rectangles indicate geographic locations for which time series of sea ice concentrations are shown in Fig. 2.9.

a region in the northern part of the Laptev Sea, where observations and the FNCEP run suggest high interannual September SIC variability. ECHAM time series show a lower STD and higher mean concentration of September SIC. In the FNCEP run, because this geographic location is very close to its sea ice edge, a stronger interannual variability can be found; nevertheless, the generally better agreement between FNCEP and GSFC is still apparent.

The middle panel represents SIC variations in the area north of the East Siberian Sea, which includes the ice edge in the GSFC data as well as central parts of the Arctic ocean. Despite the fact that the spatial distribution of STD fields in the FNCEP and GSFC fields are different, mean values are close to each other. The ECHAM run again does not simulate enough interannual variability since its ice edge is very close to the coast in this region. The bottom panel finally represents a location at the center of the Arctic Basin, where satellite data show high September SIC concentrations and low interannual variability. Here both model runs agree with observations. Common to all three panels of Fig. 2.9 is that the FNCEP run tends to produce more realistic results and that the error in the coupled ECHAM run is considerably larger.

We calculate NAO indexes for the ECHAM and NCEP runs (not shown) and find that the NAO standard deviation in ECHAM run is smaller by a factor of 1.7 than the NAO standard deviation in the FNCEP run. Lack of interannual variability suggests that our coupled model does not represent realistically some fundamental

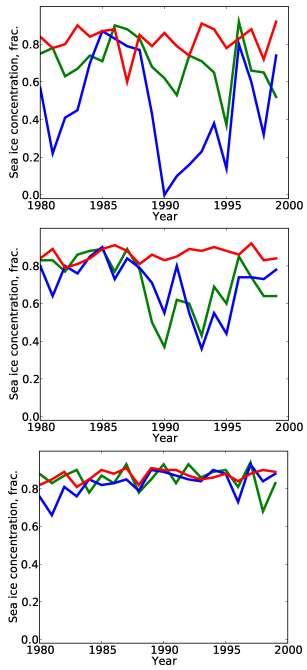

Figure 2.9— Time series of mean September sea ice concentrations from different areas for the period 1980-1999. Shown are GSFC observations (green curve), the ECHAM run (red curve) and the FNCEP run (blue curve). Shown in the top, center and bottom panels are time series from positions 1 through 3 in Figs. 2.1 and 2.8, respectively.

characteristics of atmospheric variability over the Arctic (see for example the analysis of NAO representation in ECHAM5 by Pinto et al. (2008))

2.4 Sea ice transports

Sea ice drift is an important parameter determining the distribution and thickness of sea ice in the Arctic Ocean, as well as the sea ice export into the Nordic Seas. Observations of sea ice drift are available from the Pathfinder dataset on a 25 km spatial grid (Fowler, 2003). Monthly mean sea ice velocity vectors, representing the years 1980-1999, are shown in Fig. 2.10 for March and October. (October is shown here instead of September because of problems with passive microwave radiometer observations of sea ice drifts during September (Kwok et al., 1998; Maslanik et al., 1996).)

Observed March ice transports display two main sea ice drift features, notably the Beaufort Gyre located in the Canadian Arctic Ocean, and a Transpolar Drift. In the Beaufort Gyre, ice is transported anticyclonically, bringing ice from the Canadian shelf to the north of Alaska and the Chukchi Sea. The opposite side of the Beaufort Gyre is part of the Transpolar Drift, feeding ice from the Siberian Shelf region all the way toward the Fram Strait where it is exported into the Nordic Seas. The

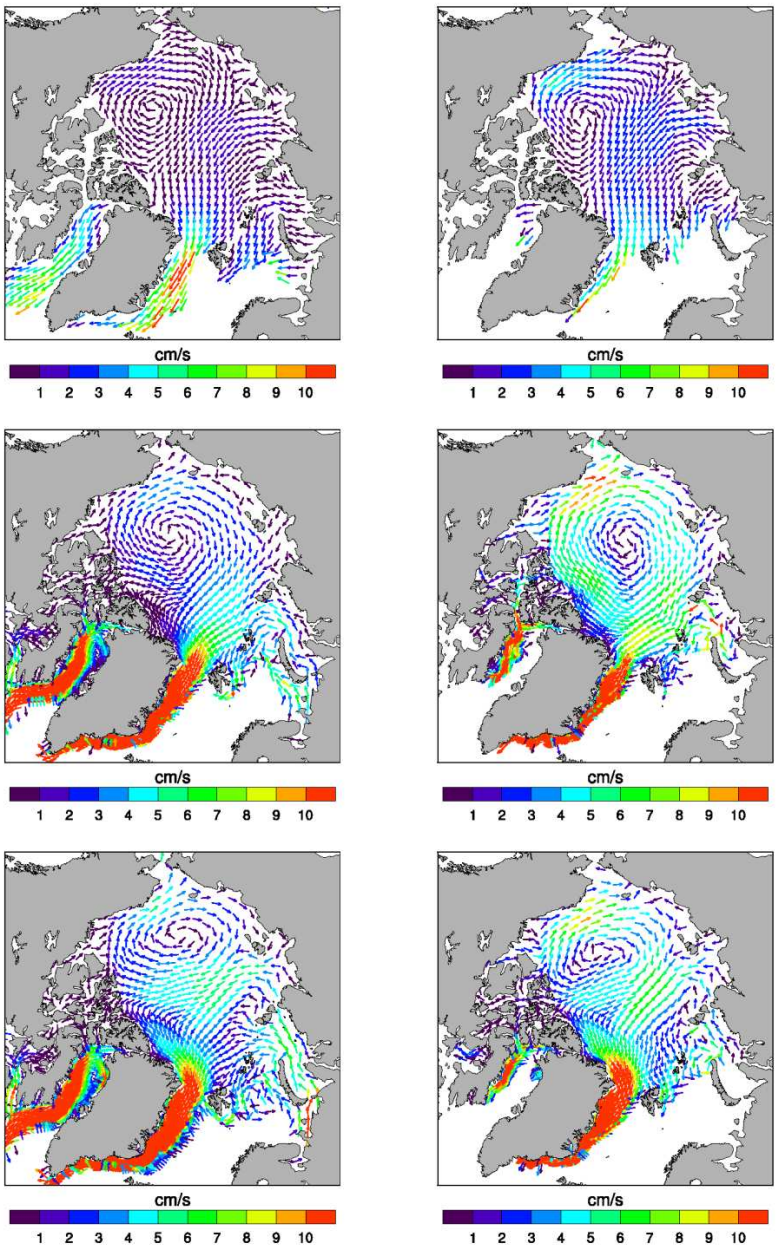

Figure 2.10— Ice motion vectors for March (left column) and October (right column) for (upper panel) Pathfinder project data, (middle panel) the ECHAM run, and (lower panel) the FNCEP run. For Pathfinder data, every fifth vector is shown, for ECHAM and FNCEP runs, every second vector is shown. Color-coded is the speed of each vector (in cm s^{-1}).

Transpolar Drift originates from the Laptev and the East Siberian Seas. Another, yet smaller feature in ice transport is the Barents Sea transport, which also feeds

sea ice toward the Nordic Seas. As compared to March, October observations show essentially similar, but enhanced, transport structures, with a stronger and larger Beaufort Gyre and a stronger Transpolar Drift.

In the ECHAM run the center of the Beaufort Gyre is shifted, forming a strong anticyclonic ice gyre in the central Arctic Ocean, and the Transpolar Drift is shifted towards Severnaya Zemlya Islands and Franz Josef Land, i.e., more toward the sea ice edge. As a consequence, the ice export from the East Siberian Sea is very small in the ECHAM run and a Transpolar Drift is quasi absent. Ice exported through the Fram Strait originates mainly from the area of the Eurasian shelf break. We note also that due to the strong Arctic ice gyre, the ice on the Siberian shelf originates to some extent from the Canadian part.

We conclude from Fig. 2.10 that the observed ice transport is very poorly represented in the ECHAM run. This problem seems much remedied in the FNCEP run (bottom row of Fig. 2.10), pointing again toward the atmosphere as the primary cause for uncertainties in high-latitude climate parameters in the coupled ECHAM model. In the FNCEP run, the center of the Beaufort Gyre and the Transpolar Drift is now much more realistic both in terms of structure and amplitude. However, the main source of the ice exported southward through Fram Strait is not the central Arctic Ocean, but the area to the north of Greenland.

Fig. 2.10 already indicates that the southward sea ice transport through the Fram Strait (and Davis Strait) in both model runs is much larger than what is observed. This is quantified in Fig. 2.11 showing a histogram of sea ice velocity magnitude for the entire Northern Hemisphere. For the comparison, observed ice velocities from Pathfinder data were interpolated to the model grid, and simulated ice velocities are used only over regions with SIC exceeding 0.15. During March, the maximum percentages in all three time series reside between 0.01 and 0.03 m s^{-1}, albeit at different levels: The Pathfinder data peak at a 19% level near 0.02 m s^{-1} velocity magnitude, the ECHAM and FNCEP data peak at 9% and 13%, respectively, near the same velocity magnitude. In Pathfinder data percentages decline rapidly for velocity magnitudes larger than 0.1 m s^{-1}, while in the ECHAM and FNCEP runs they decline more slowly, reaching values of 0.4 m s^{-1} and are more associated with the ice export through the Fram Strait. In September peaks of the ice velocity magnitude distribution in the ECHAM and FNCEP runs are shifted relative to the Pathfinder data towards higher values, but overall sea ice transports are smaller. We note that the shape of the FNCEP distribution agrees more with the Pathfinder data than with the ECHAM result especially in March. Martin and Gerdes (2007) compare AOMIP model's simulations of the ice transport with satellite observations and also found that AOMIP models tend to have a lesser percentage of low velocity magnitude and a higher percentage of high velocity amplitudes.

Only a few observation-based estimates of ice volume transports through the Fram Strait are available for a comparison (Kwok et al., 2004; Vinje et al., 1998). As expected, the model ice volume export through Fram Strait is higher than observational estimates (Fig. 2.12). In addition, the 1980-1999 time-mean FNCEP

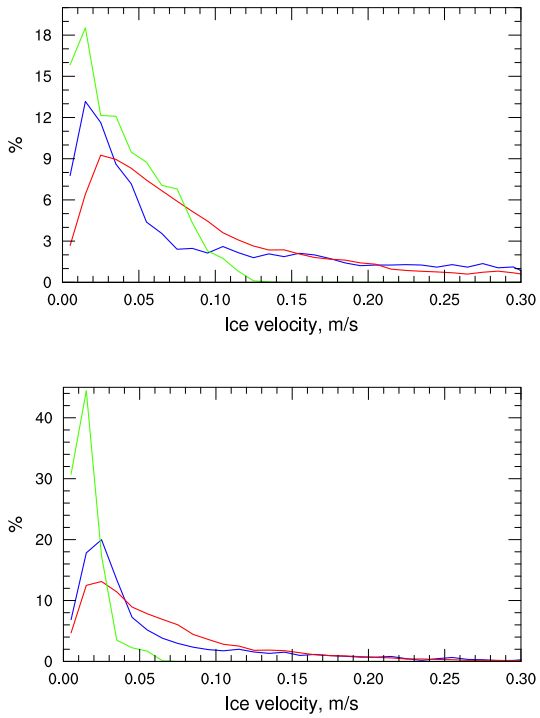

Figure 2.11— Distribution of sea ice velocities from the entire Northern Hemisphere for March (upper panel) and September (lower panel). Percentage values of the y-axis correspond to histogram bins along the x-axis with a bin width of 0.01 m s^{-1} beginning at 0.001 m s^{-1}. Shown are Pathfinder data, the ECHAM run and the FNCEP run as green, red and blue curves, respectively. Note the different vertical scale on graphs.

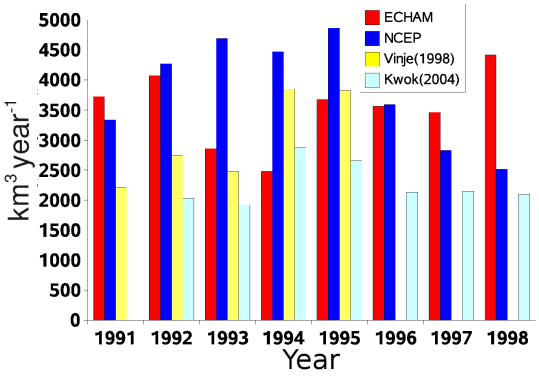

Figure 2.12— Sea ice volume transport through the Fram Strait as simulated by the ECHAM and FNCEP model runs and analyzed by previous studies.

transport (3997 km^3 $year^{-1}$) is higher than the ECHAM time-mean transport (3467 km^3 $year^{-1}$), which can be rationalized by the fact that differences exist in the sea

ice pathways feeding ice with different thicknesses toward the Fram Strait: In the ECHAM run the sea ice drifts to the Fram Strait mainly from the Eurasian part of the Arctic Ocean; this ice is relatively young and thin. In the FNCEP run the main source for the sea ice in the Fram Strait lies to the north of Greenland, where thick, multi-year ice is situated.

2.5 Forcing fields

Based on the differences between the sea ice simulations obtained from the coupled ECHAM and the FNCEP runs, we hypothesized above that these differences emerge primarily from differences between the ECHAM atmosphere and the NCEP-RA1 reanalysis in terms of surface flux fields. However, differences in the atmosphere forcing fields also lead to different Arctic ocean properties that may affect sea ice from below. In the following we will quantify the impact of atmospheric and ocean forcing on sea ice properties by analyzing differences in the fields of air temperature at 2 m height, sea level pressure (SAT and SLP, henceforth) and ocean hydrographic properties from both runs.

2.5.1 Atmospheric forcing

With respect to March SAT, Fig. 2.13 reveals that the field is biased high in the ECHAM run by 0.7°C (averaged over the Arctic Ocean north of 60°N) relative to the NCEP-RA1 reanalysis. Nevertheless spatial structures agree in that SAT increases in both fields from the Canadian Archipelago towards the Eurasian Shelf, the coast of Alaska and the Fram Strait, and the position of the ECHAM 0°C isotherm essentially coincides with the NCEP-RA1 reanalysis. In contrast, the ECHAM September SAT distribution is centered around a minimum located near the geometric North Pole, while the minimum in the NCEP-RA1 reanalysis is shifted toward Greenland and on average is higher by 0.6°C. With respect to SLP (which in the figure are superimposed on the SAT fields) the respective field for the ECHAM run indicates an anticyclonic atmospheric circulation system centered on the North Pole whereas in the NCEP-RA1 reanalysis a low pressure system spreads in a trough-like fashion from the Icelandic minimum up to the Laptev Sea.

To better highlight the differences between the two atmospheric forcing fields and to discuss their dynamical consequences for the coupled sea ice-ocean model, we show in Fig. 2.14 respective difference fields for SLP and SAT. The upper part of the figure reveals a pronounced quasi-permanent high pressure anomaly in the ECHAM run relative to the NCEP reanalysis, located over the North Pole. This is especially obvious in September when the high pressure system forms a quasi-permanent anticyclonic atmospheric gyre that occupies large parts of the Arctic. The respective Ekman transport leads to an anomalous convergence of thick ice in the central Arctic in the ECHAM run during summer months, explaining why in the ECHAM run (and potentially in other IPCC type models) too much sea

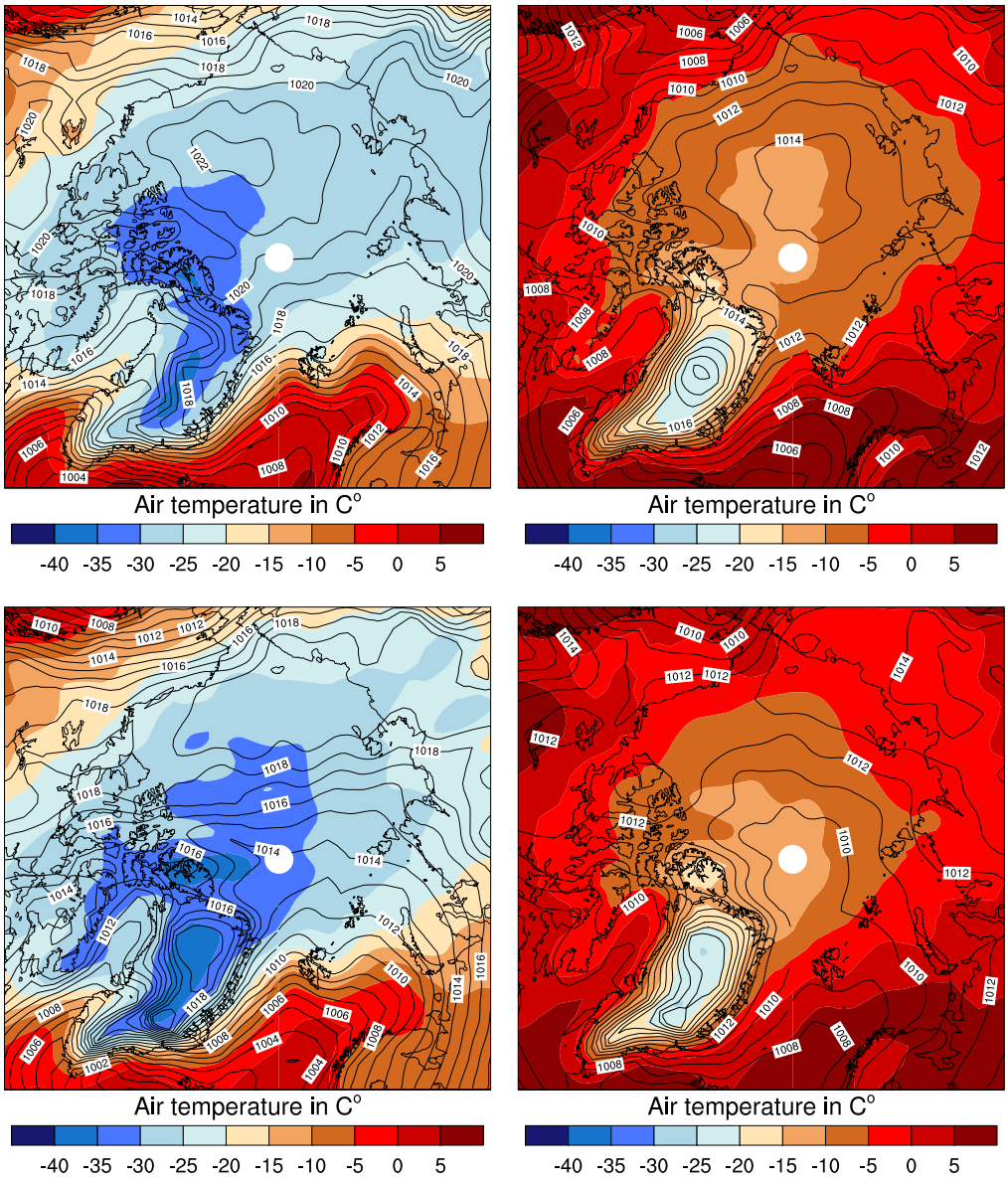

Figure 2.13— Climatological monthly mean surface air temperature (color coded in °C) and sea level pressure (contours as hPa) fields for (left) March and (right) September. Shown are results for (upper row) ECHAM and (lower row) the NCEP-RA1 reanalysis.

ice is being found in the central Arctic Basin that is hardly varying in time. In general terms, SLP gradients are associated with surface wind stress fields, and SLP therefore affects the dynamical part of the ice model. Because of this, sea ice drift is nearly parallel to the isobars (Zubov and Somov, 1940; Kwok, 2008), and this holds also for the difference fields of SLP and differences in sea ice transports shown in

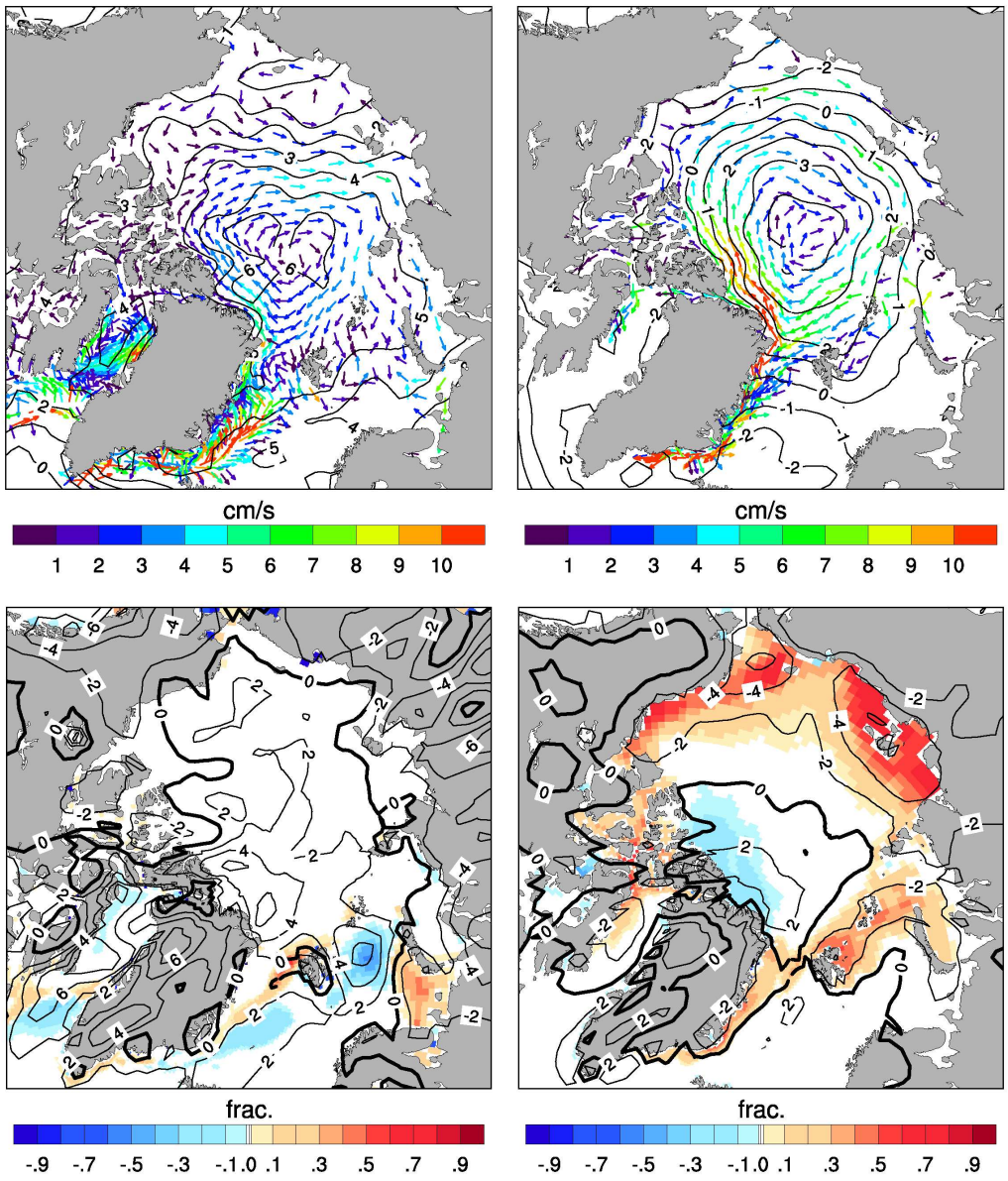

Figure 2.14— Top row: Shown as contours are differences between the climatological monthly mean (left) March and (right) September ECHAM - NCEP-RA1 SLP (contour interval is 1 hPa). Superimposed as vector field are the respective climatological monthly mean difference fields for ice motions, with only every second vector plotted and speeds color coded in cm s^{-1}. Bottom row: Shown as contour lines are differences in climatological (left) March and (right) September ECHAM - NCEP-RA1 SAT fields. Superimposed as color are respective ECHAM - GSFC SIC difference fields.

the figure. In essence, Fig. 2.14 suggests that the error in the ECHAM atmosphere in form of an anticyclonic circulation around the geographic North Pole is driving a similar, but erroneous gyre in the sea ice, which in turn is responsible for the wrong

sea ice distribution and sea ice thickness diagnosed above in the ECHAM run.

Nevertheless, errors arise also from the atmospheric thermal forcing of sea ice (lower row of Fig. 2.14). In March the ECHAM run are too warm to the north of Greenland, between Spitsbergen and the Novaya Zemlja Archipelago, and in the Baffin Bay and Labrador Sea, where the differences in SAT reach 7°C; over most of the remaining parts of the Arctic Ocean differences are typically of the order of 1-2 °C. In the ECHAM run, temperature gradients over the Arctic seas are lower than in the NCEP-RA1 reanalysis, and over large areas to the north of Greenland ECHAM is too warm. ECHAM is colder than the NCEP-RA1 reanalysis by up to 6°C in the Laptev Sea and the western part of the East Siberian Sea and over the Chukchi Sea. During September, the ECHAM SAT is lower than the NCEP-RA1 reanalysis over large parts of the Arctic, except north of Greenland and over parts of the Canadian Archipelago where ECHAM is warmer, up to 3°C near Ellesmere Island. ECHAM is colder mainly over the Arctic Seas, up to 6°C over the Laptev Sea and the western part of the East Siberian Sea and over the Chukchi Sea.

Because SAT affects the thermodynamics of sea ice, the differences in SIC between the ECHAM and the GSFC data are well correlated with the differences in SAT of ECHAM and the NCEP-RA1 reanalysis. In March the area of the biggest SIC differences, located between Spitsbergen and the Novaya Zemlya Archipelago, coincides with the region of the biggest SAT error in ECHAM. During September the too large ECHAM SAT north of Greenland can help to explain the too low ECHAM SIC there. Conversely, too low ECHAM SAT over the Siberian Seas, the Bering Strait and the Canadian coast, associated with a shift of the Arctic Gyre, may be partly responsible for too high ECHAM SIC in these regions. There is a possibility that larger areas of open water increase upward heat flux and cause SAT increase, but this process probably has a smaller impact in this case since SAT further south, over Siberia, are also too high in the ECHAM run.

While interpreting the results, one has to recall that the NCEP-RA1 SAT and SLP fields in the Arctic are far from perfect. The NCEP-RA1 was compared with observations from the "North Pole" drifting stations (NP) by Makshtas et al. (2007). The authors found that for the period of 1978-1991 in spring SAT from NCEP-RA1 is higher than observed (by 2.3°C) at the NP, but in autumn it is lower (by 1.8°C). SLP from NCEP-RA1 and NP showed good agreement between datasets in all periods, but NCEP-RA1 SLP in most cases was a bit lower than NP SLP. Taking into account these two parameters as well as a total cloudiness, specific humidity, and wind on 10m, the authors concluded that RA1 data should be used with "great caution" as forcing for sea ice models. Despite the uncertainties in the NCEP reanalysis, results of the ocean-ice model driven by the NCEP-RA1 reanalysis are nevertheless superior relative to ECHAM results and we can anticipate that with even better atmospheric forcing fields, the simulation of the coupled ocean-ice model would improve further. While interpreting the difference in atmospheric forcing between the two analyzed model runs one also has to recall that the NCEP run is performed in an uncoupled mode, while the ECHAM run is a coupled system. Clearly the comparison of two off-line model runs would be ideal. However, the ECHAM5 atmosphere already

"remembers" all feedbacks that it gets from the ocean during the coupled run. Although the surface fluxes (bulk formulas) in the FNCEP and ECHAM setups do differ, making an "offline" run with the ECHAM5 atmosphere from the coupled run would only show the sensitivity of the solution to the differences in the bulk formulas, and would not contribute to the scientific question addressed in the chapter.

2.5.2 Ocean forcing

Similar to the atmospheric forcing, the ocean circulation can influence sea ice in two different ways: (1) dynamically, through affecting sea ice transport and (2) thermodynamically, through sea ice melting and freezing. However, analyzing ocean surface currents under the ice (not shown) one finds that in both simulations ocean currents essentially follow the main pathways of sea ice transport (accounting for the respective angle of rotation) and therefore do not force the ice velocity and direction.

A more important ocean forcing mechanism might therefore be that Atlantic water entering from the Nordic Seas through the Fram Strait and Barents Sea pushes under the cold fresh surface layer, leading to a relatively warm salty layer between 200 and 600 m depth named Atlantic water (AW) layer. Although the temperature of the AW layer is higher than in water masses above and below, the heat exchange with the surface layer is suppressed by the Cold Halocline Layer (CHL) separating both water masses. The correct simulation of these two important features of the Arctic Ocean (AW and CHL) is important for simulating the correct water mass properties of the upper Arctic ocean, yet it remains a challenge, even in regional models. According to Holloway et al. (2007), models participating in the AOMIP tend to overestimate the AW layer thickness and exhibited thermally stratified upper ocean, i.e., they failed to form a proper CHL. This shortcoming can have a pronounced impact on the heat budget of the upper Arctic ocean layer and will affect sea ice on decadal to centenial time scales (Steele and Boyd, 1998; Martinson and Steele, 2001).

To test the vertical thermal and haline stratification of the ECHAM and FNCEP runs, we compare temperature, salinity and density vertical profiles with the Polar Science Center Hydrographic Climatology (PHC 3.0, (Steele et al., 2001)) in the Eurasian sector of the Arctic Ocean, where temperature of AW is highest (Fig. 2.15). Both runs show thicker, shallower and warmer AW layers. The ECHAM run shows a rapid temperature increase right from the surface without any indication of the mixed layer presence. In the FNCEP run the mixed layer is disturbed by a warmer spike in the middle, probably due to the temperature restoring process at the surface. We note that a mixed layer is lacking in all salinity profiles and a strong pygnocline starts right from the surface in the two simulations, closely following the observed salinity profile. We also note that the Brunt-Väisälä frequency (BVF) (not shown) is quite similar among the data sets in the first 50 meters of the water column, but in range of 50-150 meters the BVF is considerably smaller in the FNCEP run than in the PHC climatology and the ECHAM run.

We see from Fig. 2.15 that the heat content of the Arctic Ocean is quite different

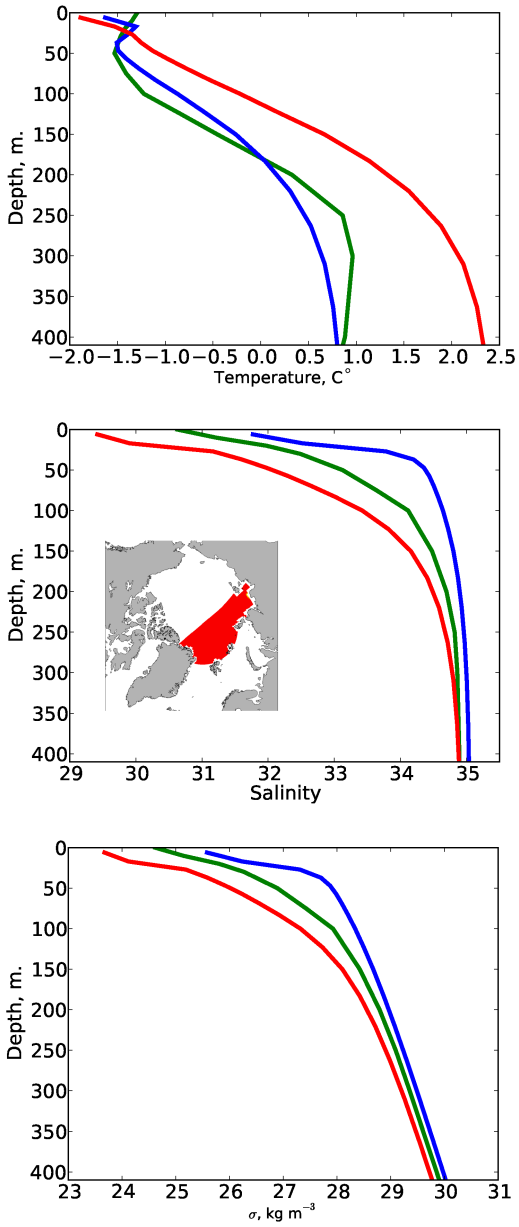

Figure 2.15— Upper row: Vertical profiles of September ocean; top:temperature, middle:salinity and bottom:density from PHC climatolofy and model runs (1980-1999). Green -PHC, red - ECHAM run, blue - FNCEP run. Parameters are averaged over the area showed at the middle panel.

between the two runs and between the model simulations and the observations. To test if this does affect sea ice budget and sea ice distribution in the model simulations, we analyze the heat convergence in the model's Arctic ocean and the associated heat loss to the ice or atmosphere. To do so, we compute the total top to bottom heat

content change and heat convergence in Area 1 (Laptev Sea; see Fig. 2.15 for the area) where heat changes are largest in both runs. While doing the computations we assume that lateral diffusion is negligible (or at least the same between the two runs) and that differences in heat content change and heat convergence will serve as a diagnostic of heat exchange through the surface of the ocean (either to sea ice or the atmosphere).

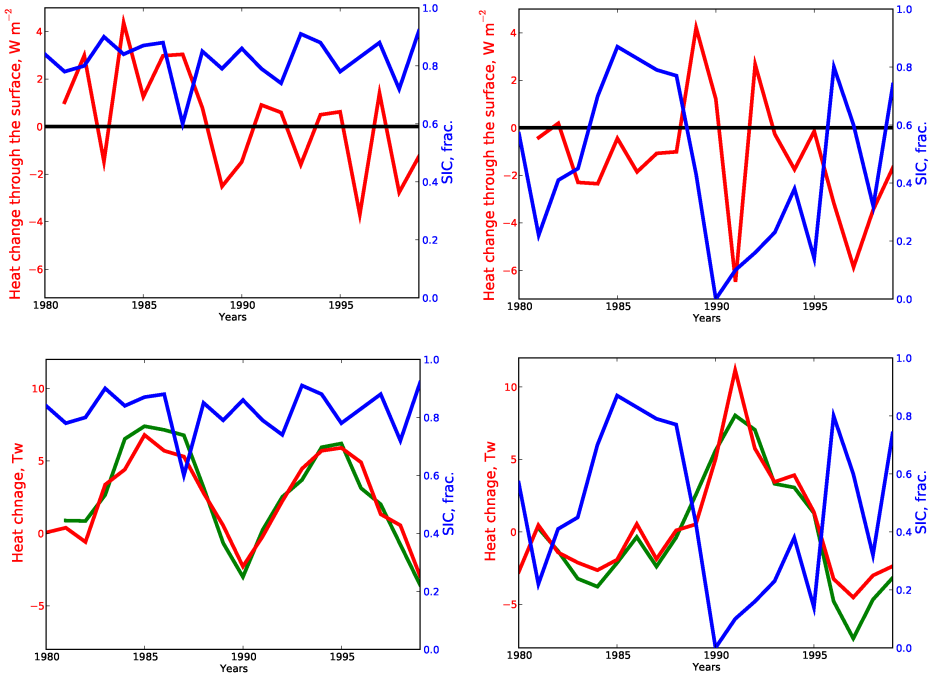

Figure 2.16— Top:Heat change throught the surface (red) and September SIC (blue). Bottom: heat convergence (red), total heat content change (green) and Septebmer SIC(blue). Left: ECHAM run, right: FNCEP run.

Results are shown in the top row of Fig. 2.16 in terms of area-averaged mean September SIC and surface heat exchange in ECHAM and FNCEP runs. Positive values indicate an oceanic heat uptake through the surface. In both runs curves are visually anti-correlated with each other (a formal correlation coefficient for ECHAM is -0.18, for FNCEP run -0.19), showing a decrease of ocean heat uptake through the surface, or increase in heat loss to the atmosphere simultaneous to an increase of SIC and vice versa. This suggests that the ocean heat content is not used to first order to melt sea ice, rather that during periods with increased amounts of open water, the ocean tends to gain heat from the atmosphere (by absorbing heat through the surface), and that during years with high SIC the ocean tend to lose the heat to the atmosphere and/or to sea ice. A noticeable exception from this tendency can be found during the year 1991, when in the FNCEP run we see a spike in heat loss from the ocean associated with close to zero SIC in the Laptev Sea,

simultaneous to high lateral heat convergence and increase in total heat content caused by the advection from aside (Fig. 2.16, bottom). We also note that the increase in ocean heat content occurs after SIC declines, not before. In contrast, two events of increased heat content (by advective heat inflow) in the ECHAM run are not associated with any change in the SIC record (Fig. 2.16, bottom).

In summary, we conclude that in both model runs heat from the ocean might influence SIC only during extreme events of strong lateral influx of heat, and even then a relation between regional heat content increase and sea ice melting is not unambiguous. We note, however, that on time scales longer than those considered here, the impact of ocean heat content on the development of SIC remains to be expected.

2.6 Discussion and Conclusion

This chapter provides a contribution to a detailed evaluation of IPCC-type coupled climate models against observations with focus on the Arctic sea ice system. The IPCC projections tend to be interpreted as forecasts of the Arctic sea ice system. However, Eisenman et al. (2007) provided already a critique of the limited skill ice forecasting models generally. The authors concluded that IPCC type models during AR4 simulated satisfactorily the present day sea ice conditions, but that uncertainties in the atmospheric cloud cover combined with a high sensitivity of equilibrium sea ice thickness to sea ice albedo lead to high uncertainties in sea ice predictions. Here we demonstrate that even for present day conditions sea ice simulations by IPCC type models show large uncertainties. Although our in depths analysis shows shortcomings of one model, the model was deemed one of the best in simulating sea ice characteristics: Parkinson et al. (2006) compared the seasonal cycle in satellite SIE with respective results from 11 models participating in the IPCC Fourth Assessment Report and reported that the ECHAM/MPI-OM model was among the most favorable models to represent the annual cycle of sea ice in the Northern Hemisphere. We can therefore expect that results reported here from the ECHAM run should be representative for other IPCC type models as well and that problems found in our own analysis and summarized above might actually apply to many other climate models. By scrutinizing our own model we attempt to identify possible sources of errors which need to be improved to improve the skill of present-day Arctic system climate simulations and projections of the Arctic system into the next century.

From a comparison of two runs of the identical MPI-M ocean-ice model (one forced by an interactive atmosphere (ECHAM run), the other forced by the quasi-realistic NCEP-RA1 reanalysis surface fluxes (FNCEP run)) against simultaneous observations of sea ice characteristics during the period 1980 through 1999, we can draw several main conclusions. Some confirming conclusions drawn by previous studies, and it can be expected that shortcomings documented here do apply more generally to IPCC type coupled climate models.

- While simulated winter time sea ice distributions are close to what has been observed, the summer sea ice conditions are highly sensitive to details of the atmospheric forcing. Simulations by the fully coupled IPCC-type ECHAM model cause significant deficits in essentially all present day ice parameters over the Arctic Ocean. In contrast, summer sea ice results are much more realistic in the NCEP-driven run, which provides quasi-realistic present day atmospheric conditions.

- A major agent for deficits in the sea ice conditions, including uncertainties in basin-scale sea ice transports, is an unrealistic high pressure system in the ECHAM run centered to the geometric North Pole in the model, which occupies the entire central Arctic. It drives a quasi-permanent anticyclonic basin-scale gyre of ice transport and causes, through an Ekman ice drift, the buildup of thick ice in the central basin. Errors in the associated surface wind stress (atmospheric circulation) leading to errors in the sea ice pathways and dynamics are a primary reason for the errors in the ECHAM sea ice.

- The ECHAM run substantially underestimates the atmospheric interannual and decadal variability over the Arctic. Accordingly the interannual to decadal variability of sea ice cover and sea ice transport is underrepresented in the ECHAM run, as is the variability in volume and heat transport from the North Atlantic into the Arctic Ocean, which in the FNCEP run is significantly correlated with the NAO/AO index.

- Sea ice transports are higher in amplitude in both model runs than in Pathfinder data, and ice transport patterns in the model simulations do not coincide with the patterns in the Pathfinder data, especially in the ECHAM run. Associated higher ice velocities lead to an unrealistically high ice export through the Fram Strait in the model simulations; differences in the sea ice advection pathways from both runs feed sea ice to the Fram Strait from different source regions, which affects the thickness and thus the ice volume leaving the Arctic toward the Nordic Seas.

- While hydrographic conditions are quite different between the two analyzed runs, we seem to find no indications of a substantial impact of the ocean heat content differences on the sea ice distribution or variation on interanual to decadal time scales - again pointing toward the atmosphere as the dominant driver for arctic sea ice variability, with the ocean on basin-scale responding more passively in its air-sea interaction to varying insulation through sea ice coverage. The situation might be quite different on centenial time scales, however, pointing toward uncertainties of IPCC sea ice projections to also originate from the ocean. This means that a good representation of the ocean circulation and its temporal variability/changes is critical for simulations of present and future ice-ocean interactions (compare also Bitz et al. (2006)).

- The uncertainties in the ECHAM atmosphere also lead to substantial differ-

ences of the Arctic Ocean circulation, its hydrography, and its water masses. In particular, the subsurface ECHAM Arctic Ocean is too warm by several °C. However, a strong near-surface halocline prevents this warm water from melting the sea ice from underneath. The halocline structure in the FNCEP run is much more similar with observed conditions, but weaker, and temperatures in the ocean interior are higher. This may lead to penetration of heat through the halocline to the ice bottom in the FNCEP run. However, not enough in-situ observations exist to evaluate the simulated ocean circulation comprehensively.

This study is the first examination of the ECHAM/MPI-OM model sea ice characteristics where in attempt to understand the causes for discrepancies between model and observations both atmosphere and ocean forcing are considered. We also for the first time compare simulated thickness of the sea ice against dataset that have reliable information about the thickness in the Arctic seas, were it play a crucial role during summer melting season. We show that not only the wrong SLP field but also lack of interannual atmospheric variability is an important cause for the difficulties in proper Arctic sea ice simulations.

We conclude that in order to improve the present-day simulations of the Arctic sea ice system, the ECHAM atmosphere needs to be improved over the Arctic in both its time-mean and time-varying components. Our findings are in line with conclusions drawn previously by Hunke and Holland (2007) who, from a comparison of the simulation of sea ice over the Arctic using three different atmospheric forcing datasets, also noted the fundamental impact of the atmospheric forcing on the thickness simulations as well as significantly different advection of heat and salt and ice-ocean stress. We identify here a quasi-permanent arctic atmospheric circulation as the primary reason for the deficits in the simulated sea ice parameters.

Causes for this artificial atmospheric circulation around the model's North Pole are unknown at this point and need a serious model improvement effort to remedy it. Also unknown is the cause for the lack of Arctic variability in the ECHAM model as well as the extent to which problems in the simulation of the summer sea ice jointly with the underestimation of atmospheric variability affect the quality of sea ice projections over the next century by the ECHAM model and needs further investigations. The same holds for the extensive warm bias in the simulated Arctic Ocean and its impact on climate projections, e.g., by melting sea ice from below.

Chapter 3

Adjoint-based sensitivities of the Arctic sea ice

3.1 Introduction

In the previous chapter we showed the importance of the proper atmospheric forcing for the sea ice simulations. The model forced by an NCEP atmosphere shows better results than the version of the model coupled with an atmospheric model. NCEP forcing is also not perfect for sea ice modeling (Makshtas et al., 2007), but using it with a regional model of the Arctic Ocean may help us to understand how the atmosphere over the Arctic affects sea ice development.

As has been shown previously, there are two main atmospheric variables that generally affect sea ice in the Arctic Ocean. One of them is the near surface atmospheric temperature (SAT), which affects sea ice thermodynamically through melting and freezing. Another is the wind field, which affects sea ice dynamically through redistribution of the thick and thin ice, opening and closing the leads and polynyas, and increasing and decreasing ridging of the ice. Interplay between these two atmospheric fields determines sea ice variability on decadal and interannual timescales. The main purpose of this chapter is to explore major patterns of possible atmospheric forcing influence on sea ice during the period 1980-2007 and to show whether these patterns change with time.

In our study we use adjoint sensitivities to explore the influence of SAT and wind on mean September Arctic sea ice area and volume for the period 1980-2007. This method allows us to see how the atmospheric forcing of the model influences sea ice parameters and how this influence evolves in time and space.

The structure of the remaining chapter is as follows: in Section 3.2 we describe present knowlege about atmosphere sea-ice interactions. In Section 3.3 we describe the model, the adjoint sensitivity analysis, and the experimental design. In Section 3.4 we compare the model results with available observations. In Section 3.5 we discuss the mean annual spatial and temporal variability of adjoint sensitivities for all simulated years and in Section 3.6 we will discuss the same for three different time

periods. Section 3.7 concentrates on time evolution of the sensitivities in different regions of the Arctic Ocean. Section 3.8 describes adjoint sensitivities on time scales longer than a year. Section 3.9 provides a discussion and concluding remarks.

3.2 Present knowlege

Harsh environmental conditions in the Arctic Ocean lead to very poor observational coverage. Only in the late 1970s with the beginning of the satellite era and the start of the Arctic Ocean Buoy Program (AOBP) have observations of the sea ice concentration (SIC), SAT, and sea level pressure (SLP) become dense enough to draw conclusions about the interaction of these three parameters.

Walsh et al. (1996) analyze SLP data from the Arctic Ocean Buoy Program for the period 1979-1994 and find increases in cyclonic circulation since the year 1988. They hypothesize that such an increase will make ice motion in the Arctic Ocean more divergent and lead to a reduction in the multiyear ice fraction and increase in the young thin ice fraction during winter. This hypothesis finds supporting evidences in later works.

Rigor et al. (2002) extend the period of analysis up to 1998 and propose the mechanism of the influence of the Arctic Oscillation (AO) on the Arctic sea ice movement, which in turn contributes to sea ice thickness and concentration changes and has an impact on surface atmospheric temperature. They determine two regimes of the sea ice motion in the Arctic Ocean. One is associated with a high phase of the AO index and characterized by a strong Beaufort Gyre and Transpolar Drift shifted towards the Atlantic. Another is associated with a low phase of the AO index and characterized by a weak Beaufort Gyre and Transpolar Drift shifted towards the center of the Arctic ocean. An increase in the AO leads to a cyclonic anomaly in the sea ice motion and increases its divergence. This causes a decrease in ice ridging and recirculation in the Beaufort Gyre and an increase in sea ice advection from the coasts of the Laptev and East Siberian seas, which lead to enhanced formation of young thin ice in areas of open water (polynyas and leads) during winter time. Both of these processes contribute to the sea ice thinning. Newly formed thin ice is more prone to summer melting, which in turn leads to a decrease in sea ice concentration in summer. Thin ice also more easily transfers heat from the ocean to the atmosphere, and the surface atmospheric temperature over the Arctic Ocean is increasing. Rigor et al. (2002) show that winter changes in sea ice motion have an effect on subsequent seasons: winter dynamical thinning of sea ice allows more heat to be released from the ocean during spring, which leads to a decrease in the summer sea ice concentration, delays the onset of autumn freezing, and lets even more heat leave the ocean during the cooling and freezing.

Changes in the influence of dynamical forcing on summer sea ice conditions through the year were estimated by Deser et al. (2000), who showed that for the period 1958-1996, spring (April-June) atmospheric circulation anomalies have considerable impact on summer sea ice changes. The southerly wind component drives

sea ice reduction in the East Siberian Sea and the northerly wind component is partly responsible for increased sea ice in the Barents and Kara seas. According to their analysis, late spring-early summer (April-June or July) atmospheric circulation anomalies have more impact on summer sea ice cover than those in high summer (June-August). The reason for such long delays between maximum sea ice response and atmospheric forcing might be a positive ice-albedo feedback.

Beside analysis of observational data, there have been several attempts to estimate the relative impact of thermodynamical and dynamical forces with the help of regional models. Zhang et al. (2000) use a coupled ice/mixed-layer-ocean model forced by the atmospheric conditions of 1979-96. They find significant differences in ice thickness distribution between periods of high (1989-1996) and low (1979-1988) AO. During high AO, ice in the eastern Arctic is thinner and less compact, while in the western Arctic it is thicker and more compact. According to the authors' sensitivity studies these differences are mainly a response to variability in the wind field patterns with a much smaller impact of thermodynamical factors. Dynamical and thermodynamical factors interplay with each other, establishing a negative feedback of ice growth to ice advection, reducing the sensitivity of ice thickness to dynamical perturbations. When advection of thicker sea ice from the western Arctic to the eastern Arctic decreases, it is compensated by increased ice formation in the eastern Arctic and decreased ice formation in the western Arctic.

Rothrock and Zhang (2005) use a regional model forced by NCEP reanalysis (1949-1999) to investigate causes for the thinning of the sea ice in the Arctic Ocean (excluding the Kara, Barents, Greenland, and Norwegian seas). They also try to separate the effects of wind and atmospheric temperature influence on the Arctic sea ice. The estimated variance in volume appears to be equally due to wind- and temperature-forced responses, but the temperature response has a smoother structure and gradually declines over the last 30 years. There was no dominating effect of one or another force found in association with extreme events. Both wind and atmospheric temperature may dominate extreme ice accumulation or retreat. Rising temperatures determine long-term downward trend with a reduction of 25% in sea ice volume over 5 decades, while winds cause large oscillations (for example in the late 1980s to mid-1990s) but not multidecadal downward trend.

Makshtas et al. (2003) use a dynamic-thermodynamic sea ice model with 50 km resolution to show that there is a correlation between thinning of the sea ice and a decrease in the concentration of ridged ice, which in turn correlates with cyclonic and anticyclonic regimes of the wind-driven ice motion in the Canadian Basin. The results of a zero-dimensional model simulation show very high sensitivity of ice to small changes in the summer air temperature, but only 20% of the decrease in sea ice can be attributed to those changes. The notion that increased sparsity of the sea ice increases its mobility is supported by the work of Rampal et al. (2009), who use data from the International Arctic Buoy Program for the period 1979-2007 to estimate the mean speed of sea ice transport in the Arctic Ocean. They found a substantial positive trend that was related to increased sea ice fracturing and lead opening rather than to the increased atmospheric forcing.

If we assume that cyclonic and anticyclonic wind circulation over the Arctic Ocean determine sea ice variability (Rigor et al., 2002), then a decrease in the AO index will increase sea ice thickness and extent. But after AO becomes close to neutral or negative, sea ice extent and thickness continue to decrease. According to Rigor and Wallace (2004), a transition to a sea ice thickness distribution dominated by young thin ice happened in 1989-1990, when the AO index was extremely high. During 1989-1995, the AO continued to be high, helping to reduce the amount of thick ice in the Arctic Ocean. The change in the AO to lower values after the year 1995 did not increase the presence of thick multiyear sea ice due to strong preconditions created during the period 1989-1995. Rigor and Wallace (2004) believe that in the case of low-index AO conditions of significantly long duration, summertime sea ice thickness and concentration can return to the higher values of the 1980s.

With the course of time, the data record becomes longer and the allocation of further periods in the atmospheric circulation becomes possible. Deser and Teng (2008) compare two different periods of the sea ice satellite record, one (1979-1993) associated with positive and the other (1993-2007) with negative trends in the "Northern Annular Mode" (NAM) (which includes both the NAO and the AO). During the summer of the first period, anomalous southerly winds cause negative SIC trends in the East Siberian, Chukchi, and Beaufort seas and anomalous northerly winds cause positive SIC trends in the Barents and Kara Seas. The connection between wind anomalies and trends in SIC is not that clear for the second part of the record, suggesting that other forces drive summer SIC trends during this period. Nevertheless, easterly rather than southerly wind anomalies are associated with negative SIC trends in the East Siberian and Beaufort seas.

Apart from pan-Arctic studies of atmospheric influence on sea ice there have been works that concentrate on the regional aspects of such influence. The ice edge area should be more sensitive to changes in atmospheric forcing due to the presence of thinner and less compact ice. Francis and Hunter (2006) estimate the impact of downward longwave flux (DLF), zonal and meridional winds (U,V), and temperature advection (ADV) on variability of the summer perennial ice edge in the Arctic seas. They integrate forcing fields backwards in time from zero to 80 days before the date of maximum ice retreat for every year from 1979 to 2004 and estimate the variance in maximum ice retreat anomalies attributable to anomalies in each forcing field. In all regions, DLF is found to be a dominant driver of the maximum ice retreat anomalies. In the Barents Sea, southerly (from the south) wind anomalies and ADV play a significant role in the forcing integrated backwards for 25 and 50 days before the date of maximum ice retreat. In the Kara Sea, a significant amount of variance is determined by southerly wind anomalies in the forcing integrated backwards for 80 days. Striking differences were found when the authors estimated the relative importance of forcings for the periods 1979-1991 and 1992-2004. During the first period, in the Barents Sea the dominant forcings were the DLF and southerly wind anomalies, while in the Chukchi Sea the dominant forcing was also southerly wind anomalies. During the second period, in the Barents Sea the dominant forcing became ADV, while in the Chukchi Sea it was DLF. Francis and Hunter (2006)

conclude that the continuous decline in ice extent despite the return of the AO to the near-neutral phase suggests that in the last years, anomalies in the surface energy balance have played a more important role than wind anomalies.

Francis and Hunter (2007) explore factors that affect winter (March) ice edge variability in the Barents and Bering seas, areas relatively free to respond to changing atmospheric and oceanic conditions, which account for much of the variability in hemispheric winter ice-cover. For the Barents Sea, the two main factors are found to be SST anomalies and southerly wind anomalies.

Drobot and Maslanik (2003) concentrate on only one region and examine the influence of winter and summer surface meteorological conditions on summer sea ice in the Beaufort Sea. During the winters that precede light summer ice conditions, atmospheric circulation favors an increase in ice advection from the west-central Arctic by Transpolar Drift and a decrease in ice transport into the Beaufort Sea due to a weaker Beaufort Gyre. Surface atmospheric temperatures are significantly warmer in the Bering Sea and significantly colder in the Barents Sea, but are estimated to be less important than wind for summer sea ice conditions. Summer winds during the years with light ice conditions have enhanced the easterly and southeasterly components in the Beaufort Sea, which transport ice away from it. Summer air temperatures seem to contribute to summer ice variability only in the southern portion of the Beaufort Sea. The authors also found a close linkage between atmospheric conditions that determine light and heavy ice summers and the AO/NAO index.

The trend in sea ice extent in the Arctic Ocean from the beginning of the satellite era in 1979 to 2006 was -3.4 $\pm$ 0.2% per decade (Comiso et al., 2008). The extreme sea ice concentration minimum in September 2007 made it even more negative. Such a fast retreat has attracted considerable attention from the scientific community and has led to many publications considering possible reasons for such an event. In the following we briefly describe key publications on this topic, since they represent attempts to investigate not decades of ice variability but one individual year, and try to look into the reasons that led to that particular September sea ice distribution. This approach is interesting for us since most of our further analysis will consider atmospheric conditions not more than one year before individual Septembers.

Thinning of the ice pack was considered by Maslanik et al. (2007a) as one of the main reasons for the substantial ice loss in 2007. Old ice melted during transport in the parts of the Beaufort Gyre close to the Alaskan and eastern Siberian coast, creating conditions for easier melting in the summer.

Kwok (2008) also found that SLP patterns during 2006 and 2007 according to satellite observations favored the export of sea ice from Pacific to Atlantic sectors of the Arctic Ocean. Zhang et al. (2008) came to similar conclusions on the basis of a PIOMAS model, naming thinner ice in the previous years, transport of sea ice from the Pacific sector to the Atlantic one, and positive ice-albedo feedback as main reasons for the extreme ice loss.

In other works, Maslanik et al. (2007c) and Stroeve et al. (2008) discuss unusual

clear skies formed due to the anticyclone that persisted for a long time over the central Arctic Ocean as one of the key factors that contributed to extreme sea ice conditions during September 2007. But Schweiger et al. (2008) show on the basis of the model study that "sunny skies" during the summer of 2007 did not contribute substantially to the sea ice extent anomaly. In contrast, Kay et al. (2008) conclude that reduced cloudiness was one of the contributing mechanisms for the 2007 event.

Comiso et al. (2008) compare satellite-derived maps of the sea ice concentration and temperature for 2007 and find a good correlation between positive temperature and negative sea ice concentration anomalies. However Schweiger et al. (2008) mention that it is not clear whether higher temperatures are the cause of or a response to the sea ice anomaly.

Perovich et al. (2008) show the results of the surface and bottom melt made from an autonomous ice mass balance buoy drifted in the area of the Beaufort Sea where the greatest ice loss occurred in 2007. There was a dramatic increase in the bottom melting, while the amount of surface melt was not significantly different compared to the earlier years. Observed heating of the upper ocean, with anomalies up to 5°C (Steele et al., 2008), was enough to cause this bottom melting. The authors believe that the ice albedo feedback mechanism was the key factor in the extreme 2007 sea ice loss, but it is still unclear how widespread this bottom melting was and what initially triggered the increase in the area of open water; it may have been the strengthening of the ice transport and transpolar drift, as mentioned by Zhang et al. (2008).

It is believed that solar radiation is not the only source of heat that might have increased the temperature in the upper ocean and stimulated the sea ice melt in 2007. The temperature in the Atlantic layer of the Arctic Ocean increased dramatically by up to 0.8°C in the beginning of the 2000s (Polyakov, 2005; Dmitrenko et al., 2008). This additional amount of heat might penetrate the halocline and reach the sea ice (Polyakov et al., 2007).

So there are several proposed reasons for the extreme 2007 September ice loss, but the degree to which each of them contributed to this event is unclear. On the decadal time scale, it seems that the wind field dominated the interannual variability and atmospheric temperatures responsible for the downward trend in sea ice thickness and extent. Important details of the mechanisms by which the atmosphere affects sea ice such as increased ice melting along ice edges and increases in thin ice fraction due to dynamical effects are more or less clear. But how these influences are distributed spatially and especially how they change through the year are still open questions that we would like to address in this research.

One of the possible instruments for conducting such research would be sensitivity analysis as carried out for example in Zhang et al. (2000), Rothrock and Zhang (2005), and Köberle and Gerdes (2003). They drive regional models by a multiyear mean seasonal cycle of surface temperature with interannually changed winds and then drive them with a repeating seasonal cycle of the wind with changing air temperature. This approach allows them to estimate the relative importance of each

force globally, but it is hard to estimate regional differences in dynamical and thermodynamical influence or to show their time evolution through the year. In our study we use adjoint-based sensitivities of Arctic sea ice to atmospheric forcing.

3.3 Methodology

3.3.1 MITgcm model setup

We use an Arctic Ocean setup based on the Massachusetts Institute of Technology general circulation model (MITgcm) (Marshall et al., 1997a,b). The ocean part of the model consists of conservation equations for horizontal and vertical momentum, volume, heat, and salt as well as an equation of state. A detailed description of the model is provided by Marshall et al. (2004). One of the key features of MITgcm is its capability for automatic generation of tangent linear and adjoint code, which permits sensitivity and optimization studies (Marotzke et al., 1999). In the following we will briefly describe the MITgcm sea ice model and its adjoint, the two parts that are most relevant for the present work.

The MITgcv sea ice model is based on the Hibler type (Hibler, 1979, 1980) viscous-plastic (VP) dynamic-thermodynamic sea ice model.

Ice thermodynamics

The thermodynamical part of the model is the so-called zero-layer formulation following the Appendix in Semtner (1976) with snow cover as in Zhang et al. (1998). The temperature profile in the ice is assumed to be linear with constant ice conductivity. Upward conductive heat flux is expressed as:

$$Q_c = \frac{K}{h}\left(T_{water} - T_0\right) \tag{3.1}$$

where K is the ice conductivity, h the ice thickness, and $(T_{water} - T_0)$ the difference between water and ice surface temperatures.

Such a formulation means that the sea ice does not store heat, and as a result the seasonal variability of sea ice is exaggerated. To reduce this effect we use parameterization of the sub-grid scale distribution of heat flux computations. The mean sea ice thickness in grid cell h is split into seven thickness categories H_h. These categories are equally distributed between $2h$ and a minimum sea ice thickness of 5 cm by

$$H_h = \frac{2n-1}{7}. \tag{3.2}$$

for $n \in [1, 7]$. The heat flux is computed separately for each category and then area-averaged to give the total heat flux (Hibler, 1984).

The oceanic heat flux from below balances the atmospheric heat flux and is proportional to the difference between the ocean surface temperature and the freezing point temperature of sea water:

$$Q_o = \rho c_p \left(T_{water} - T_{freezing}\right) \tag{3.3}$$

were ρ is the density, c_p is the heat capacity of sea water, and $T_{freezing}$ is the local freezing point temperature, which remains constant in our setup and equals -1.96 °C. Lateral and vertical growth of sea ice are parameterized according to Hibler (1979, 1980), and the so-called lead closing parameter has a value of 0.5 m.

There is a snow layer on the top of the ice, formulated according to Zhang et al. (1998), which changes heat flux and albedo. Snow modifies the effective conductivity in the following way:

$$\frac{K}{h} \rightarrow \frac{1}{\frac{h_s}{K_s} + \frac{h}{K}}, \tag{3.4}$$

where K_s is the conductivity of snow and h_s the snow thickness. Snow flooding due to ice submerging is not considered in our setup.

Effective ice thickness (ice volume per unit area, $c \cdot h$), concentration c, and effective snow thickness ($c \cdot h_s$) are advected by ice velocities:

$$\frac{\partial X}{\partial t} = -\nabla \cdot (\vec{\mathbf{u}}\, X) + \Gamma_X + D_X \tag{3.5}$$

where Γ_X are the thermodynamic source terms and D_X the diffusive terms for quantities $X = (c \cdot h), c, (c \cdot h_s)$.

Advection schemes are multidimensional second- and third-order advection schemes with flux limiters (Roe, 1985; Hundsdorfer and Trompert, 1994).

Ice dynamics

The evolution of the sea ice drift is determined from the momentum balance, which includes air and water stress, Coriolis force, internal ice stress, and ocean tilt in the form:

$$m\frac{D\vec{\mathbf{u}}}{Dt} = \vec{\tau}_{air} + \vec{\tau}_{ocean} - mf\vec{\mathbf{k}} \times \vec{\mathbf{u}} + \vec{\mathbf{F}} - mg\nabla\phi(0), \tag{3.6}$$

where m is the sum of ice and snow mass per unit area; $\vec{\mathbf{u}} = u\vec{\mathbf{i}} + v\vec{\mathbf{j}}$ is the two-dimensional ice velocity vector; $\vec{\mathbf{i}}$, $\vec{\mathbf{j}}$, and $\vec{\mathbf{k}}$ are unit vectors in the x, y, and z directions, respectively; $\vec{\tau}_{air}$ and $\vec{\tau}_{ocean}$ are forces due to air and wind stress, respectively; f is the Coriolis parameter; $\vec{\mathbf{F}} = \nabla \cdot \sigma$ is the divergence of the internal ice stress tensor σ_{ij}; g is the gravity acceleration; and $\nabla\phi(0)$ is the gradient (or tilt) of the sea surface height, where $\phi(0) = g\eta + p_a/\rho_0 + mg/\rho_0$ is the sea surface height potential in response to ocean dynamics ($g\eta$) due to atmospheric pressure loading (p_a/ρ_0, where ρ_0 is a reference density) and a term due to snow and ice loading (Campin et al., 2008).

There are several approaches to treat the sea ice interactions available in the MITgcm, but we keep to the default viscous-plastic (VP) rheology scheme of Hibler (1979) with an extended line successive over-relaxation (LSOR) method (Zhang and Hibler, 1997). VP rheology allows compressive and shear deformations in the sea ice, but also has no resistance to the divergence in the ice drift, so there are no problems with opening leads in the ice. For very small strain rates, for example in a relatively motionless situation, ice shows viscous behavior, while for bigger strain rates ice behaves like a plastic material. The bulk and shear viscosities as well as ice pressure depend non-linearly on both ice thickness and compactness (concentration). A detailed description of the rheology scheme in the MITgcm is given by Marshall et al. (2004), and a comparison of different rheology schemes in MITgcm is performed by Losch et al. (submitted to Ocean Modelling).

3.3.2 Adjoint calculation of sensitivities

Often we would like to know how sensitive some measure constructed from the model solution (e.g. mean monthly sea ice area, mean daily atmospheric temperature over some region) is to input variables (e.g. initial conditions, forcing fields). There are generally two main approaches in geophysics to answer this question: classical sensitivity analysis and adjoint sensitivity analysis. Errico (1997) gives a good description of the differences between the two, and we will follow his explanation.

Let us consider a numerical model M that takes some input a and produces an output $b = M(a)$. From output b we can construct our measure $J = J(b)$, which might be the mean September sea ice area calculated from daily sea ice area fields. To understand how sensitive J is to changes in a, for example, a wind field, in classical sensitivity analysis one has to perturb a and apply model M to it again, resulting in perturbed output $b_{pert} = M(a_{pert})$, and to calculate $J_{pert} = J(b_{pert})$; then $\Delta J = J_{pert} - J$ will be the sensitivity of J to the perturbation in a. The problem with this approach is what we get as ΔJ is the impact of one particular perturbation ($\Delta a = a_{pert} - a$) on J. Another perturbation, although very close to the first perturbation, might lead to a considerably different ΔJ. In order to answer the question of how sensitive J is to changes of a in, say, some particular place, one should examine an ensemble of perturbations.

In essence the adjoint method allows us to obtain derivatives of $\frac{\partial J}{\partial a}$ for every grid point and every timestep in such a way that we can estimate the impact of any (sufficiently small) perturbation on J by simply multiplying the perturbation by the gradient. The adjoint calculation of J sensitivities can be performed with respect to a multiple number of input variables at once, so compared to classical sensitivity analysis it is more efficient in terms of computer time. Another remarkable feature of adjoint sensitivities is their ability to track down the influences that come from remote places or distant times relatively easily. This can help to discover some teleconnections or processes that were previously unexplored.

To obtain the gradient of the cost function by using the adjoint method, first we have to construct a tangent linear version of the initial model. To do so one

can decompose the model code to elementary mathematical functions (+, -, sin), get the derivatives of these functions, and then, following the chain rule, construct the derivatives of the initial model functions. Information obtained during the non-linear forward run is used for the adjoint run, where the adjoint of the tangent linear model is integrated backwards in time. The resulting gradients show the sensitivity of the cost function with respect to the input.

The code for the tangent linear and adjoint models is automatically generated by the Transformation of Algorithms in Fortran (TAF) source-to-source translator (Giering and Kaminski, 1998; Giering et al., 2005). MITgcm is adapted for use with the TAF and the description of the MITgcm adjoint construction together with its first application for the sensitivity studies has been published by Marotzke et al. (1999). Later MITgcm adjoint were successfully applied for ocean state estimation (e.g. Stammer et al. (2002); Köhl and Stammer (2008)) as well as for sensitivity studies (e.g Köhl and Stammer (2004); Stammer et al. (2008)).

3.3.3 Experimental design

The model domain covers most of the Arctic Ocean (except for the small part of the Laptev Sea) and most of the GIN Sea (Fig. 3.1). It has 130 × 102 grid points and 25 vertical levels. The resulting horizontal resolution is 40 km. The model is solved on an Arakawa C grid with a time step of 30 min. We will refer to this setup as MITarc40.

The setup is initialized with the Polar Science Center Hydrographic Climatology (PHC 3.0, (Steele et al., 2001)) annual mean temperature and salinity fields. The forcing fields are fluxes of momentum, heat, and freshwater, computed using bulk formulae from daily NCEP-RA1 reanalysis (Kalnay et al., 1996). All lateral boundaries of the model are closed. The sea surface temperature of the model is relaxed to the monthly Extended Reconstruction SST version 2 (ERSST.v3) database (Smith et al., 2008) and sea surface salinity is relaxed to WOA2005 monthly climatology (Boyer et al., 2005).

Model runs performed to obtain adjoint sensitivities schematically are presented in Fig. 3.2. To simulate September sea ice characteristics for a particular year (Y_{target}), first the four-year spin-up is performed. It starts at 1 October, five years before the "target year" ($Y_{target} - 5$) from the zero sea ice conditions and PHC 3.0 climatology. Due to the closed boundaries of the setup, a longer spin-up might cause an unrealistic ocean simulation that, in turn, can affect the sea ice. The forward run of the model starts at 1 October of the year prior to the "target year" ($Y_{target} - 1$) and ends at the end of September of the "target year".

This procedure is repeated for every year from 1980 to 2007. Then an adjoint run is performed backward in time from 1 October of the "target Year" to 1 October of the previous year, producing one year of cost function adjoint sensitivities. We choose two cost functions: mean September sea ice area (AREA in the following) and mean September sea ice volume (VOLUME in the following). For each cost function, runs were performed separately. The adjoint model generates adjoint sensitivities

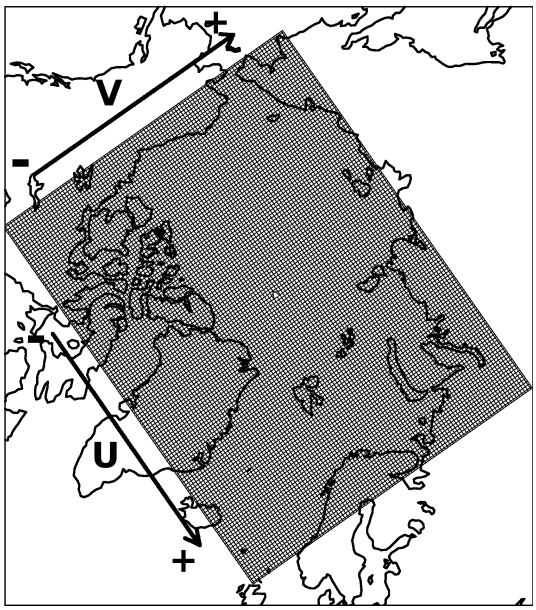

Figure 3.1— Model grid and directions of model U and V wind components.

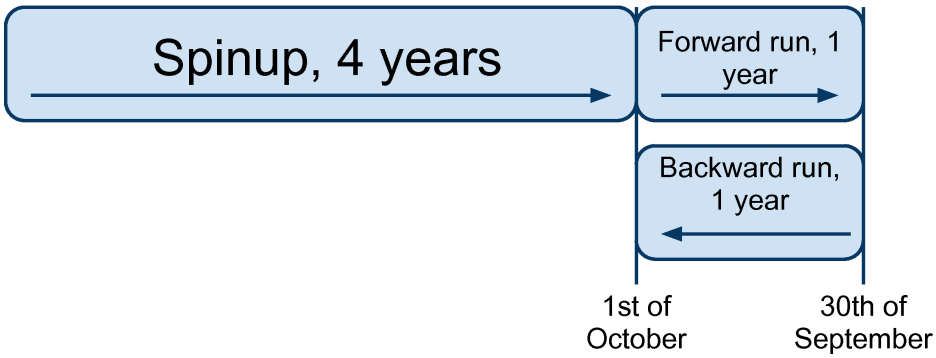

Figure 3.2— Schematic representation of model runs for each year performed from 1980 to 2007.

of the cost function to the following parameters: surface atmospheric temperature (SAT) (referred to in figures as "adxx_atemp"), zonal near surface wind (referred to in figures as "adxx_uwind"), meridional near surface wind (referred to in figures as "adxx_vwind"), near surface specific humidity, and precipitation. We will consider only the first three.

3.4 Comparison of satellite and simulated SIC

Here we evaluate monthly fields of SIC simulated during the forward run initialized from a four-year spin-up.

Figure 3.3 shows total September sea ice extent in the Arctic Ocean from satellite data and as simulated by MITarc40. The model produced more ice in September almost every year except for the very beginning of the data set where it was close to the observations. Overall variability is reproduced in the model. Both satellite and MITarc40 time series show an increased downward trend in sea ice extent since the end of the 1990s. Years with increasing and decreasing sea ice extent generally coincide. The correlation coefficient between datasets is 0.9.

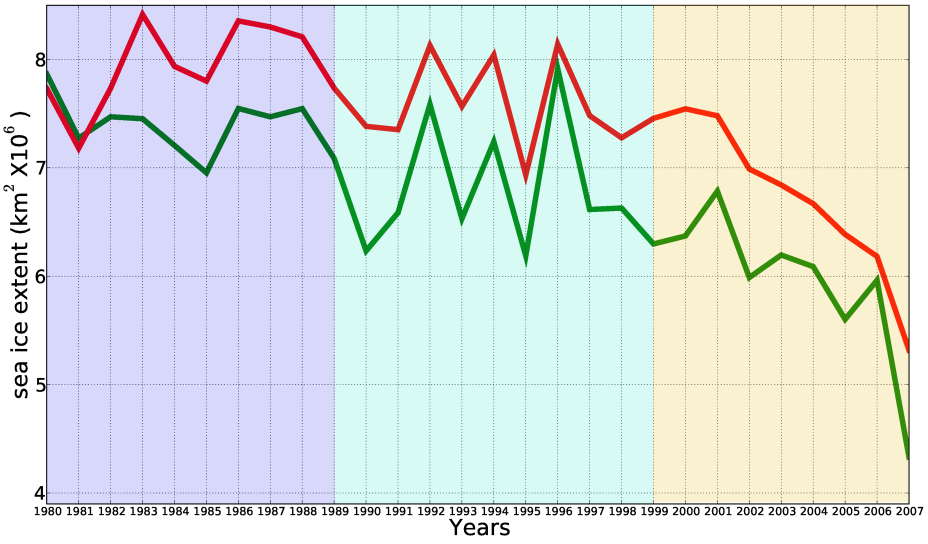

Figure 3.3— Total September SIE in the Arctic Ocean. Green: satellite data from GSFC dataset; red: simulated by MITarc40. Background colors denote three periods that were chosen for the analysis in Section 3.6.

To show how well MITarc40 captures the spatial distribution of sea ice extent (SIE) during the years with different sea ice conditions, we choose three years that according to satellite observations differ in their total September SIE relative to the previous year (see Fig. 3.3). In the year 1988, total September SIE changed very slightly compared to 1987. In 1996 there was a very strong increase in September SIE compared to 1995. In 2007, conversely, there was a significant decrease in September SIE compared to 2006.

In Fig. 3.4, March SIC is shown for these three years. The interior of the Arctic Ocean and all shelf seas, in both satellite data and model simulations, are

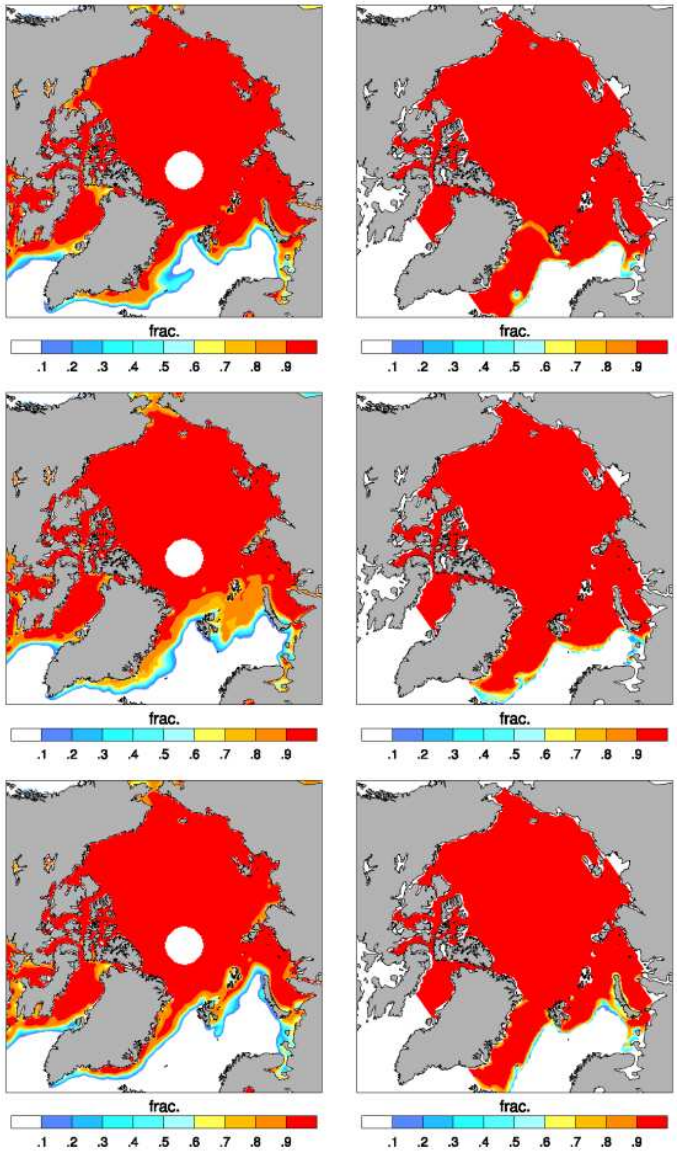

Figure 3.4— March sea ice concentration. Left: GSFC, right: MITgcm. Top row: 1988; middle row: 1996; bottom row: 2007.

covered by SIC of more than 0.9 frac. The differences emerge in the Barents and Greenland seas, where the model tends to overestimate SIC for all three years. A notable feature is the build-up of ice at the southern edge of the model domain. The model's boundaries are closed, and ice, exported from the Arctic Ocean along the Greenland coast, builds up at the model domain edge. Nevertheless the model

represents relative changes in SIC reasonably well in that years with relatively bigger SIC according to GSFC data also have larger SIC in the model simulations and vice versa. A good example of this is a situation in the Barents Sea, where in the year 2007 sea ice concentration was minimal out of three years according to GSFC. The model also demonstrates a minimum of the SIC in the Barents Sea out of the three years in 2007.

In Fig. 3.5, September SIC for three years is shown. Generally SIC in the model is higher than in the GSFC data, especially in the Canadian Archipelago and Baffin Bay. The spatial structure of SIC in GSFC data is more inhomogeneous than in the model, with uneven distribution of areas with different SIC values. But general features of the ice edge are captured well everywhere in the Arctic basin except for the East Siberian Sea, where the SIC is too high. For the year 2007, simulated sea ice occupies a much bigger area than in GSFC data, but the general shape of the ice edge and spatial distribution of the SIC inside the ice field of the model are still sufficiently close to the GSFC data.

Maps of the 1980-2007 mean SIC for March and September (Fig. 3.6) summarize the difficulties of the model in simulating sea ice conditions. For March there is too much ice in the Barents and Greenland seas and ice build-up near Greenland. For September there is too much ice in the Canadian Archipelago, Baffin Bay, and Arctic shelf seas, especially in the East Siberian Sea.

Despite some differences between GSFC data and model results, the latter reflects observed SIC quite well for winter and in summer months. The degree of resemblance between GSFC and simulated data allows us to use our model setup to reveal the main factors affecting the SIC distribution in September with the hope that they will represent the situation in the real world.

Fig. 3.7 represents the seasonal cycle of SIE averaged over 1980-2007. The zigzag shape of the graph for the satellite data is related to the fact that before July 1987, satellite data were collected for every other day. The model sea ice minimum is shifted towards August by about half a month. This is a common problem of models with zero-layer sea ice thermodynamics (Semtner, 1984). Since our cost functions are the mean area and volume for September, sensitivities will represent not only the possible influence of melting but also to some extent freezing processes, especially sensitivities in September itself; this should be remembered during interpretation of the data.

There are only few estimates of climatological mean sea ice thickness (SIT) distribution for the whole Arctic Ocean and we will compare our simulation with data from Romanov (1995). For extensive discussion of these data, refer to Chapter 2.

For April, the overall structure of the spatial SIT distribution is captured well by the model. Ice is thick to the north of Greenland and becomes thinner towards the ice edges. The model shows thinner sea ice in the central basin of the Arctic Ocean, especially in its Eastern part, and SIT distributed unevenly, with multiple regions of thicker ice inside the areas of thinner ice. To the north of Alaska, SIT is underestimated, in the Chukchi sea SIT it is 240-180 cm instead of 180-120 cm, and

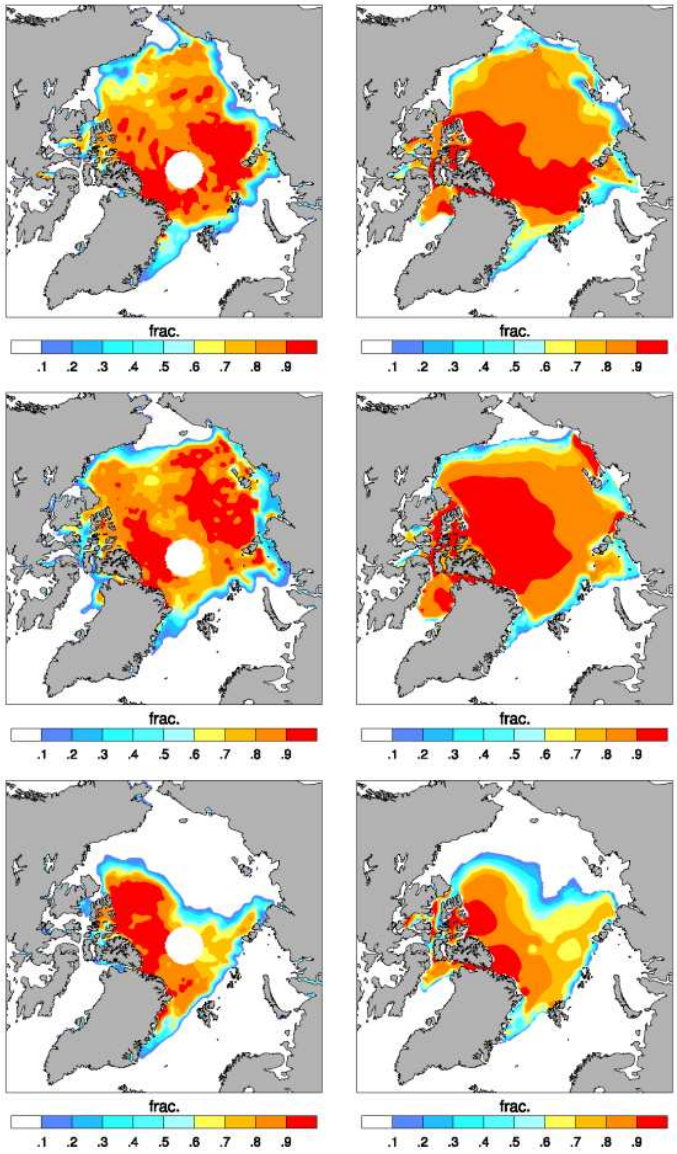

Figure 3.5— September sea ice concentration. Left: GSFC; right: MITgcm. Top row: 1988; middle row: 1996; bottom row: 2007.

in the East Siberian sea an isoline of 240 cm SIT goes to close to the shore in the western part, but in the eastern part values are close to observations (240-180 cm). In the Laptev Sea, thickness is overestimated, showing values of 180-240 cm when they should be less than 120-180 cm. In most parts of the Kara Sea, the model captures SIT nicely, and in the Barents Sea the model produces slightly thinner ice

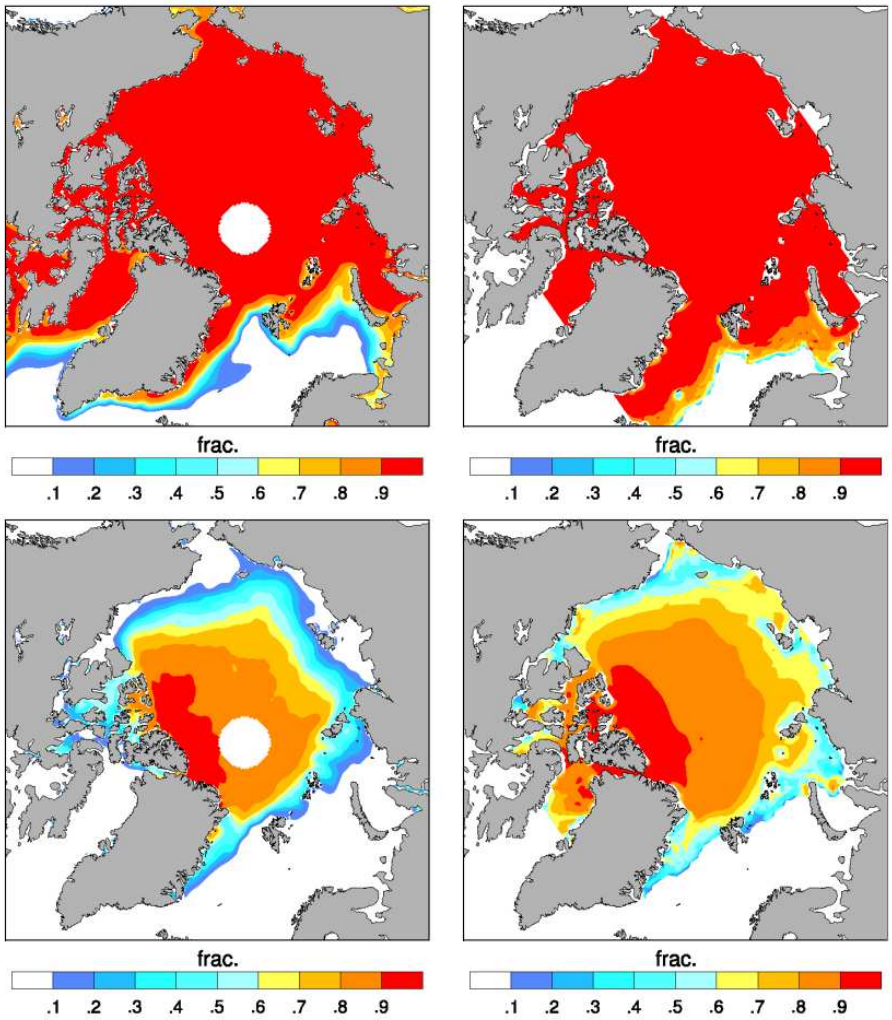

Figure 3.6— Mean sea ice concentration. Left: GSFC; right: MITgcm. Top panel: March; bottom panel: September.

with extended sea ice coverage.

In August-September, SIT in the model is distributed more evenly with thicker ice to the north of Greenland and thinner ice in the shelf seas. Similarly to April, SIT is underestimated in the central part of the Arctic Ocean and especially in the Eastern part. A tongue of ice thicker than 180 cm extends from the Beaufort Sea towards the East Siberian Sea. Values of 120-180 cm are close to the observations to the north of Alaska, while in the Chukchi Sea, the ice is thicker, showing values of 180-120 cm instead of 0-70 cm. Both isolines of 120 cm and 180 cm SIT go too far

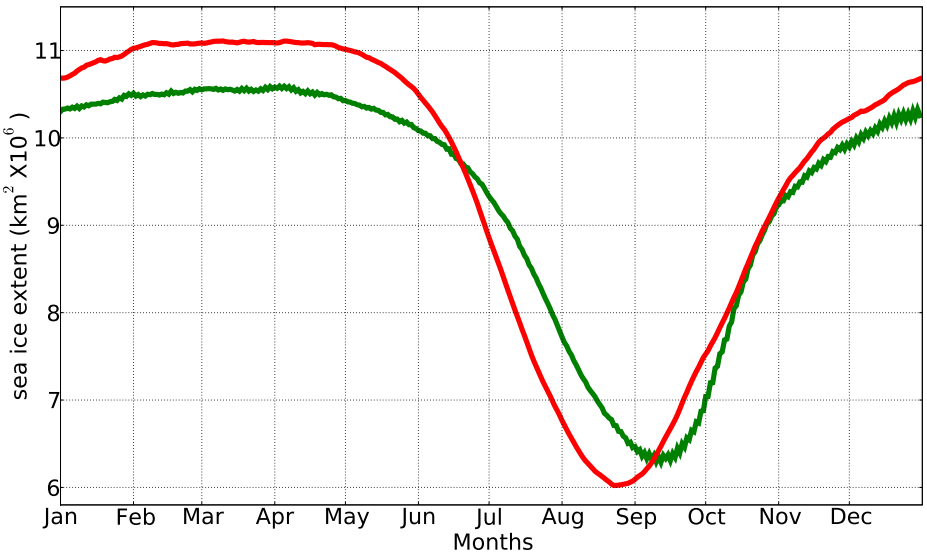

Figure 3.7— Mean seasonal cycle of Arctic SIE for 1980-2007.Green: satellite data; red: MITarc40 simulation.

into the East Siberian sea and the model shows hardly any ice, with SIT less than 120 cm along the coast where, according to observations, the ice should be less than 70 cm thick. Ice with a thickness of around 70-120 cm occupies most of the eastern part of the Laptev Sea, where only young 0-70 cm thick ice should be observed. In the eastern part of the Kara Sea, ice with a thickness of 70-120 cm extends too far to the west and then due to the expanded ice edge, ice with thicknesses of 30-70 cm is observed in the western part of the Kara Sea where there should not be ice at all. The position of the ice edge in the Barents Sea is also shifted to the south and slightly thicker values of SIT can be observed there.

Despite the fact that SIT is mostly underestimated in the central Arctic Ocean and to the north of Greenland and mostly overestimated along the ice edges in the Arctic shelf seas, we think that overall representation of SIT spatial distribution in the MITarc40 is satisfactory. Differences between the model and Romanov (1995) do not usually exceed 50 cm. The data on which the Atlas of Romanov (1995) is based were collected during the 1970s and 1980s when ice in the central Arctic Ocean was considerably thicker. Kwok and Rothrock (2009) showed on the basis of submarine and ICESat SIT measurements that in the central Arctic Ocean the average thickness at the end of the melt season has decreased by 1.6 m in over 40 years. This decrease might account for the differences in SIT between Romanov (1995) and MITarc40. On the other hand Polyakov et al. (2003) do not find a statistically significant trend in the ice thickness of fast ice along the Russian coast

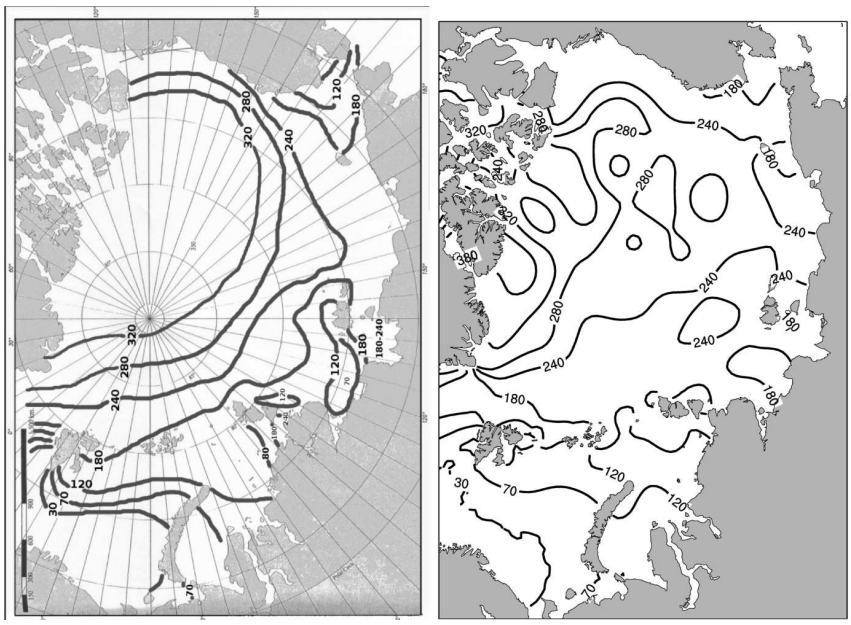

Figure 3.8— Mean sea ice thickness for April. Left: according to Romanov (1995); right: as simulated by MITarc40.

for the period from 1936 to 2000. Therefore SIT differences between the model and observations are more reliable along the Russian coast.

3.5 Spatial variability of mean adjoint sensitivities

In the following we describe spatial and temporal variability of AREA (mean September sea ice area) and VOLUME (mean September sea ice volume) adjoint sensitivities to atmospheric forcing. During the analysis we will consider only the years when sensitivities most of the time over most of the area do not exceed three standard deviations from the mean of all 28 years. This is done to exclude very high sensitivity values that originate from the instabilities in the linearized model, when very small changes in the parameters may lead to a sizable response over the big area and time span. These kinds of sensitivities are found to be not useful in estimating climate sensitivities (Lea et al., 2000). Our task here is to explore general patterns in sensitivity distribution, and such extreme behavior of sensitivities distorts the mean signal considerably. Consequently the years 1986, 1989, 1998, 2000, and 2003 were excluded from the analysis, and all averages in the following will not consider values from these years. We will also not consider Baffin Bay in our analysis since most of the time extremely high sensitivity values are observed in this area.

Figure 3.10 shows monthly means of AREA sensitivities to SAT from April to September. We demonstrate only negative values of this type of sensitivity, since

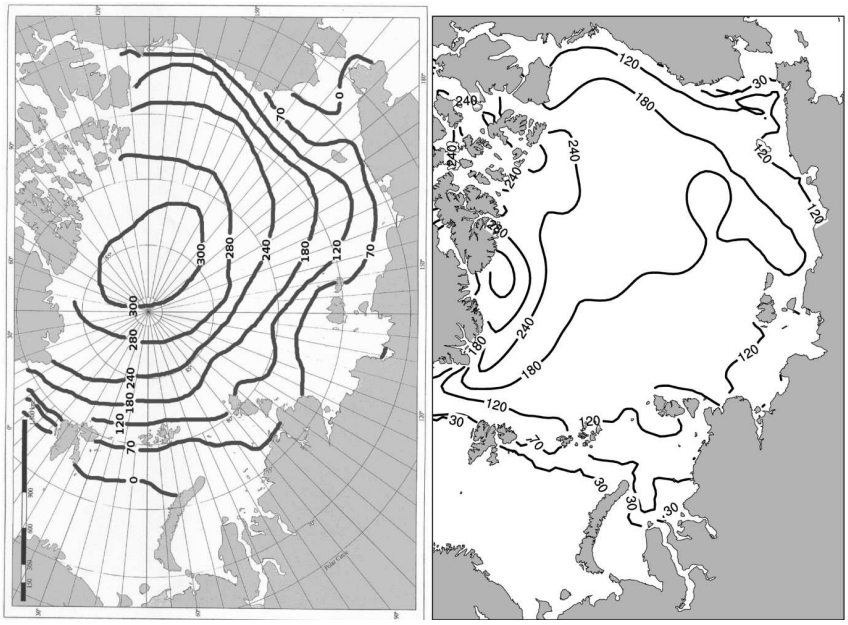

Figure 3.9— Mean sea ice thickness for August-September. Left: according to Romanov (1995); right: as simulated by MITarc40.

positive values are very rare. Maps of the sensitivities for October-March look much the same as the one for the April, demonstrating low sensitivities over the larger part of the Arctic Ocean. Stronger sensitivities start to evolve in May and reach their maximum in June. Especially high values are located close to the future ice edge, in the East Siberian Sea, Laptev Sea, eastern part of the Kara Sea, and northern part of the Barents Sea as well as in the coastal part of the Beaufort Sea. Comparatively weaker sensitivities are located to the north of the Greenland and Canadian Archipelago. Most of the central part of the Arctic Ocean is covered by the sensitivities with values from -0.5 to -1.5 $km^2/°C$. The strength of the sensitivities declines in August and even more in September, suggesting that a higher impact of SAT on AREA happens in June-July.

Temporal evolution of VOLUME sensitivities to SAT (Fig. 3.11) is also characterized by weak sensitivities during April and March, sudden strengthening in June, and gradual decline in July-August towards weak values in September. But the spatial distribution is different compared to the AREA sensitivities. Stronger values are located all over the central Arctic Ocean, while over the ice edges sensitivities are weaker. In June there are several areas with especially strong sensitivities located to the north of Spitsbergen, in the eastern part of the Kara Sea, and in the northern Laptev Sea. All of them except for the one in the Kara Sea continue to express comparatively stronger values during July, when sensitivities generally become weaker. In August all of the Arctic Ocean is dominated by uniformly distributed

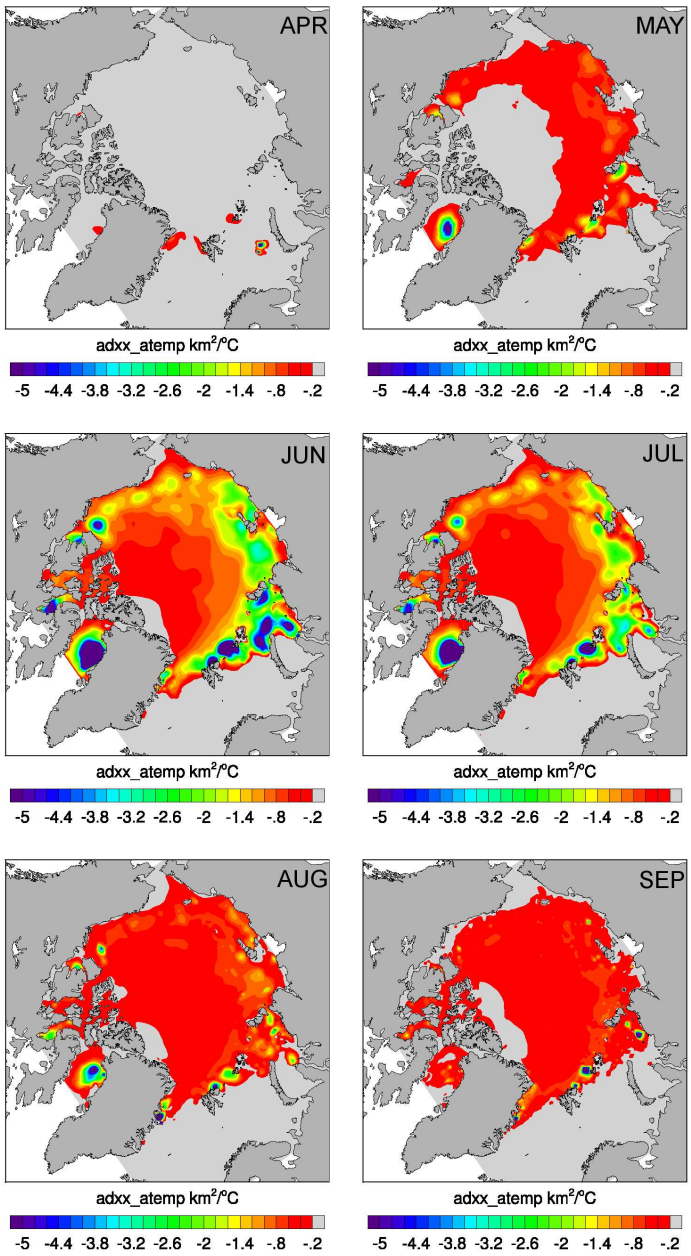

Figure 3.10— Monthly means of September mean sea ice AREA sensitivities to SAT. Top: April, May; middle: June, July; bottom: August, September.

weak sensitivities.

Stronger AREA sensitivities to SAT were observed in the regions where ice is thin and more prone to the summer melting. Melting of the thin ice may have an

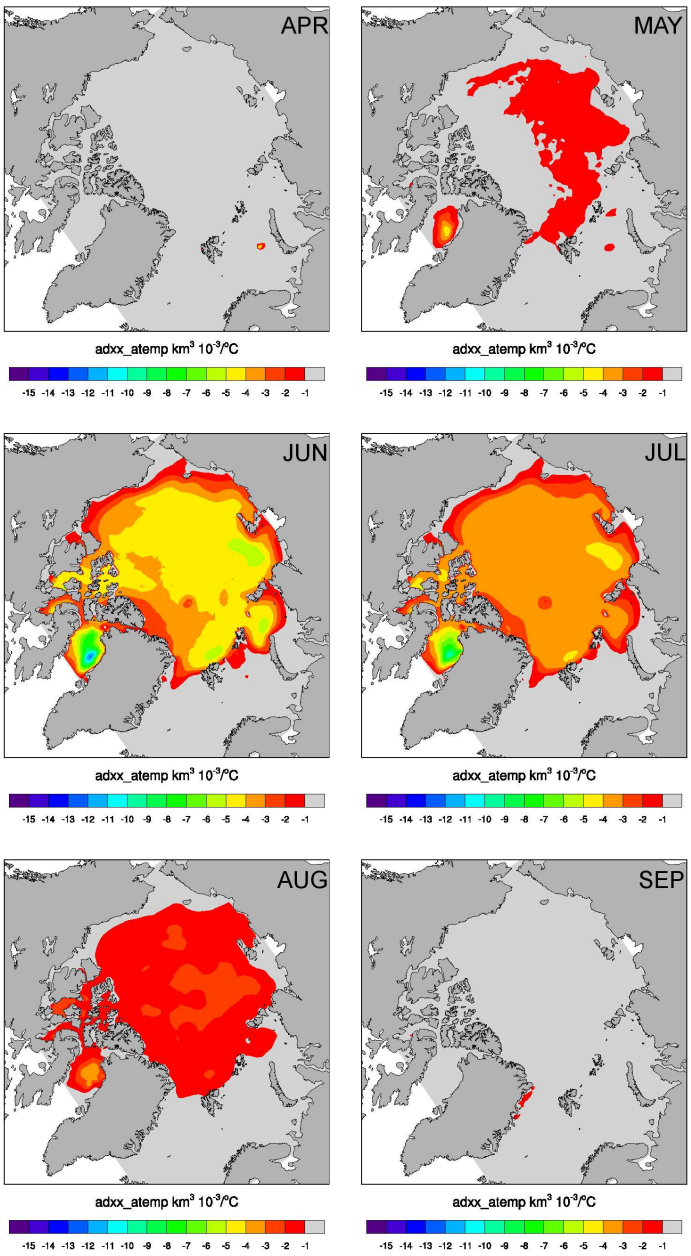

Figure 3.11— Monthly means of September mean sea ice VOLUME sensitivities to air temperature. Top: April, May; middle: June, July; bottom: August, September.

immediate impact on the total ice area, while in the case of thicker ice, intensive melting may just reduce the sea ice thickness, but not remove it completely, leaving the sea ice area at the same level. This, though, will have an effect on the sea ice

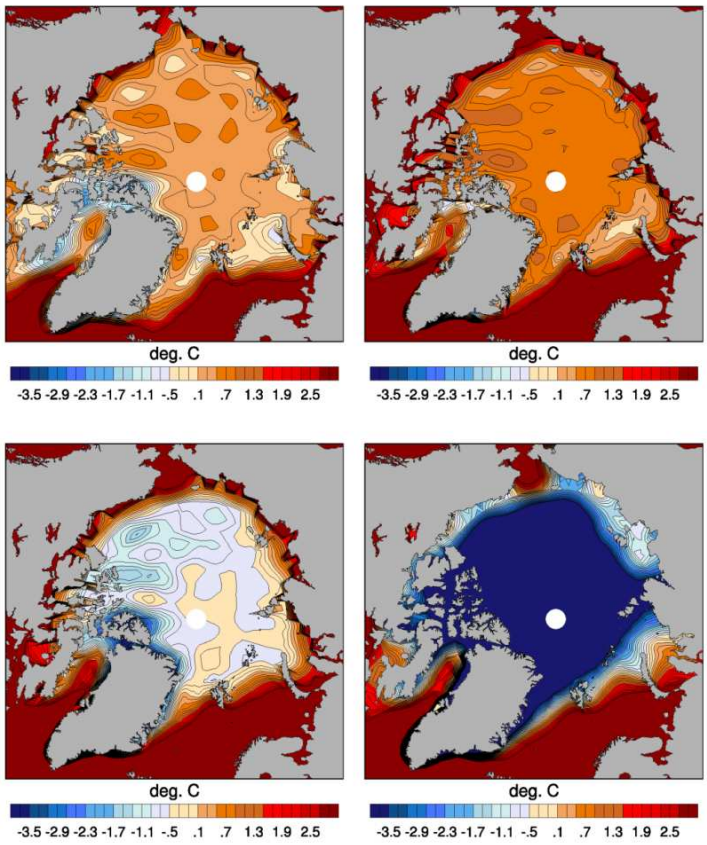

Figure 3.12— Monthly means of 2 m SAT for the period 1980-2007. Top: June, July; bottom: August, September.

volume. Sensitivities of the VOLUME to SAT are weak to the north of Greenland, a region with thick ice and high sea ice concentration, since it is harder to melt thick ice (the conductivity of ice is inversely proportional to its thickness). In the areas close to the ice edge, the sea ice is thin, but the sea ice concentration is low, so the sensitivities are weak as well. Regions of relatively strong sensitivities in the Kara and the Laptev seas are associated with both relatively high sea ice concentrations and thin ice. Thin ice can be melted more easily and high concentrations provide higher impact on the resulting VOLUME.

It is interesting that the stronger AREA sensitivities to SAT in June were located over the areas where the ice will have a concentration of about 0.7-0.8 in September. This might be related to the fact that ice located closer to the shore will melt anyway under any realistic temperature conditions, and indicates the importance of the early stage of the melting season, when the "cores" of the melting are formed. These might be areas of open water that have small albedo, take up heat very quickly, and help to

melt the ice around, increasing the area of open water even more (positive ice-albedo feedback).

Figure 3.12 shows monthly means of SAT distribution for June-September. The color scale is limited to a range from -3.5 to 3°C. This allows us to emphasize the details of SAT distribution over the sea-ice-covered regions during the summer months. Temperatures over the Arctic Ocean in July are higher than in June, while sensitivities to air temperature of both AREA and VOLUME are conversely stronger in June. This may lead to an equal impact of the surface atmospheric temperature on AREA and VOLUME during June and July. Comparisons between fields of air temperature and AREA and VOLUME sensitivities do not allow us to clearly separate any region where the impact of the air temperature is considerably larger due to a combination of strong sensitivities and higher temperatures.

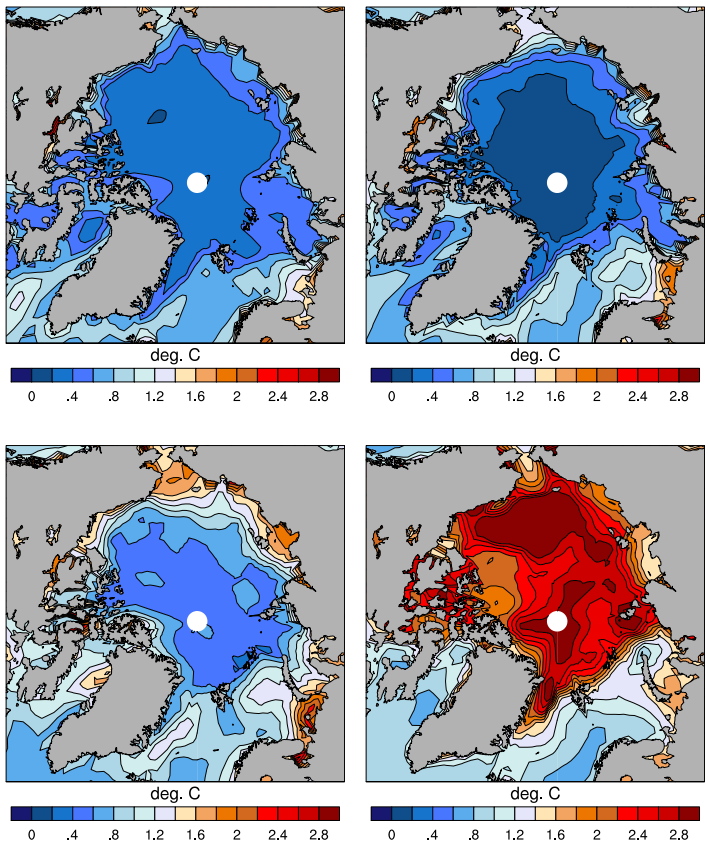

Figure 3.13— STD of SAT monthly mean for the period 1980-2007. Top: June, July; bottom: August, September.

The standard deviation of monthly mean SAT during June, July, and August is relatively small (Fig. 3.13). This is due to the fact that SAT over the sea ice during

the summer months oscillates slightly around 0°C until all snow and ice have melted (Rigor et al., 2000). Since interannual changes in the SAT are small, temperature forcing over the sensitivities during June and July is close to the constant on the interannual scale, making it very unlikely that a situation will occur in which, for example, in one year SAT over the area with strong sensitivities is high, and in another year it is low, determining the differences in AREA of VOLUME between this two years. Taking into account the small variability of the monthly mean SAT we believe that on the monthly time-scale most probable candidates for the main parameters that control sea ice variability related to thermodynamical reasons are SIT and SIC. We will take a closer look at the relations of these parameters and sensitivities in the next section, where a comparison of different time periods will be performed.

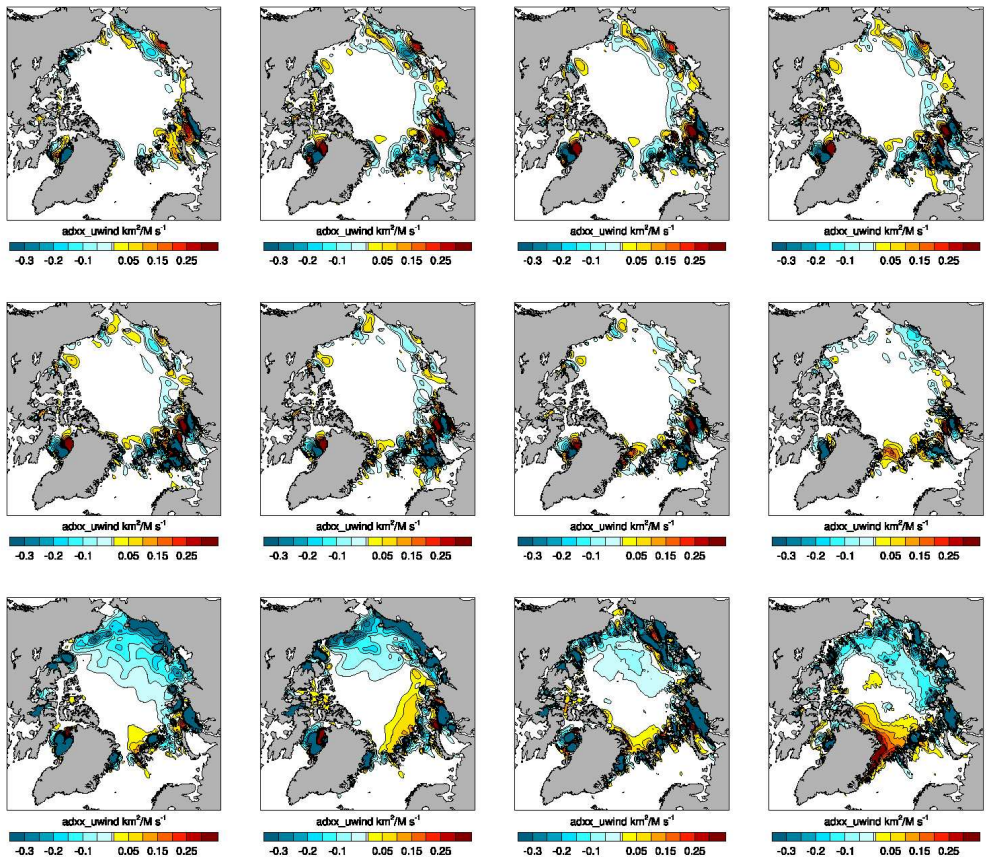

Figure 3.14— Monthly means of AREA sensitivities to U wind component. Top: October, November, December, January; middle: February, March, April, May; bottom: June, July, August, September.

Figure 3.14 shows monthly means of AREA sensitivities to the U component of the wind. Note that the direction of the wind components differs from the usual geographical direction and is shown in Fig. 3.1. During autumn, winter, and spring, high sensitivities located along the coastal areas, especially in the East Siberian and Laptev Seas, mostly have negative signs. A very complicated situation is found in the eastern part of the Kara Sea and in the Barents Sea, where very strong positive and negative sensitivities form several bipolar structures. In October to May, general weakening of the sensitivities is observed over the whole Arctic Ocean, with a sudden increase in June, probably associated with the beginning of the ice melting. In June, negative sensitivities to U wind are dominant with stronger negative values over the Eurasian part of the Arctic Ocean and north of Alaska. In July considerable positive sensitivities appear as a narrow zone over the shelf break to the north of the Barents, Kara, and Laptev seas. During the next month, August, this zone becomes smaller and shifted towards the north of Greenland, while in the Siberian shelf seas to the north of Alaska and over large parts of the central Arctic Ocean, negative sensitivities are still dominant. During September, positive sensitivities strengthen and expand more to the north and to the west of Greenland, while negative sensitivities also become stronger and occupy a larger area in the central Arctic Ocean.

The sensitivity of VOLUME to the U wind component (Fig. 3.15) shows much weaker values in October-May than in June-September. During October-May positive and negative values are located close to the coastal areas, especially in the Chukchi and the East Siberian seas, the eastern part of the Kara Sea, and north of the Barents Sea. In April there is a minimum in sensitivities' areal coverage and strength. In June negative sensitivities occupy most of the central Arctic Ocean and shelf seas, except for the small zone of positive values to the north of Greenland. This zone disappears in July and negative sensitivities dominate over almost the whole Arctic Ocean. Later, in August, the strength of the sensitivities weakens, with negative sensitivities staying mostly in the Amerasian Basin and weaker positive sensitivities in the Eurasian Basin. During September, small negative sensitivities are left only in the Beaufort, the East Siberian, and the Laptev Seas, when small positive sensitivities are located along the eastern coast of the Greenland, to the north of the Spitsbergen, and around Franz Josef Land.

Both sensitivities of AREA and VOLUME to U wind component express some, mostly weak, positive and negative values during the winter period near the coast of the Siberian shelf seas that reach a minimum in April and come back to some degree as negative sensitivities in the East Siberian Sea during May. Several studies (e.g. Rigor et al. (2002); Deser et al. (2000)) suggest that winter atmospheric circulation creates sea ice preconditions that are important for the consecutive September. In our experiments, during October-May we only see sensitivities in some coastal areas and they are not very strong, meaning that the effect of winter circulation is probably much smaller than the effects of atmospheric circulation during June-September.

Mostly negative sensitivities to the U wind component dominate over the basin for AREA and VOLUME. Positive values occupy a much smaller area located to the north of Greenland and the Barents and Kara seas.

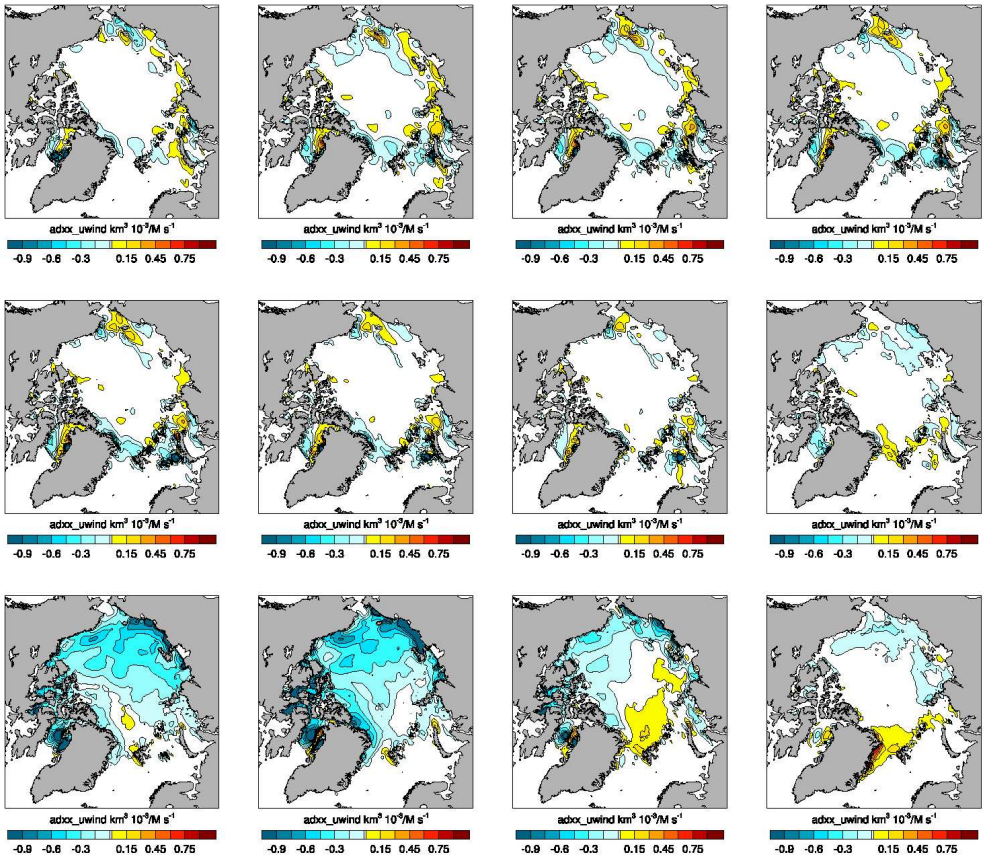

Figure 3.15— Monthly means of VOLUME sensitivities to U wind component. Top: October, November, December, January; middle: February, March April, May bottom: June, July, August, September.

Figure 3.16 shows monthly means of AREA sensitivities to the V wind component. In contrast to sensitivities to the U component, strong values are observed in all shelf seas, including the Beaufort Sea. In October through May, sensitivities become weaker with a minimum in May. In June strong negative sensitivities located close to the shore and weaker positive sensitivities are more characteristic for the central Arctic Ocean. During July, the spatial distribution of sensitivities generally stays the same, but they are getting stronger. In August and especially in September, negative sensitivities occupy the western part of the Arctic Ocean and strong positive sensitivities the eastern part of the Arctic Ocean.

During October-May, the sensitivity of VOLUME to the V wind component (Fig. 3.17) shows some weak positive values in the central part of the Arctic Ocean and also in the coastal seas. There is a notable dipole to the north of Alaska, along

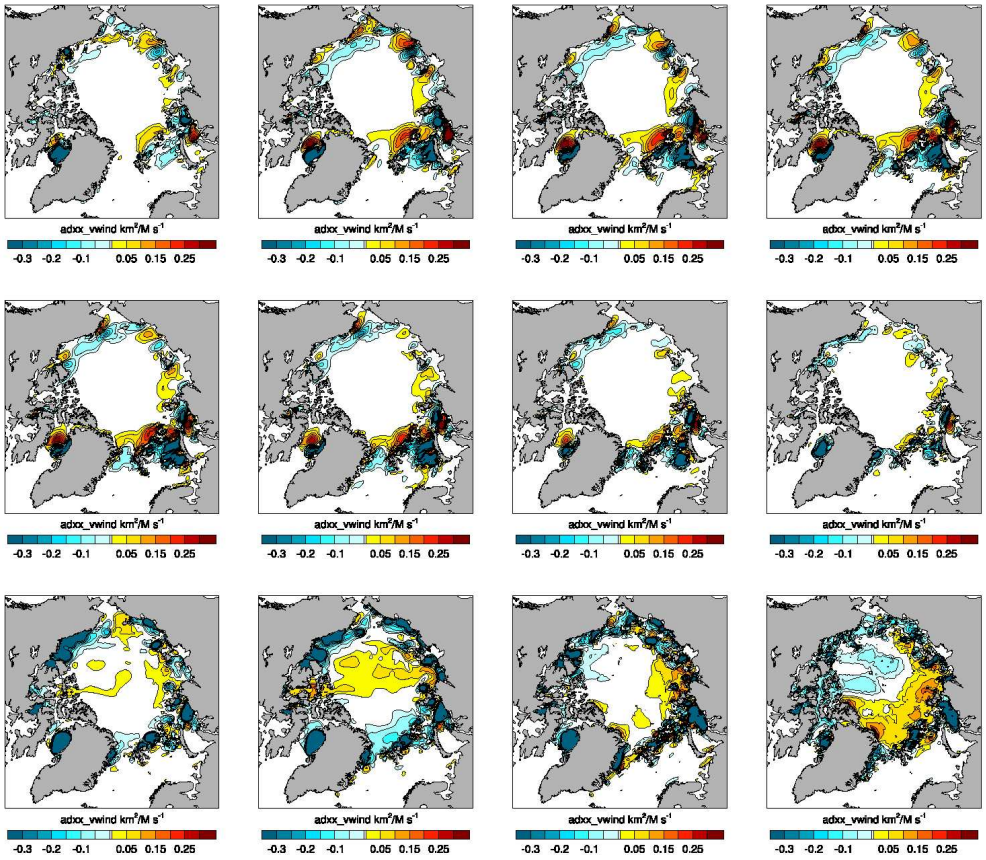

Figure 3.16— Monthly means of AREA sensitivities to V wind component. Top: October, November, December, January; middle: February, March, April, May; bottom: June, July, August, September.

with mostly negative values in the eastern Kara and northern Barents seas. During June, large parts of the central Arctic Ocean are occupied by the zone with positive sensitivities, surrounded by the negative values extended towards coastal seas. In July, the strength of positive and negative sensitivities increases but the area of positive ones shrinks. During August most of the Amerasian Basin is covered by the positive sensitivities, while in the coastal areas negative sensitivities are still dominant. In September the only considerable sensitivities stay along the ice edges in both the Eurasian and Amerasian basins.

In order to analyze sensitivities to U and V wind components in a combined way and estimate how important forcing over the different regions might be for the interannual changes of sea ice, we make plots where sensitivities to U and V wind components are combined to obtain vectors and overlaid on the interannual

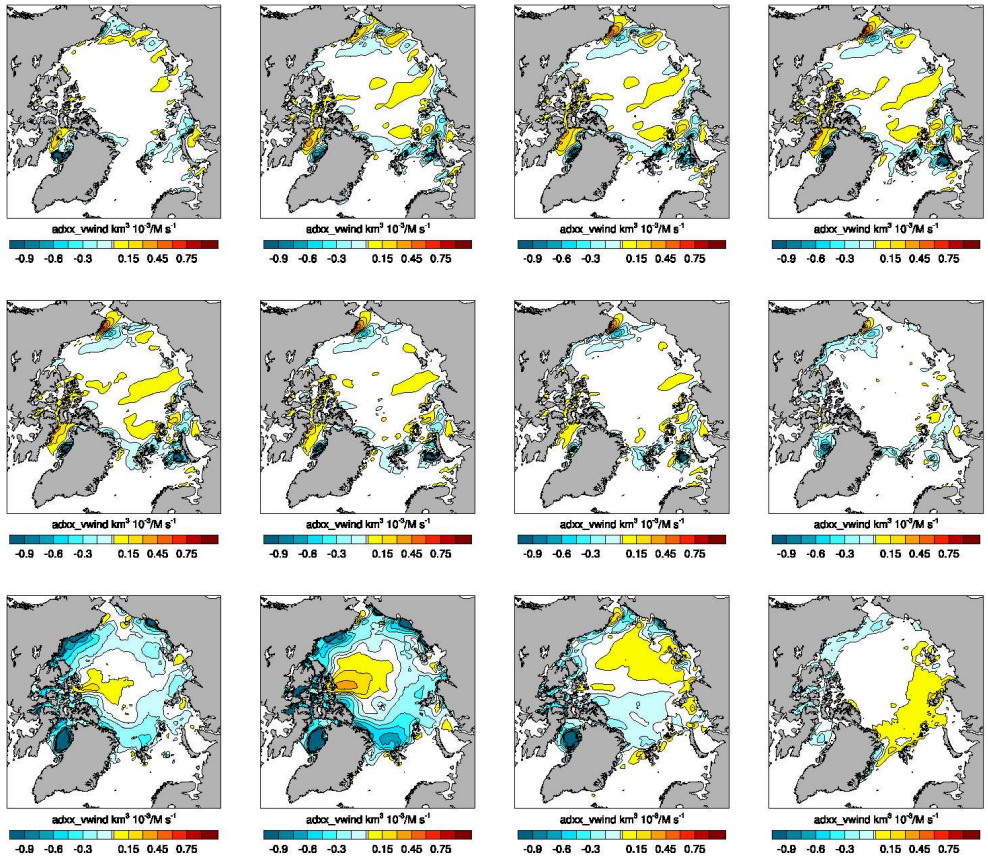

Figure 3.17— Monthly means of VOLUME sensitivities to V wind component. Top: October, November, December, January; middle: February, March April, May; bottom: June, July, August, September

standard deviation of monthly mean U and V wind components. The direction of arrows should be interpreted as the most preferable direction of the wind for the *increase* in the AREA and VOLUME, hereafter referred to as preferable wind direction (PWD). The length of the arrows should be interpreted as follows: the longer the arrow, the stronger the positive sensitivity to the wind in the location of the arrow tail. To cut out extremely high local sensitivities that are related to the instabilities in the linearized model, we take into account only the sensitivities that do not exceed a certain threshold, which for AREA equals 0.2 $km^2/m\ s^{-1}$ and for the VOLUME equals 0.9 $km^3\ 10^{-3}/°C$. We show only every third vector for the purpose of better visualization.

First we will analyze PWD and strength of the sensitivities for the AREA (Fig. 3.19). In June-August the strongest sensitivities can be found in the Canada Basin,

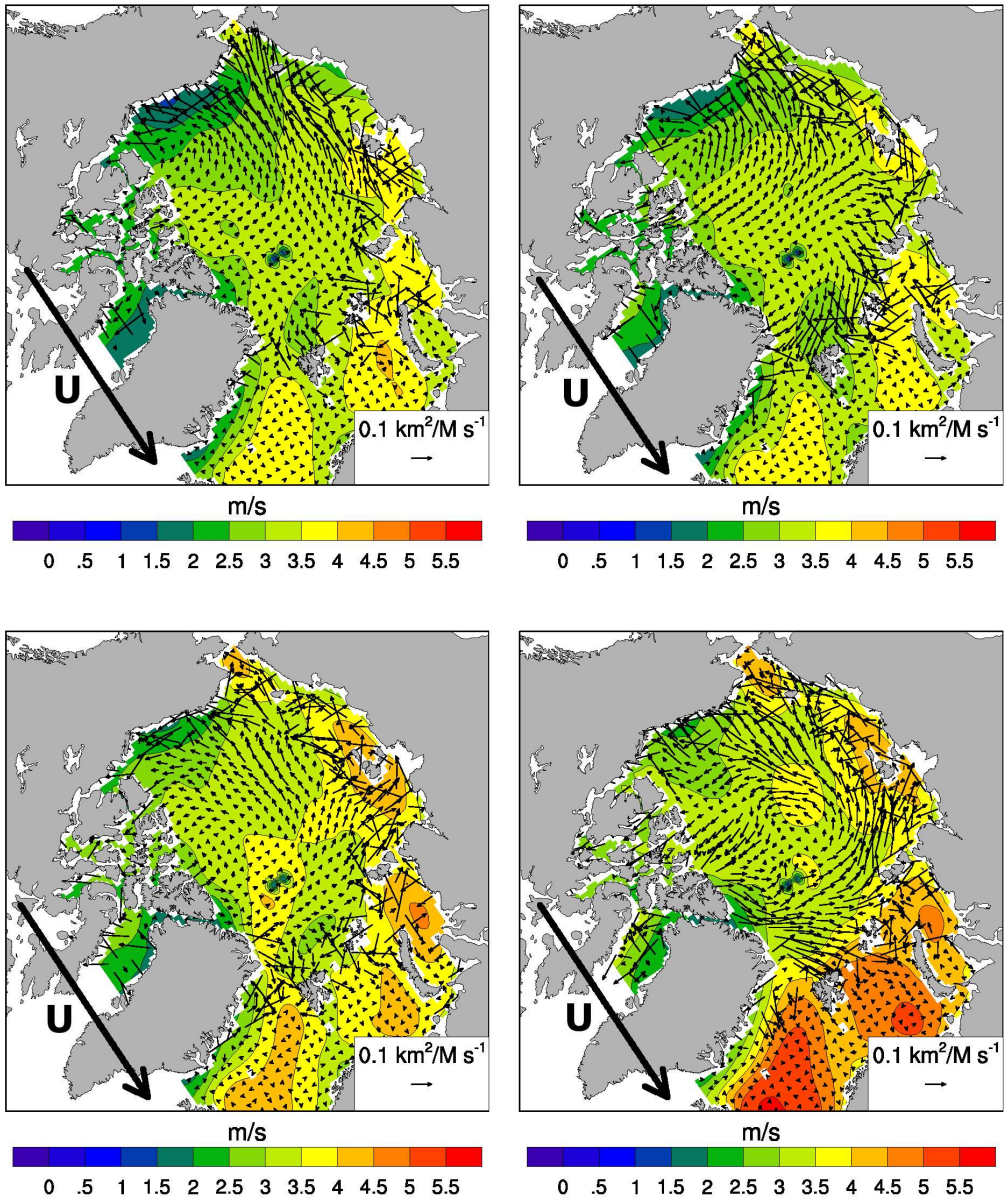

Figure 3.18— Arrows: combined sensitivities of AREA to U and V components of the wind. Colors: standard deviations of the monthly mean U wind component. Top: June, July; bottom: August, September.

and the PWD is towards the coast of Alaska and the western part of Canada. In June to the north of the Siberian Seas, PWD is towards the east, and the sensitivities are especially strong to the north of the East Siberian Sea. Then in July PWD turns

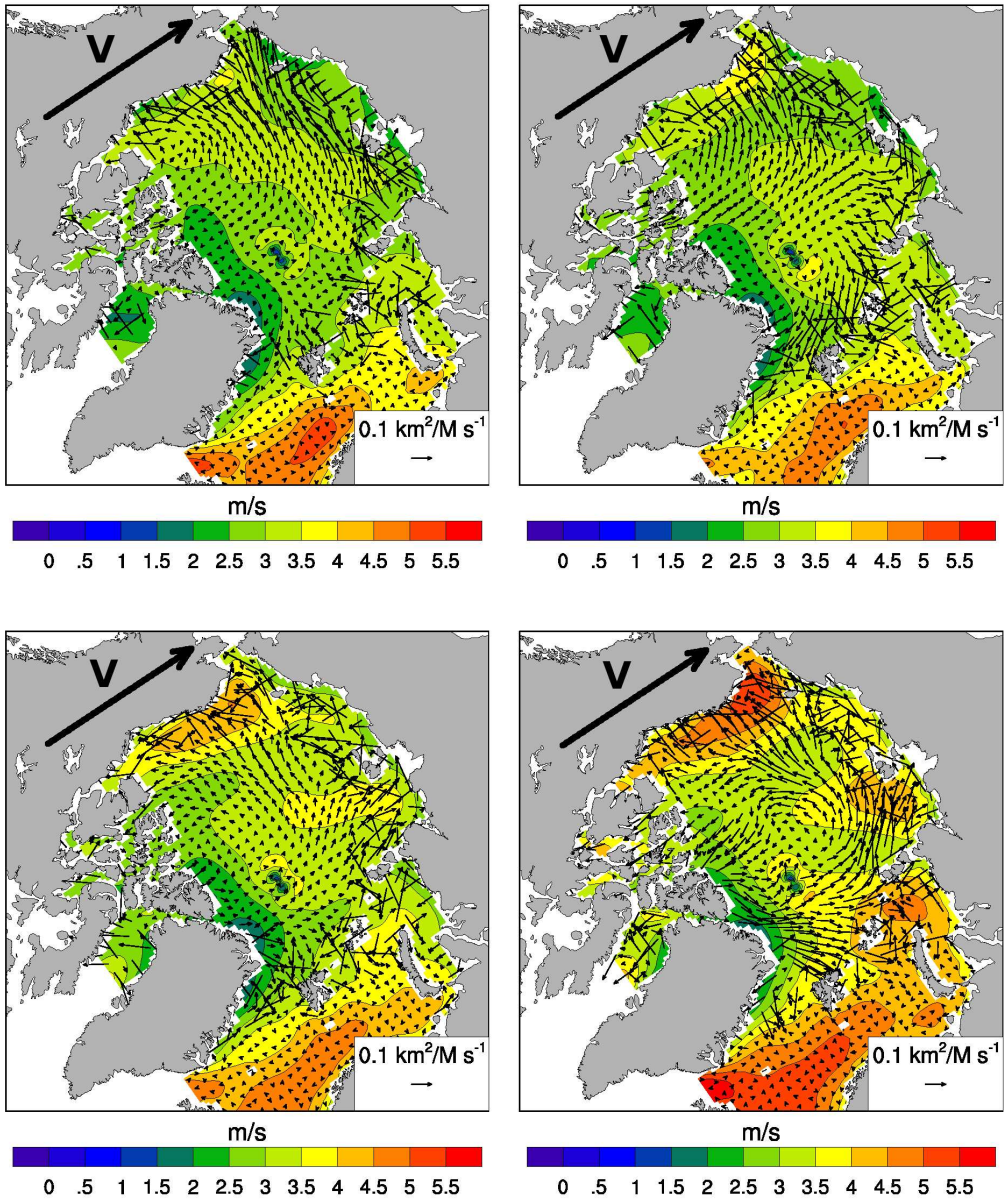

Figure 3.19— Arrows: combined sensitivities of AREA to U and V components of the wind. Colors: standard deviations of the monthly mean V wind component. Top: June, July; bottom: August, September.

more towards the interior of the coastal seas while the strength of the sensitivities increases considerably to the north of Spitsbergen. In August the strength of the sensitivities is weakened and then in September they become stronger again and

PWD is organized in a basin-wide cyclonic feature.

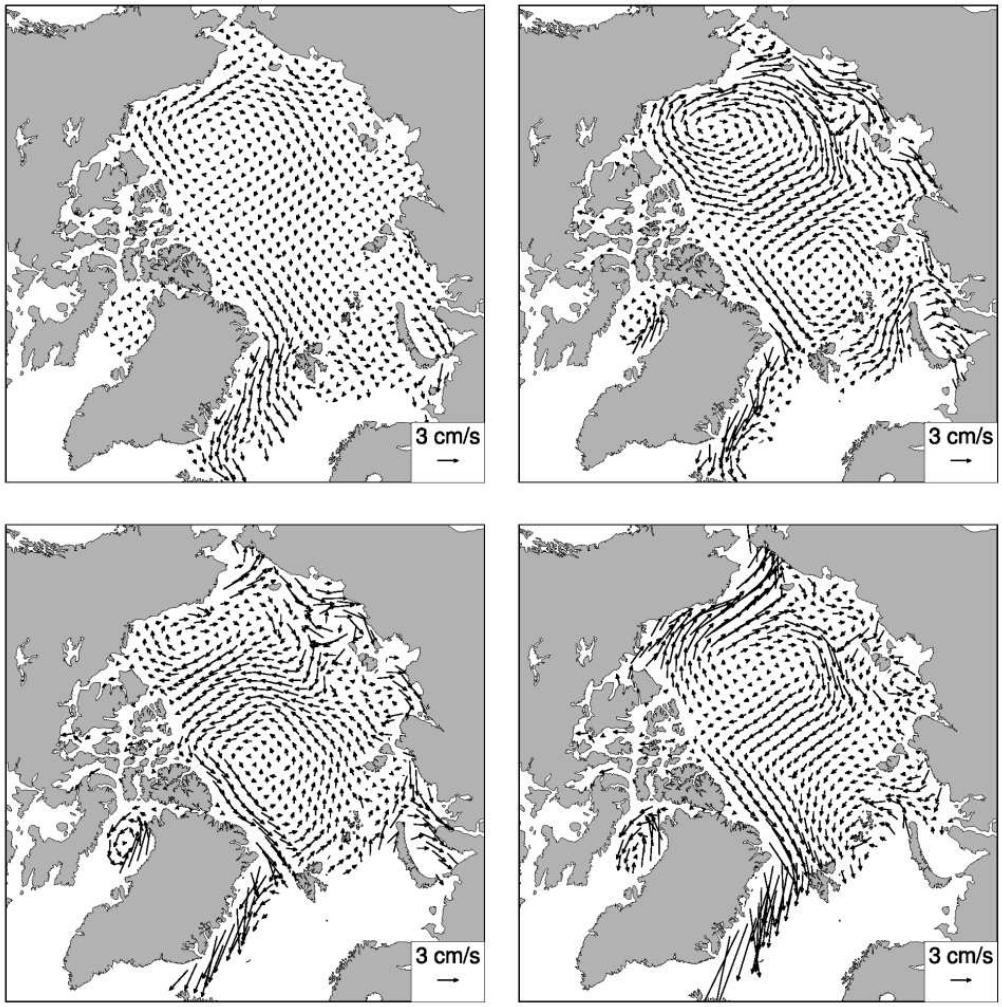

Figure 3.20— Mean sea ice transport for 1980-2007 in MITarc40. Top: June, July; bottom: August, September.

In the beginning of May the sea ice transport in the Arctic Ocean (not shown) is minimal since most of the model domain is covered by the ice with SIC close to 100%. Later, with the onset of ice melting, transport starts to increase slightly in June and becomes very strong in July (Fig 3.20). Sea ice sensitivities of AREA and VOLUME to the wind and temperature during this time indicate the importance of this period in shaping the state of September sea ice. The transport of thicker sea ice from the center of the basin and from the north of the Canadian Archipelago towards coastal seas increases the resistance of the ice to summer melting. Movement of the

ice towards the center of the basin will open more water in coastal areas, increase ocean heat absorption, and, as a consequence, warm the atmosphere and melt more sea ice. Positive ice-albedo feedback probably starts to work actively already in June, when the first big leads are formed in the areas with thinner ice. These leads may serve as a nucleus for the following ice retreat. That makes redistribution of the sea ice in June and July very important for the development of sea ice melting and consecutive September sea ice state.

Regionally our results agree with previous studies. For the Beaufort sea, Drobot and Maslanik (2003) found that enhanced easterly and southeasterly winds are dominant during the years with light ice conditions. Our results show the PWD for an increase in AREA to be north easterly. Deser et al. (2000) show for the Barents, Kara, Laptev, and East Siberian Seas that reduction in sea ice concentration is associated with an anomalous southerly wind component over the seas and increase in sea ice concentration associated with an anomalous northerly wind component. They also found that during 1979-1996 atmospheric circulation anomalies in May-July have a stronger influence on sea ice cover than those in June-August or April-June. The importance of the late spring atmospheric circulation for shaping the late summer sea ice extent was also shown by Serreze et al. (1995) and Maslanik et al. (1996).

Two things should be noted when analyzing the figures of wind components' standard deviations together with PWD. First, wind components' STDs presented here are on the model grid and the direction of each component is indicated on the figures. Second, while analyzing figures with STD for a particular wind component, one has to consider the PWD that is directed more along the axis of this wind component.

Standard deviations of the monthly mean wind speed of the U component are presented in Fig. 3.17. In June and July the U wind STD is fairly uniform over the Arctic Ocean, exceeding values of 3.5 m/s only in some Siberian seas. Slightly lower values of the U wind STD coincide during these months with the strongest values of sensitivities in the Beaufort Sea and to the north of Spitsbergen. This might be interpreted to mean that while sensitivities are strong in these areas, they might have a lesser or equal impact on the interannual changes in the sea ice conditions in the Arctic Ocean compared to surrounding areas with weaker sensitivities but higher U wind STD. In August and September, the U wind STDs are less uniform over the Arctic Ocean with regions that have values up to 4 m/s appearing over the central Arctic. In the Siberian seas, U wind STDs reach 4.5-5 m/s. While in August areas with high U wind STDs to the north of the New Siberian Islands are associated with onshore PWD, which is along the V axis of the model and not affected by the U wind, in September PWD turns to the east and becomes affected by the U winds that have high STD here. This means that instant dynamical forcing of the ice by U wind in the areas surrounding the New Siberian Islands might be important for ice formation in September (note that in our model during September, ice freezing processes are dominating).

June and July V wind STD (Fig. 3.19) distribution is even more uniform than

for U wind STD. Minimum values of 1.5-2 m/s are observed only to the north of Greenland, and maximum values of 3.5-4 m/s are observed in a small area to the north of Alaska. In June there are no PWDs associated with strong sensitivities to the V wind. In July there are areas with strong sensitivities to the north of the Laptev Sea with PWD to the shore and to the north of Spitsbergen, where PWD is more towards the Fram Strait. In August the V wind STD increases to the north of Alaska and over the Laptev Sea, where strong sensitivities related to the V wind component are observed. In September the V wind STD over the Arctic Ocean increased even more and the combination of strong sensitivities and high V wind STD becomes prominent over the Nansen and Amundsen basins. Another area of strong sensitivities and PWD along the V axis of the model is in the north of the Canadian Archipelago, but it is associated with lower V wind STD.

After analysis of Fig. 3.17 and Fig. 3.19 we can name several good candidates for areas where wind changes can determine the interannual AREA variability due to the combination of strong sensitivities and high wind STD. For the U wind it is north of the New Siberian Islands in June and to a greater extent in September. For the V wind it is to some extent north of the Laptev Sea in August and the area to the north of Frans Josef Land and the Laptev Sea in September.

PWDs and the strength of the sensitivities for VOLUME are presented in Fig. 3.21. From Fig. 3.15 and Fig. 3.17 it is clear that sensitivities of VOLUME to wind components are much weaker in August-September than in June-July, which is why we will demonstrate figures only for the last two mentioned months. The spatial distributions of PWDs during both June and July are very similar, while during July sensitivities are stronger in the Beaufort Sea and over the Nansen and Amundsen basins. In the Beaufort Sea, PWD is favors transport of thicker ice from the north of the Canadian Archipelago towards the coast of Alaska and the eastern coast of Canada. This thicker ice is more resistant to the summer ice melt and will contribute to an increase in the VOLUME. In June, PWDs to the north of the Laptev and East Siberian seas are quite close to the one that we have for the AREA with PWD to the east. But in July, PWD for the VOLUME is more from the Laptev and to some degree from the East Siberian seas while PWD for the AREA is towards these seas. Winds that blow onshore in July bring thicker ice from the central parts of the Arctic Ocean to the Siberian Seas and increase the sea ice area. At the same time, atmospheric thermodynamical conditions favor melting in these regions. This ice probably survives the summer but becomes thinner than if it were to stay in the central Arctic Ocean. In the Eurasian Basin, strong sensitivity values presented during July for both AREA and VOLUME, but in the case of VOLUME, PWD there turned more towards the west, indicating that a positive impact on VOLUME will have winds that drag ice away from the Kara and Barents seas but towards the north of Greenland where it can be accumulated.

U and V wind STDs in June-July, as mentioned before, are distributed quite uniformly. Only the matching of relatively high U wind STDs with strong sensitivities in the Laptev Sea and relatively low U wind STDs again with strong sensitivities near the coast of Canada can be observed. Low V wind STDs coincide with strong

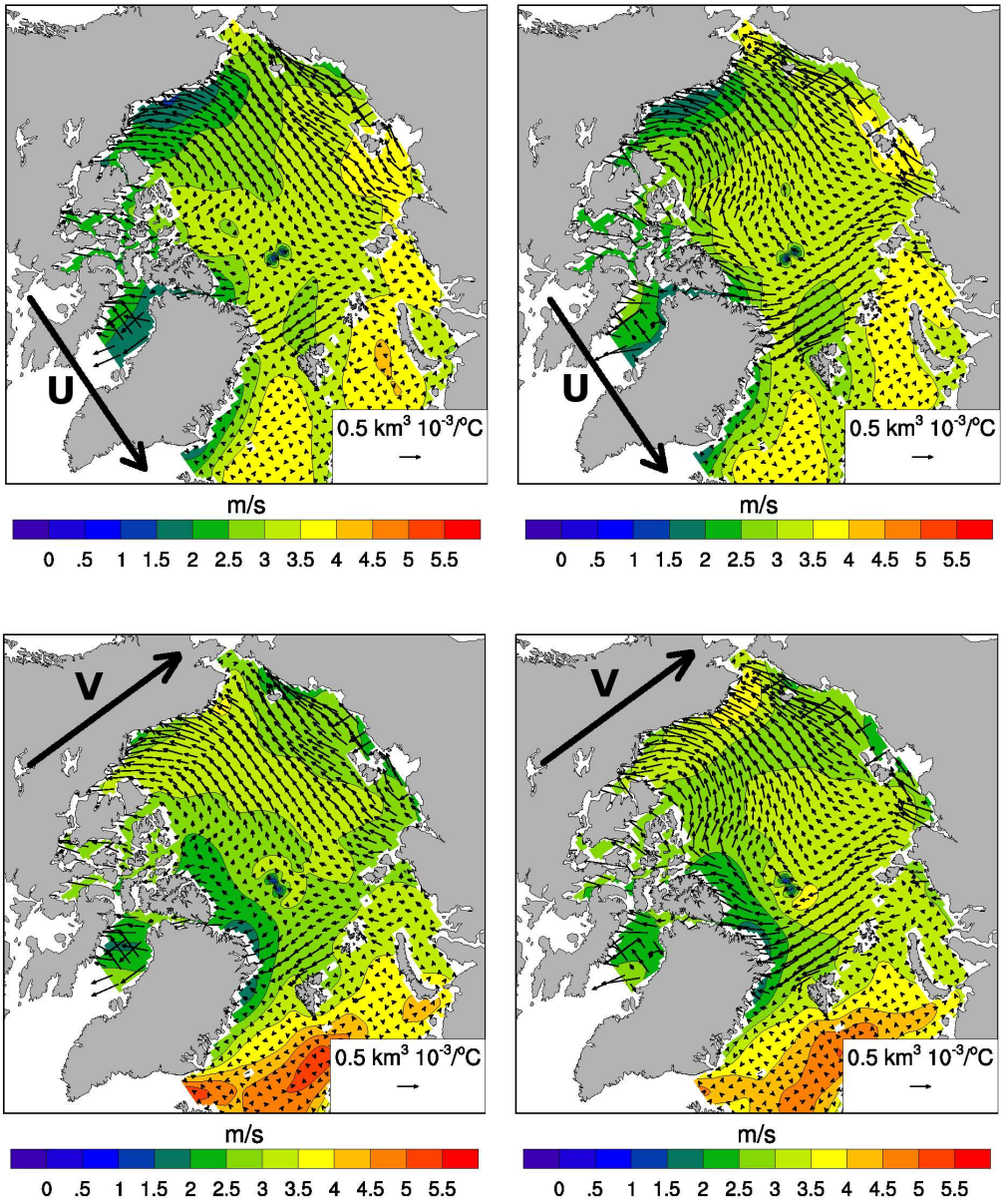

Figure 3.21— Arrows: combined sensitivities of VOLUME to U and V components of the wind. Colors: standard deviations of the monthly mean wind component. Top: STD of U wind component; bottom: STD of U wind component. Left: June; Right: July.

sensitivities to the north of Greenland. It is hard to name any areas that would contribute more than others to the interannual changes in VOLUME due to interannual changes in wind, since the STD of wind components for the Arctic Ocean is

mostly within 2.5-4 m/s.

We can conclude that in some regions, winds of particular directions will have different effects on AREA and VOLUME. Onshore winds during July in the Laptev and East Siberian seas will increase the AREA and decrease the VOLUME. Winds blowing in July along the axis of the Nansen and Amundsen basins towards Greenland will be favor an increase in VOLUME, but will be not that good for the AREA, which has PWD turned more to the south. Nevertheless PWDs for AREA and VOLUME are very similar in the Canadian sector of the Arctic, indicating that movement of the ice towards the Canadian coast with redistribution of the thick ice from the north of the Canadian Archipelago more towards the center of the Arctic Ocean leads to increases in both AREA and VOLUME.

At the end of this section we emphasize the main conclusions drawn from the analysis of the mean AREA and VOLUME sensitivities:

- Both mean AREA and VOLUME sensitivities to SAT have weak values during October-March. Sudden strengthening occurs in June and then values of the sensitivities gradually weaken during July-September.

- Maximum AREA sensitivities to SAT are located close to the ice edge over the areas where in September there will be ice with concentrations of about 0.7-0.8 frac.

- Both mean AREA and VOLUME sensitivities to wind components showed the highest values in the period June-September; however VOLUME sensitivities in August-September are much weaker than in June-July.

- PWD for AREA favors spreading sea ice toward the marginal seas, while PWD for VOLUME is mainly from the Siberian seas toward central parts of the Arctic Ocean and to the north of Greenland and the Canadian Archipelago. PWDs for both cost functions are toward the coast in the Beaufort Sea and to the north of Alaska.

- The STD of monthly mean wind components over the Arctic Ocean is fairly uniform and we can name only the area to the north of the Laptev Sea as a region where a combination of the high sensitivities and high STD of the wind components may determine interannual AREA and VOLUME variability.

- There might be situations in which the wind blowing in a certain direction favors an AREA increase and a VOLUME decrease, and vice versa. We can see it happen in the case of the onshore winds during July in the Laptev and East Siberian seas and in the case of winds blowing in July along the axis of the Nansen and Amundsen basins toward Greenland.

3.6 Adjoint sensitivities during the three time periods: 1980-1989, 1990-1999, and 2000-2007

During the period of our analysis, sea ice characteristics are varying considerably. To see whether sensitivities vary as well we look at three separate time periods that show substantially different distributions of mean sea ice characteristics. Division to the periods will also help us to check and expand the conclusions drawn in the previous section about the ways in which sensitivities are related to the SIT and SIC. Following the studies of sea ice variability mentioned in the introduction we choose the periods 1980-1989, 1990-1999, and 2000-2007 (Fig. 3.3). The first (1980-1989, hereafter 1980s) is characterized by mostly anticyclonic atmospheric circulation, extended summer sea ice cover, and a relatively big fraction of thick multiyear ice. The second (1990-1999, hereafter 1990s) is characterized by more cyclonic atmospheric circulation, shrunken summer sea ice cover, and a decrease in the fraction of thick multiyear ice. The third (2000-2007, hereafter 2000s) is characterized by a return to slightly more anticyclonic conditions but with a continuous summer sea ice concentration retreat and decrease in the sea ice thickness.

Figure 3.22 shows the monthly means of AREA sensitivities to SAT for three different periods. The distributions of sensitivities for June and July show no big differences between the 1980s and the 1990s, except for the fact that coverage by stronger negative sensitivities is a little larger during the 1990s. Differences are much greater between these two periods and the 2000s. During the 2000s, stronger sensitivities occupy a larger area and propagate further towards the center of the Arctic Ocean to the north of the East Siberian Sea and the Alaskan coast. Nevertheless, development of the sensitivities during the 2000s through the summer months remains the same with the maximum in June and the minimum in August. In the Eurasian sector, the differences between the three periods are not very big. In September, weak sensitivities cover almost the whole area of the Arctic Ocean during all three periods with slightly stronger values during the 2000s.

A comparison of AREA sensitivities to SAT with mean thickness distributions for June and July (Fig. 3.25) shows their close relation. On average, strong sensitivities with values less than 1.5 $km^2/°C$ are associated with a certain range of thicknesses. In June in the Amerasian Basin this range is from 1.6 m to 2.4 m, and in the Eurasian Basin it is from about 1.4 m to 2 m. In July in the Amerasian Basin this range is from 1.4 m to 2.2 m, and in the Eurasian Basin it is from about 0.8-1 m to 1.8 m. Differences between June and July are due to melting and reach about 20 cm in each region. Probably all sea ice that is below this range will be melted during the summer season. Ice that is in this range has a chance of surviving summer melting, and ice that is above this range will most probably survive over the summer. The reason why we have strong sensitivities in the regions where ice is in this certain thickness range is its uncertain fate. Higher than usual temperatures over these regions may melt more thin ice and decrease the resulting AREA, while lower temperatures will preserve this ice. The consistency of these thickness ranges

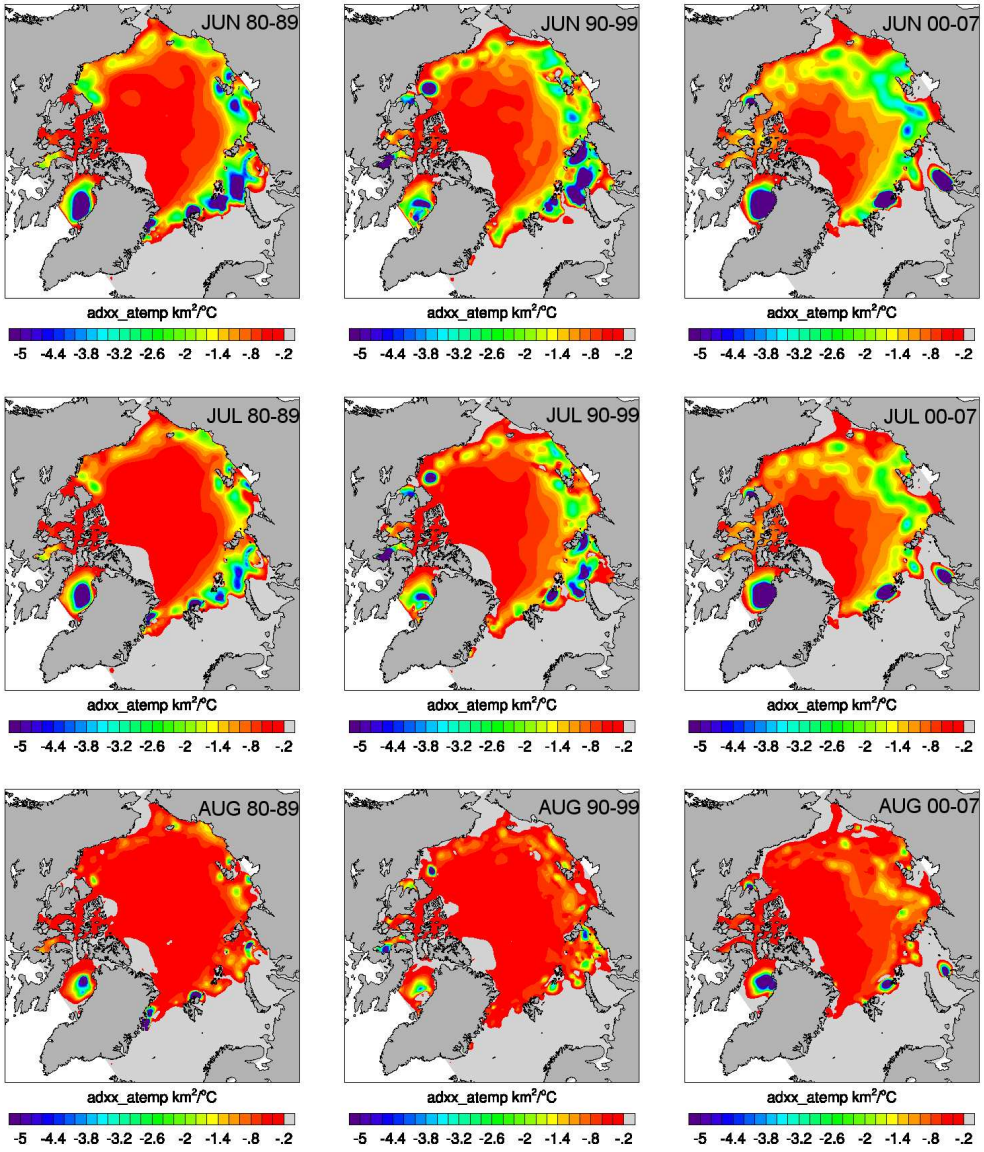

Figure 3.22— Monthly means of AREA sensitivities to SAT. From left to right: left: 1980s; middle: 1990s; right: 2000s. From top to bottom: top: June; middle: July; bottom: August.

through the different periods emphasizes importance of the background thickness for the thermodynamical forcing of the sea ice on short time scales and its interannual variability.

Maslanik et al. (2007b) combine ICESat data with estimations of ice age for February-March of 2003-2006 and get mean thickness values of 1.5 m for the one-

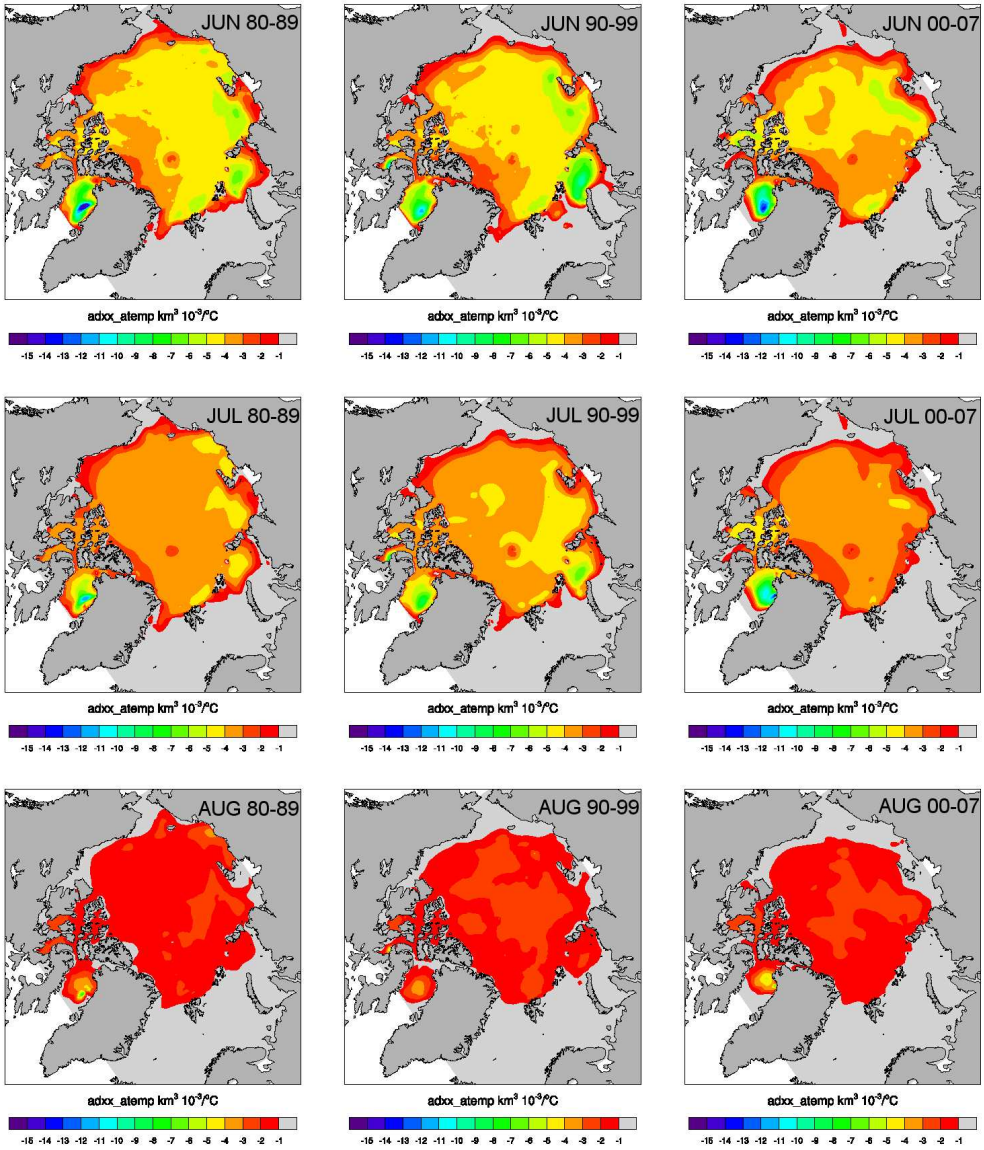

Figure 3.23— Monthly mean VOLUME sensitivities to SAT. From left to right: left: 1980s; middle: 1990s; right: 2000s. From top to bottom: top: June; middle: July; bottom: August.

year-old ice, 2 m for two-year-old ice, 2.3 m for three-year-old ice, and 2.5 m for four-year-old ice. The mean thickness in the model runs changes very slightly between March and June, so we can compare June values in the model with Febrary-March means from Maslanik et al. (2007b). The upper limit in the range of thicknesses associated with high values of AREA sensitivities in June is 2.4 m for the Amerasian

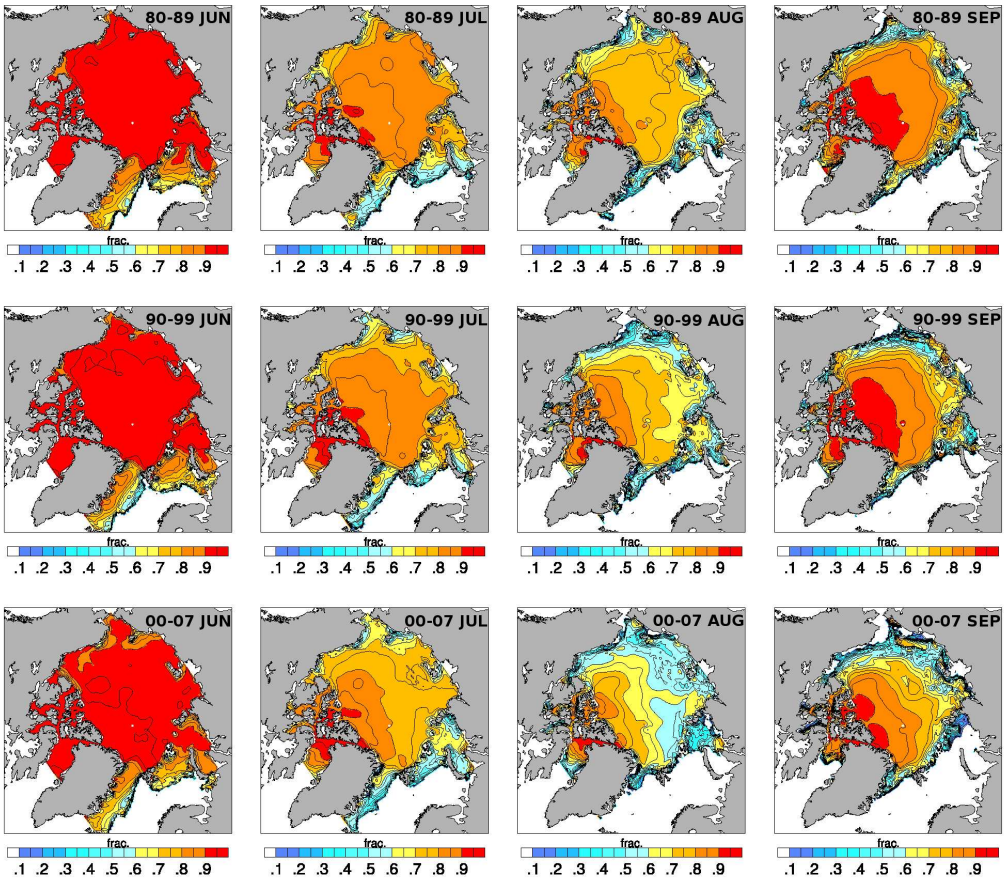

Figure 3.24— Monthly means of SIC for three different periods.

Basin, which gives us an ice age of 3-4 years, and 2 m for the Eurasian Basin, which gives us an ice age of about 2 years. Lower limits in both basins are in good agreement with values for one-year-old ice. Using this information together with satellite methods of ice age retrieval, we could localize the areas where more attention to the surface air temperature should be paid in order to predict the sea ice state in September. Direct information about sea ice thickness from the ESA CryoSat-2 satellite, whose launch is planned for the beginning of 2010, may increase our skill in predicting summer sea ice conditions. Note that due to the thermodynamical scheme we used, the ranges we found might be thinner in reality.

Figure 3.24 shows the monthly means of VOLUME sensitivities to SAT. The strongest sensitivities in June are observed during the 1990s, especially in the eastern part of the Kara Sea, the Laptev Sea, and the western part of the East Siberian Sea, while weaker sensitivities are found during the 2000s, especially over the Eurasian

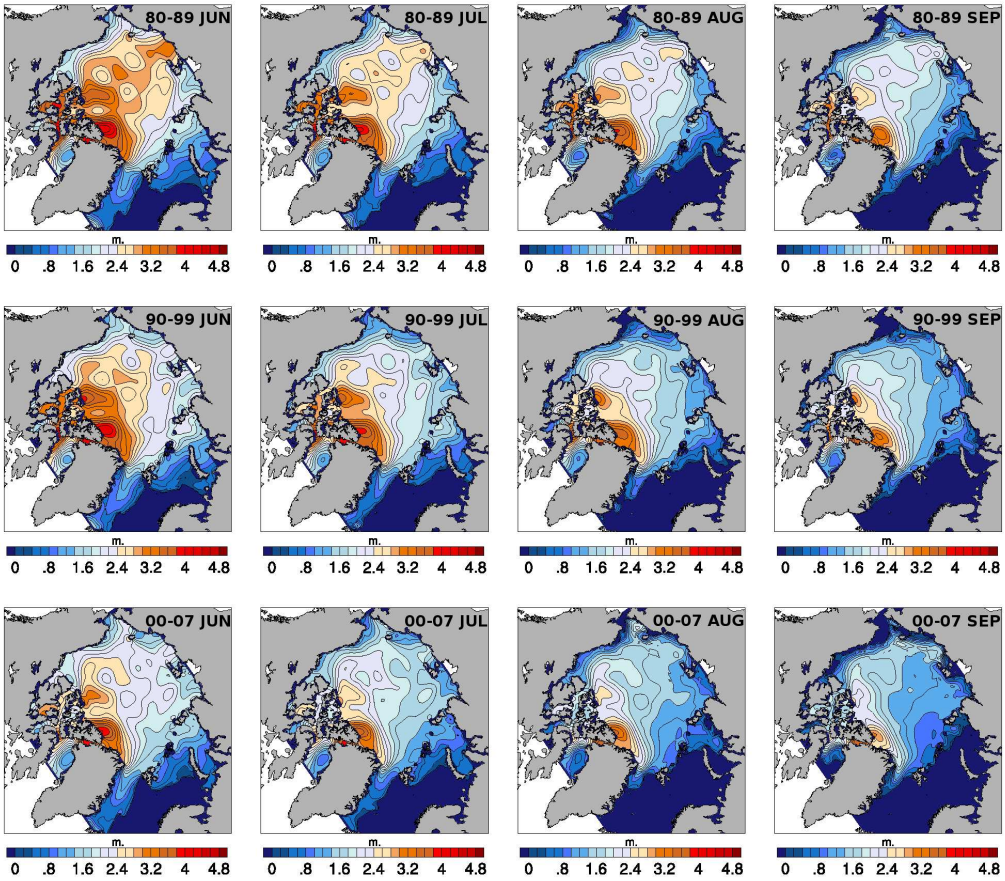

Figure 3.25— Monthly means of SIT for three different periods.

Basin. In July this tendency continues and the 1990s have the strongest sensitivities, especially over the Eurasian Basin. A decrease in VOLUME sensitivity to SAT in the Eurasian Basin during the 2000s is probably related to the slight increase in snow cover in this region (not shown), which has lower conductivity than sea ice and makes the sea-ice-snow system more resistant to melting. A simultaneous slight decrease in sea ice concentration may also play a role. Relatively strong sensitivities to the north of the Siberian Seas in July in the 1990s come from the strong sensitivities in the year 1993. During this year, sea ice thickness in this area is close to average but the sea ice concentration exceeds the average by about 0.15 frac. This leads to strong sensitivities that affect the mean value for the 1990s.

The balance between sea ice concentration and thickness is very important for the resulting VOLUME. In a simplified manner, sensitivities of the VOLUME to air temperature could be expressed as c/h, where c is the sea ice concentration and

h is the thickness. Sensitivities are weak where either both$c$ and h are high (like in the area to the north of Greenland) or low (like near the ice edge), or c is very small. Sensitivities are high where c is high and h is low, like in the areas where the new thin ice is formed during the winter. But this is of course a very simple way of thinking about it; other factors could also play a role, like in the case of the snow thickness.

Figure 3.26 shows PWD for AREA in three different periods for the June-September. In June of the 1980s and 1990s, the biggest PWD differences are located in the Amerasian Basin. For the 1990s, sensitivities in the middle of the Arctic Ocean are weaker than for the 1980s, and PWD near the Alaskan coast turns more towards the Bering Strait and the East Siberian Sea. The latter might be explained by the fact that during the 1980s ice in the East Siberian and Chukchi seas was thick, and adding even more thick ice would not considerably affect the resulting AREA, while in the 1990s, ice in these regions, and especially in the eastern part of the East Siberian Sea, became thinner and incoming transport of the thicker ice may affect the resulting AREA.

PWDs in June of the 2000s are close to those in the two previous periods but the strength of the sensitivities increased considerably. Strong sensitivities occupy large parts of the Arctic Ocean to the north of Eurasia. It is not possible to see whether PWDs to the north of the Barents and Kara seas still have a strong southern component since we restrict our analysis to sensitivities that are not stronger than 0.2 $km^2/m\ s^{-1}$. The same is true for the regions to the north of the East Siberian and Chukchi seas, where instabilities in the linearized model are very strong, probably due to the absence of the sea ice during some of the years of this period. A combination of the ice thinning and a decrease in SIC over the Arctic Ocean is probably the main reason for the increase in the sensitivities' strength during the 2000s. Sea ice concentration in June of the 2000s is only about 0.05 frac. less compared to the previous periods (Fig. 3.24), but this seems to be enough to increase sea ice mobility and lead to considerable strengthening of the sensitivities.

In July the strength of the sensitivities for the 1990s is increased in the central Arctic Ocean compared to the 1980s. This is the opposite to the situation of June, for which the 1980s show slightly stronger sensitivities in the central Arctic. This is probably related to the fact that the "bridge" of ice thicker than 2.4 m between the Canadian Archipelago and the western part of the East Siberian Sea that exists in July of the 1980s disappears in the 1990s. Combination with the lower SIC makes the ice more mobile and increases the sensitivities. The whole PWD in July of the 1990s experiences some sort of shift in anticyclonic direction over the major parts of the Amerasian and Eurasian Basins in relation to the 1980s period, but stays the same over the Lomonosov ridge. In the Amerasian basin it is related, as mentioned before, to the increase in the areas with thinner ice to the north of the Chukchi and East Siberian Seas, while to the north of the Barents Sea and Fran Strait there is a tendency to preserve ice inside the central basin since it became thinner in the 1990s and can no longer serve as a stabilizing factor for the AREA but will be melted away. PWD in July of the 2000s resembles the 1990s more closely, but with a more

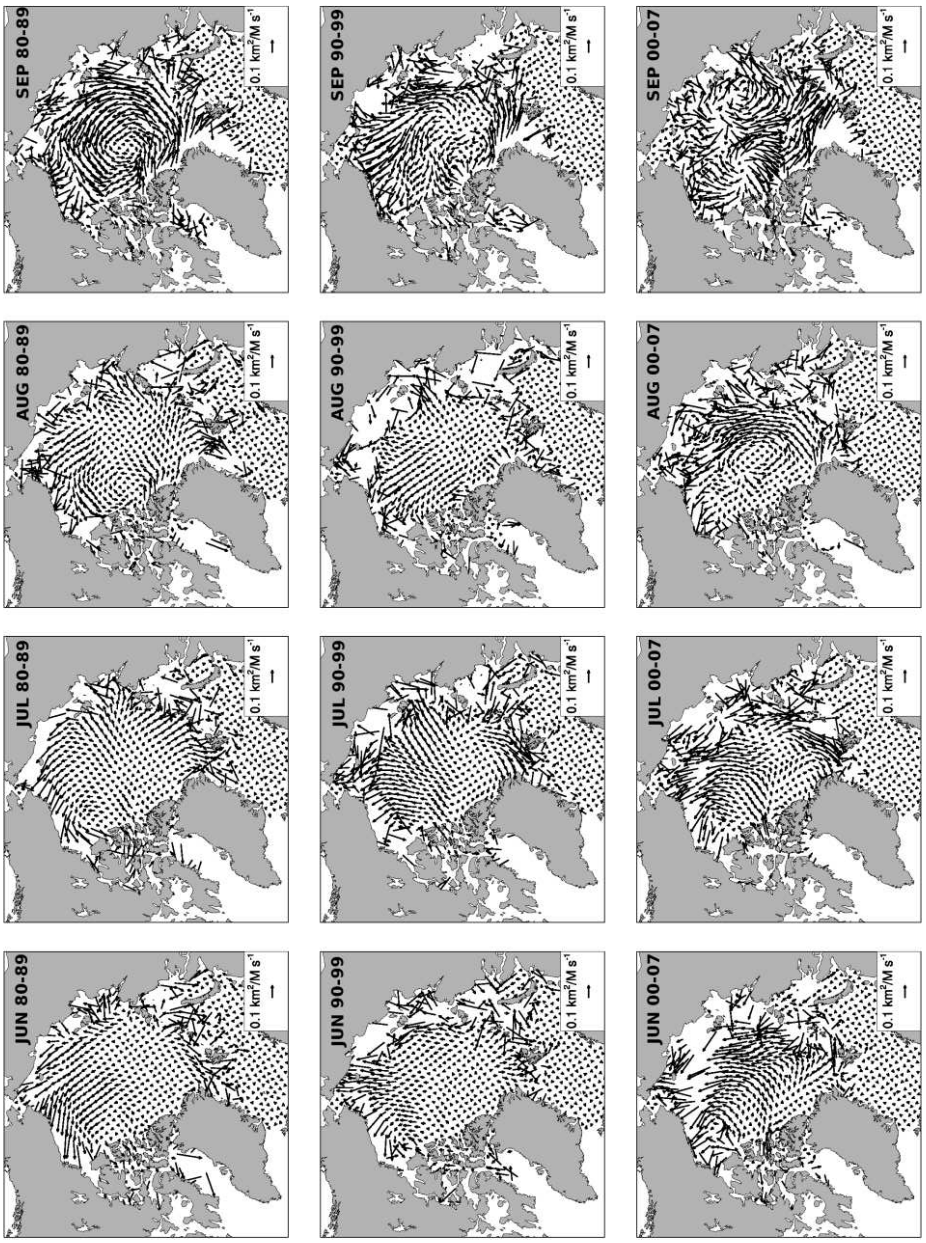

Figure 3.26— Combined sensitivities of AREA to U and V components for three different periods.

easterly component over the big part of the Lomonosov ridge and a more westerly component to the north of the Laptev Sea. This indicates the same tendency to save ice from being exported to the marginal seas, but now for all seas except the Chukchi and Beaufort seas. Sensitivities are further strengthened in comparison

with the previous periods, which coincide with decreased thickness and SIC over the whole Arctic Ocean.

In August, PWDs in the 1980s and 1990s are quite similar except that there is again an anticyclonic shift in the Amerasian Basin during the 1990s and generally weaker values of sensitivities, especially in the Eurasian Basin. PWDs in August of the 2000s are substantially different from those in the two other periods. In the Eurasian Basin along the Siberian shelf break, most of the PWD are to the east and are associated with very strong sensitivities. This is probably related to the combination of the decrease in SIC compared to the 1990s by about 0.10 frac. and decrease in SIT compared to the 1990s by about 40 cm. Ice with these characteristics that is exported to the Shelf Seas probably would not contribute to the increase in AREA and it is better to "preserve" it in the regions along the northern borders of the Shelf Seas. There it will not be melted due to high temperatures in the Shelf Seas, but also will not decrease the total sea ice area due to moving towards the center of the Arctic Ocean.

September PWD during the 1980s forms a cyclonic feature around the North Pole associated with strong sensitivities. PWDs are opposite to the dominant anticyclonic circulation, which exports sea ice through the Fram Strait and favors preserving the "status quo", where the main body of the sea ice does not move either to the center or to the border of the Arctic Ocean. In the 1990s there is no such anticyclonic structure in PWD and there are more grid points with PWD from the center of the Arctic towards the Alaskan and Canadian coast. Sensitivities to the north of the Canadian Archipelago are smaller than during the 1980s and PWD is mostly onshore there. September of the 2000s is characterized by strong sensitivities all over the Arctic Ocean with PWD in the Eurasian basin mostly directed towards the Atlantic Ocean and in the Amerasian sector towards the Pacific Ocean. During both the 1990s and the 2000s there is a tendency for PWD to be towards the borders of the Arctic ocean, spreading thicker ice from areas with higher SIC to the seas, while in the 1980s ice in the seas has characteristics that favor freezing without "injections" of older ice.

Sensitivities of VOLUME to U and V wind components during August and September are very small, due to both decreased SIC and SIT, so we will analyze only June and July (Fig. 3.27). PWDs during June of the 1980s and 1990s are different in the region to the north of the Canadian Archipelago, while in the 1980s PWD is from the center of the basin towards the Beaufort Sea and in the 1990s PWD are first from the shore of the Canadian Archipelago and then towards the Alaskan coast. In the Beaufort Sea and adjacent waters, a slight anticyclonic shift can be observed that is the same as that in PWD for AREA. To the north of the East Siberian Sea, sensitivities during the 1990s are stronger than during 1980s. To the north of Spitsbergen and Greenland, sensitivities in the 1990s are smaller than in the 1980s, and PWD is out of the basin, while in the 1980s they are towards Greenland. June PWD for the 2000s is characterized by a strong component out of the Barents, Kara, and Laptev seas towards central parts of the Arctic Ocean and an easterly component in the East Siberian Sea associated with strong sensitiv-

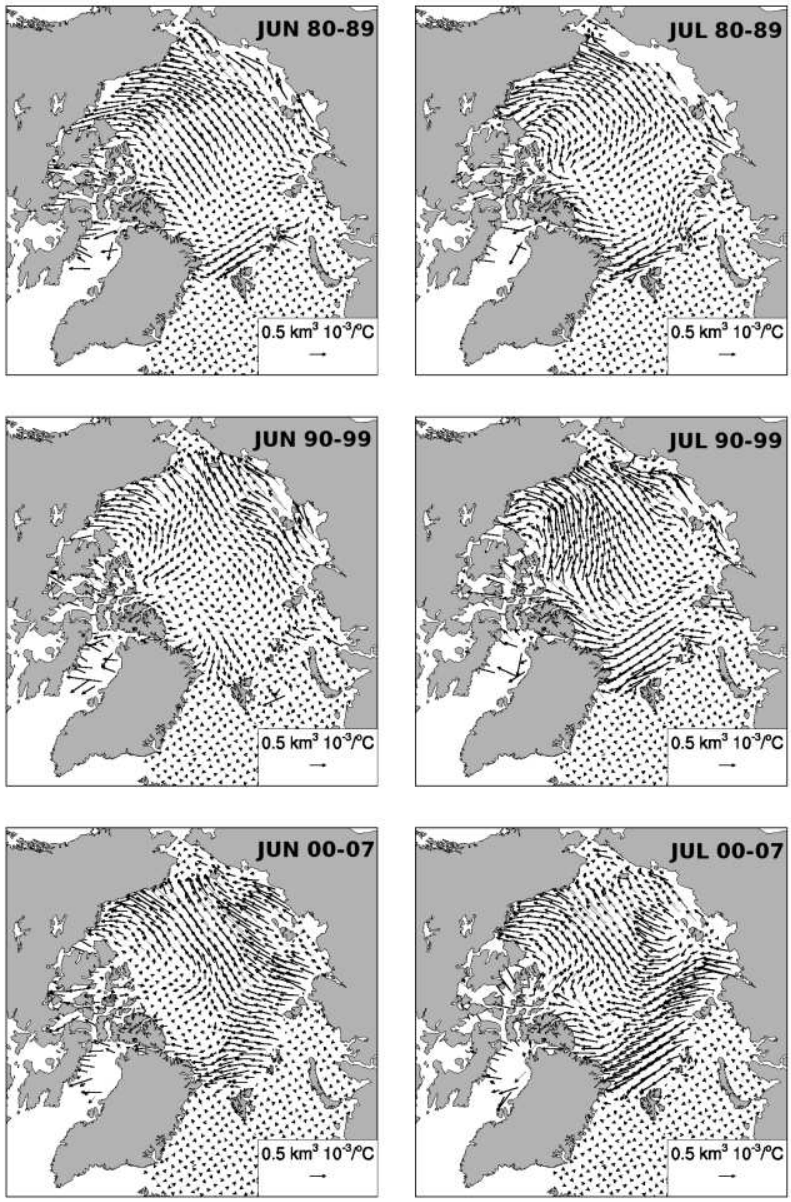

Figure 3.27— Combined sensitivities of VOLUME to U and V components for three different periods of the wind.

ities. Sensitivities in the central Arctic Ocean and the Beaufort Sea are also strong and PWD in these regions resembles those of the 1980s more closely. Differences between the three periods are probably completely explained by differences in the ice thickness (Fig. 3.24). PWD favor thicker ice redistribution towards the Alaskan

and Canadian coast and thinner ice redistribution from the Eurasian Basin towards areas with thicker ice in the central parts of the Arctic Ocean and to the north of the Greenland and Canadian Archipelago.

In July of the 1980s, PWD stays almost the same as in June with only slightly different PWD in the central part of the Arctic, turning more towards the East Siberian Sea, with increased sensitivities to the north of the Kara Sea. In the 1990s, July PWD stays close to PWD for June in the Amerasian Basin but sensitivities are considerably strengthened. In the Eurasian Basin, PWD are more towards Greenland and the strength of the sensitivities is also increased. This increase is explained by the ice thinning, since SICs in this region during the 1980s and 1990s are the same. In July of the 2000s PWD and the strength of the sensitivities in the Amerasian Basin stay very similar compared to June, but in the Eurasian Basin PWD shifted counterclockwise towards Greenland and the overall strength is increased. This might be associated with both the decrease in SIT and SIC.

In this section we analyze sensitivities for three different time periods. We try to connect changes in sensitivities with changes in SIC and SIT for these periods in order to show how sea ice characteristics during the summer months shape the impact of the atmospheric forcing on the resulting AREA and VOLUME. Our main findings can be summarized as follows:

- Distribution and strength of the sensitivities for the three periods do differ. There are especially big differences between the 2000s and the other two periods. During the 2000s, strong AREA sensitivities to SAT occupy larger areas of the Arctic Ocean in comparison to the 1980s and 1990s, while strong VOLUME sensitivities occupy smaller areas.

- There is a close relation between the distribution of AREA sensitivities to SAT and SIT that is consistent throughout the whole three periods. In the beginning of the melt period strong AREA sensitivities to SAT are associated with ice thickness from 1.6 m to 2.4 m in the Amerasian Basin and 1.4 m to 2.0 m in the Eurasian Basin. High resolution data about SIT distribution are required, since closer investigation of this relationship may lead to an increase in our skill in predicting September SIC.

- The balance between SIC and SIT is very important for sensitivities of VOLUME to SAT. In regions where both SIC and SIT are high or low, sensitivities are low. In regions where SIC is high, but the SIT is low, sensitivities are high, since large amounts of thin sea ice that are more prone to melting may largely affect VOLUME.

- The differences in SIC and SIT control the differences in AREA and VOLUME sensitivities to wind for our three periods. Mean sensitivities in the 2000s become stronger in comparison with sensitivities for the 1980s and 1990s. Due to thinning of the sea ice, PWDs in the 2000s are changed such that sea ice export toward the Siberian Shelf seas during July-August is no longer the best way to increase the AREA.

- In PWD for VOLUME in June-July of the 2000s, the component directed from the Siberian Shelf seas toward the center of the Arctic Ocean increased considerably, showing that VOLUME became more sensitive to the sea ice redistribution between central regions of the Arctic Ocean and the Siberian Shelf seas. Ice export toward the Siberian Shelf seas in the 2000s might lead to stronger VOLUME decrease in comparison to the 1980s and 1990s.

3.7 Time evolution of sensitivities in different regions

In the previous two sections we analyzed monthly means of the sensitivities' spatial distribution. As has been shown, differences between monthly averaged fields in the summer months are usually quite big, and it is interesting to see how sensitivities evolve over time on a smaller time scale. It is not possible to present maps of the sensitivities distribution for every day of the year, so we decide to "condense" this information. We choose several boxes (Fig. 3.28) from our model domain: Box 1 covers the Beaufort Sea and the areas to the north of the Alaskan coast; Box 2 is located to the north of the Greenland and Canadian archipelago; Box 3 represents the areas around Spitsbergen, Frans Josef Land, and the eastern part of the Kara Sea; and Box 4 covers the region to the north of the Laptev Sea. According to the analysis done in the previous sections, behavior of the sensitivities in these regions is interesting and important for the cost functions. Taking a closer look at these boxes will allow us to explore the seasonal cycle of the sensitivities and to better understand the reasons for the changes in values of the sensitivities. Sensitivities in the regions covered by the boxes are averaged for every day, and these values are then averaged across the years of the time period in which we are interested. All values are smoothed by a moving average with a window of 10 days.

Figure 3.29 shows the evolution of the mean daily AREA and VOLUME sensitivities to SAT for two boxes that are representative for the demonstration of the seasonal cycle. Sensitivities in Box 2 are characterized by weaker values, and Box 4 covers the regions where the sensitivities are relatively strong. In both boxes, seasonal changes in the sensitivities in general have similar shapes but differ in strength and details. When we talk about the strength of the sensitivities to the air temperature and their maximums and minimums we mean absolute values. During winter, sensitivities are close to zero and start to emerge rapidly with the beginning of the melting season in the middle of May. They reach the first local maximum in the middle of June and then start to decrease until the local minimum, associated with the beginning of freezing, is reached (we have shown that, in general, freezing in our model simulations starts in the second half of August; Section 3.4, Fig. 3.7). This is followed by the peak in the middle of September, and then sensitivities become close to zero. VOLUME sensitivities to the SAT (Fig. 3.30) repeat the behavior of AREA sensitivities until August, but then instead of having a second peak the slope is slightly increased after the beginning of the freezing period. The relative strengths of the sensitivities in Box 2 and Box 4 for AREA differ considerably, as

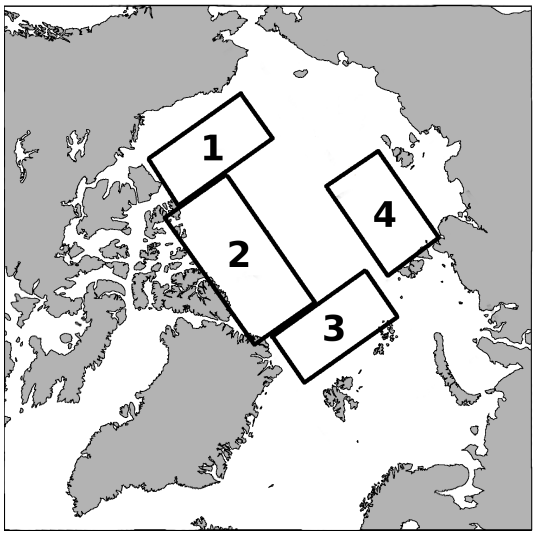

Figure 3.28— Division of the model domain into boxes.

in the case of VOLUME they are close to each other with still stronger values in Box 4. The presence of the second peak in values of the AREA sensitivities to SAT demonstrates how sensitive the SIC is to the changes in the temperature. VOLUME sensitivities to the SAT do not have a second peak since the newly formed ice is very thin, and the ice that survives the summer increases its thickness very slowly.

To show the evolution of the mean daily AREA and VOLUME sensitivities to the wind components, we choose Box 1 and Box 4. In Box 1, sensitivities to the U and V components for AREA and VOLUME have similar signs, while in Box 4 sensitivities to the V component have a period in which the signs are opposite. Sensitivities to the U wind component are presented in Fig. 3.30. For both cost functions, sensitivities in winter are close to zero and start to emerge in the middle of May with the beginning of the melting period. In Box 1, sensitivities are mostly negative during the whole summer for AREA and VOLUME, showing that to the north of Alaska and the western part of Canada, wind that will increase both cost functions should blow onshore. The VOLUME sensitivities become close to zero in the middle of August as a result of the thinning of sea ice and decrease in its concentration, while sensitivities of AREA continue to be strong through the whole summer period, indicating that dynamical redistribution of the ice in this region is important for the AREA during all summer months.

For sensitivities in Box 4, behavior is more complicated. Sensitivities there are also mostly negative, but for the AREA they have two negative peaks with close to zero values from the middle of June to the middle of August, while values for VOLUME show one negative peak in the middle of June and one positive peak in August. The period of weak AREA sensitivities might be explained by the comparatively uniform distribution of thickness and SIC in this box along the axis parallel to

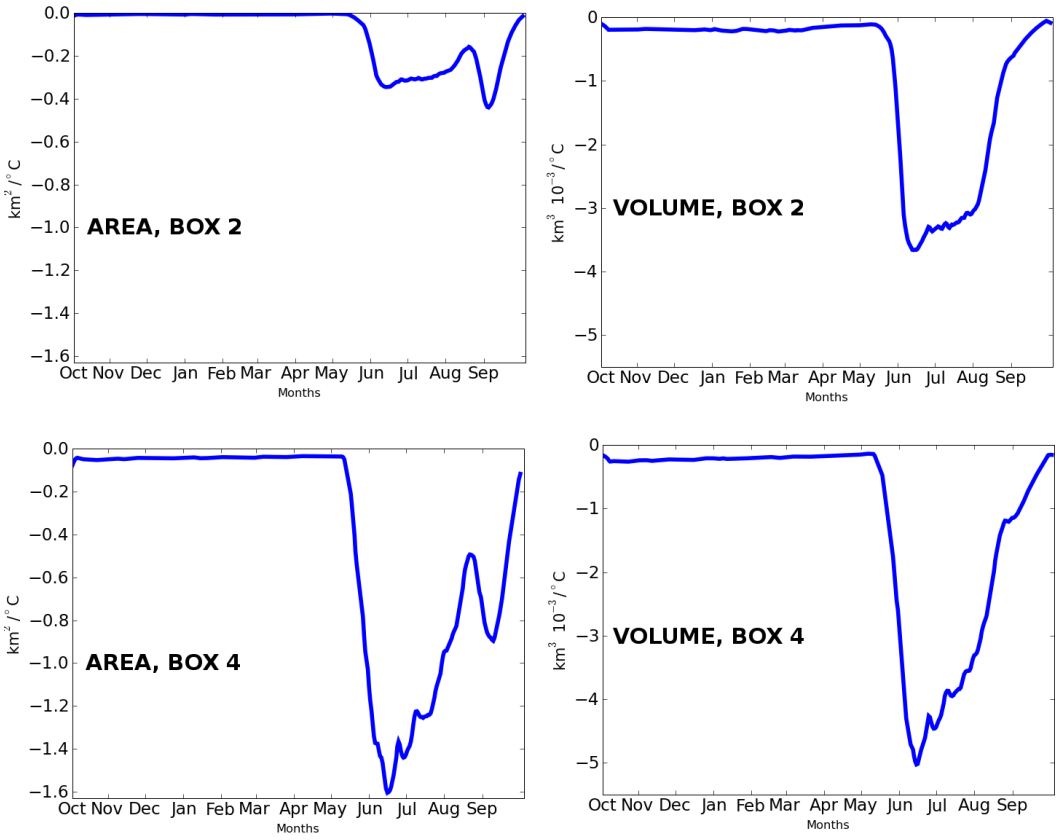

Figure 3.29— Evolution of the mean daily AREA and VOLUME sensitivities to SAT. Top: Box 2; bottom: Box 4. Left: AREA sensitivities; right: VOLUME sensitivities.

the northern border of the Laptev Sea. The U wind is responsible for the movements of the sea ice along this border but ice redistribution in this direction should not affect the resulting AREA. Periods of strong AREA sensitivities might be related to the fact that moving relatively thick ice to the west instead of exporting it to the Laptev Sea (see next paragraph) leads to a decrease in the resulting AREA. The shape of the curve that describes VOLUME sensitivities to the U wind in Box 4 is explained by negative effects that the export of the thick ice from the north of the East Siberian Sea might have on the resulting VOLUME during the melting period, and by positive effects that the same transport might have during the freezing period.

Sensitivities to the V wind component are presented in Fig. 3.31. In Box 1 sensitivities for both AREA and VOLUME show mostly negative values that favor pushing the ice more to the Canadian coast. Sensitivities to air temperatures there are small and ice area and thickness have a big chance to be preserved and contribute to the resulting AREA and VOLUME. The situation to the north of the Laptev Sea

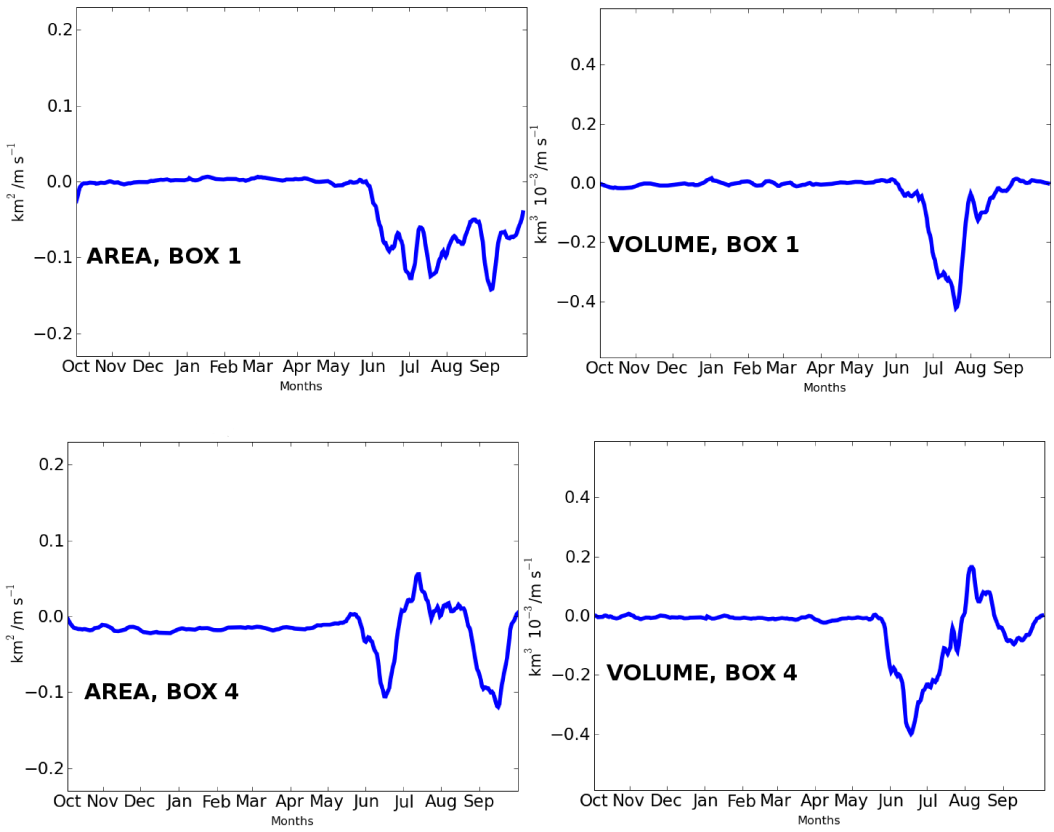

Figure 3.30— Evolution of the mean daily AREA and VOLUME sensitivities to U wind component. Top: Box 1; bottom: Box 4. Left: AREA sensitivities; right: VOLUME sensitivities.

in Box 4 is different. Sensitivities for AREA demonstrate mostly positive values here, indicating that export of the thicker sea ice from the areas with high SIC to the Laptev Sea will increase the resulting AREA. Sensitivities for VOLUME, on the contrary, show mostly negative values, indicating that export of the thicker ice from the central parts of the Arctic Ocean to the Laptev Sea, where sensitivities to the SAT are high, will have a negative impact on the resulting VOLUME. This example shows that the same dynamical forcing in some regions of the Arctic may lead to different consequences for different characteristics of the sea ice. What is good for the sea ice area is not necessarily good for the sea ice volume, despite the fact that volume is dependent on area.

As we have shown in the previous section, interdecadal differences in sensitivities are considerably high. Therefore it is worth looking at the time evolution of the mean sensitivities through the year for our three periods in order to see how differences in sea ice characteristics affect the seasonal cycle of the sensitivities.

Evolution of the mean daily AREA and VOLUME sensitivities to surface air

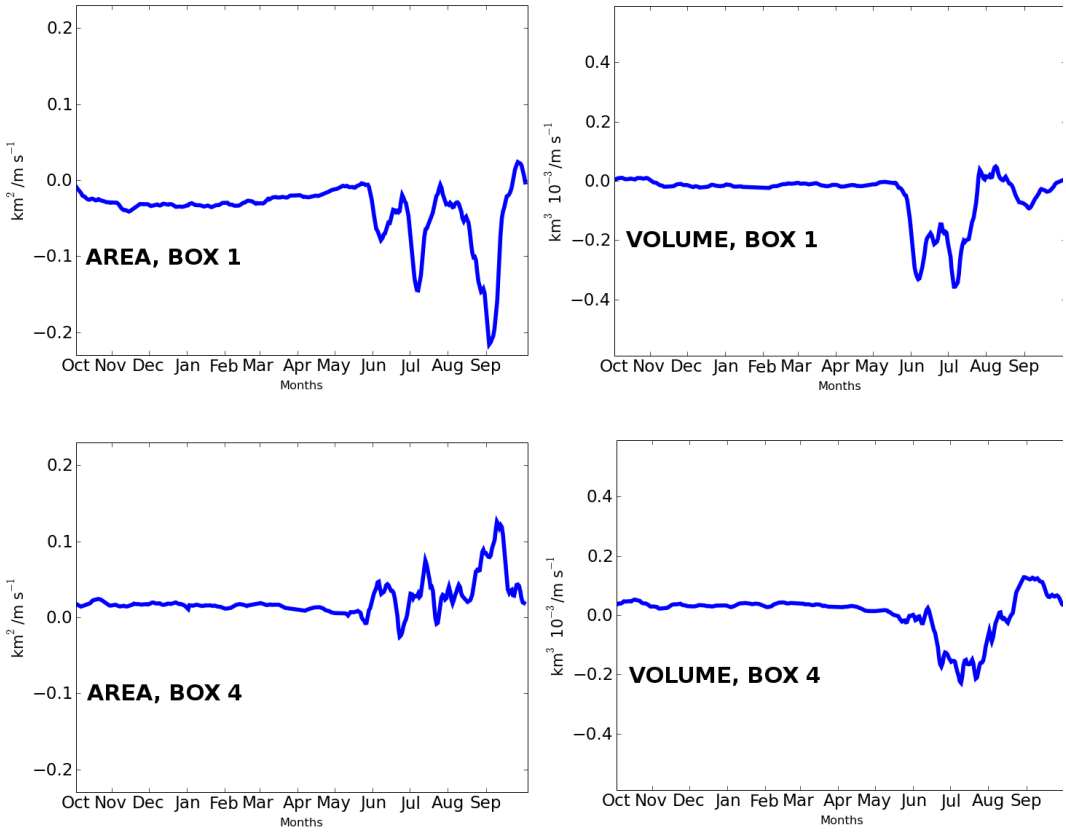

Figure 3.31— Evolution of the mean daily AREA and VOLUME sensitivities to V wind component. Top: Box 1; bottom: Box 4. Left: AREA sensitivities; right: VOLUME sensitivities.

temperature in Box 3 is shown in Fig. 3.32. Sensitivities for both cost functions in this box are relatively high, but do not reach extreme values like, for example, in Box 4. Sensitivities for AREA during the 1980s and 1990s are close to each other, while in the 1990s they are a bit stronger. In the 2000s, sensitivities increase considerably due to thinning of the sea ice in the area of Box 3. Sensitivities for VOLUME during the 1980s and 1990s are also close to each other, when in the 2000s there is a slight decrease in strength of the sensitivities, probably due to both decreased sea ice thickness and sea ice concentration. So sensitivities of AREA tend to be stronger in the 2000s, while sensitivities of VOLUME, on the contrary, tend to be weaker compared to previous periods. Note that the evolution of the sensitivities to air temperature through the year is relatively smooth and in general repeats the shape of the mean curve. This is not the case for the sensitivities to the wind components.

Sensitivities of both cost functions to wind components have very high variability and general tendencies can be seen only on the smoothed means. As we show on the PWD distribution maps, the differences in sensitivities to the wind components

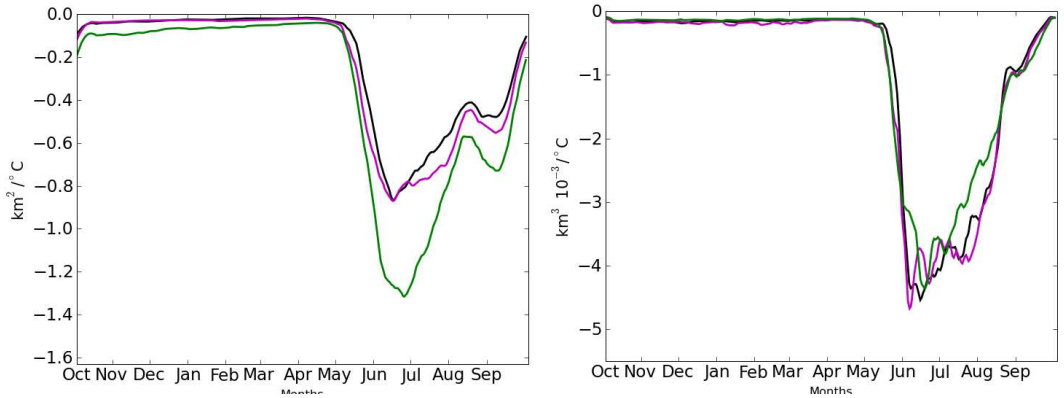

Figure 3.32— Evolution of the mean daily AREA (left) and VOLUME (right) sensitivities to surface air temperature in Box 3. Black: 1980-1989; magenta: 1990-1999; green: 2000-2007.

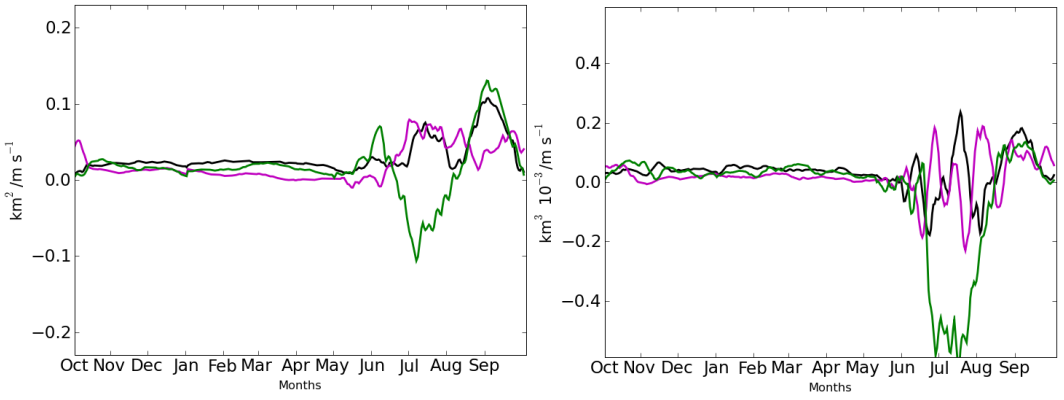

Figure 3.33— Evolution of the mean daily AREA (left) and VOLUME (right) sensitivities to the V wind component in Box 4. Black: 1980-1989; magenta: 1990-1999; green: 2000-2007.

between time periods might be sufficient. A good illustration of this is an evolution of the mean daily AREA and VOLUME sensitivities to the V wind component in Box 4 (Fig. 3.33). Mean values for AREA sensitivities to the V wind component in Box 4 are presented in the lower panel of Fig. 3.31 and one can see how different they are from the means for the individual periods. While in the 1980s and 1990s there is a general agreement on the sign, in the 2000s the sign during the melting period has changed, indicating that ice located in Box 4 being exported to the Laptev Sea is not able to survive summer melting any more, and this will make a negative contribution to the resulting AREA. Values for the VOLUME sensitivities to the V component during the 1980s and 1990s are mostly negative during the melting season, although showing some positive peaks, but values for the 2000s are

strongly negative, reflecting changes in the ice concentration and thickness. This again shows that similar dynamical forcing in one particular region may have different consequences depending on the background SIC and SIT situation.

In this section we explore the seasonal cycle of the mean sensitivities for the whole 28 years and for the three different time periods. Our main findings can be summarized as follows:

- The AREA and VOLUME sensitivities to SAT are characterized by close-to-zero values during the winter and rapid increases in strength associated with the beginning of the melting season. AREA sensitivities to SAT have a second maximum in September, associated with the beginning of the freezing period.
- The AREA and VOLUME sensitivities to wind components rapidly increase in strength after the onset of the melting season due to increased mobility of the sea ice. In different regions, the seasonal cycle of these kinds of sensitivities may differ considerably, and rapid changes from positive to negative sensitivities are possible during the melting season. Time evolution and signs may differ for the AREA and VOLUME sensitivities to the wind in the same region, as happens, for example, to the north of the Laptev Sea.
- Seasonal cycles of AREA and VOLUME sensitivities to SAT for the three time periods differ mostly in the strength of the sensitivities, but the shape of the curve stays almost the same. For the regions close to the ice edge, AREA sensitivities to SAT tended to be stronger in the 2000s compared to the previous periods, while VOLUME sensitivities to SAT tend to be weaker. The thinner ice along the ice edges is more prone to melting, so the AREA sensitivity to SAT is increasing in the 2000s. The combined effect of thinner ice and lower concentrations have decreased VOLUME sensitivities to SAT in the 2000s.
- Seasonal cycles of AREA and VOLUME sensitivities to wind for individual periods showed big differences. While sensitivities for the 1980s and 1990s mostly agree in magnitude and sign, sensitivities for the 2000s showed stronger values and may differ in sign in comparison with the two preceding periods. To the north of the Laptev and East Siberian seas this effect is explained by the thinning of the sea ice in this region. Export of thicker ice to the Laptev and East Siberian seas during the 1980s and 1990s led to increase in AREA, while export of ice that became thinner during the 2000s from the same regions will lead to a decrease in AREA, since this ice is more prone to melting.

3.8 Five-year run

To explore whether the sensitivities of AREA and VOLUME to the atmospheric forcing extend further back in time we perform a five-year adjoint run. The scheme we use is similar to the one-year runs but with increased time of the adjoint run. For

this experiment we choose the year 1990. The first spin-up is performed from 1981 until 1985, and then from the spin-up initial conditions in October 1985 a forward run is performed until September 1990 and then an adjoint run is performed backwards until October 1985.

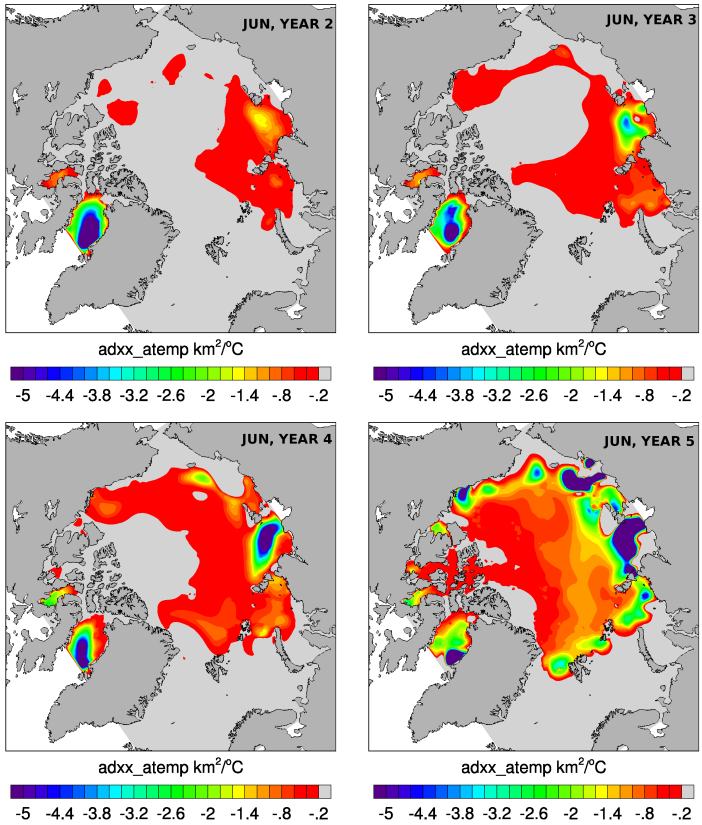

Figure 3.34— Mean June sensitivities of AREA to SAT for different years of the five-year run.

We choose June to show monthly means of AREA sensitivities to the surface air temperature (Fig. 3.34) since it is during this month the sensitivities are strongest. We did not show the first year, since the strength of the sensitivities there is very low (although they still exist). Year 2, Year 3, Year 4, and Year 5 are 1987, 1988, 1989, and 1990 respectively. The spatial coverage and relative strength of the sensitivities increase from year to year gradually until they reach maximums during the final year. Higher values of the sensitivities are associated with regions of thin ice, especially in the Laptev Sea and eastern part of the Kara Sea. The "bridge" of relatively thick ice that develops in the model from the north of the Canadian Archipelago to the East Siberian Sea is associated with weaker sensitivities; this is especially clear during Year 3.

Figure 3.35 shows mean June sensitivities of VOLUME to SAT. Similar to the

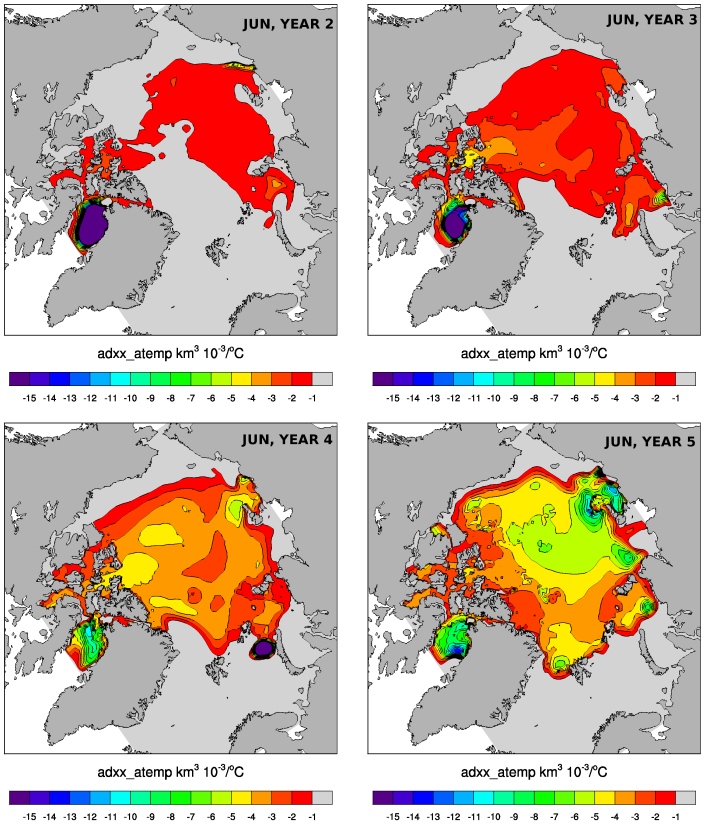

Figure 3.35— Mean June sensitivities of VOLUME to SAT for different years of the five-year run.

AREA sensitivities, sensitivities of VOLUME increase in area and strength through the years. Regions to the north of the Siberian Seas are covered by relatively strong sensitivities in each June. During June of Year 5 we see the distribution of sensitivities characteristic for the above described monthly mean July values of one-year adjoint runs, with strong sensitivities in the areas of the relatively high sea ice concentration with relatively thin sea ice (sea ice thickness in the central Arctic Ocean during 1990 is relatively small). But during Year 3 and especially Year 4, the region of stronger sensitivities appears to the north of the Canadian Archipelago. This indicates that while VOLUME is less sensitive to the temperature changes over the thick ice to the north of the Canadian Archipelago during the "target year", it is sensitive to the temperature changes over this region one and, to some degree, two years before. This might be explained by the fact that the region to the north of the Canadian Archipelago is a very important source of the thick ice that later could be exported to the central areas of the Arctic Ocean and affect resistance of the sea ice to summer melting. However stronger sensitivities do not cover the whole region to the north of the Canadian Archipelago, but only some part of it. Comparison with

thickness distribution for Year 3 and Year 4 (not shown) demonstrates relatively thin ice in the area associated with stronger sensitivities, so the thickness of the multiyear ice also matters in the sense of its impact on the characteristics of future years' September sea ice.

The existence of the AREA and VOLUME sensitivities to the atmospheric temperature that goes back in time for at least four years shows the importance of the initial conditions for the resulting September sea ice characteristics. Since the mean atmospheric thermodynamical forcing during the months of the strongest sensitivities probably does not change considerably between the years, the background state of the ice during June and July, even several years before, is an important factor in shaping the future state of the September sea ice.

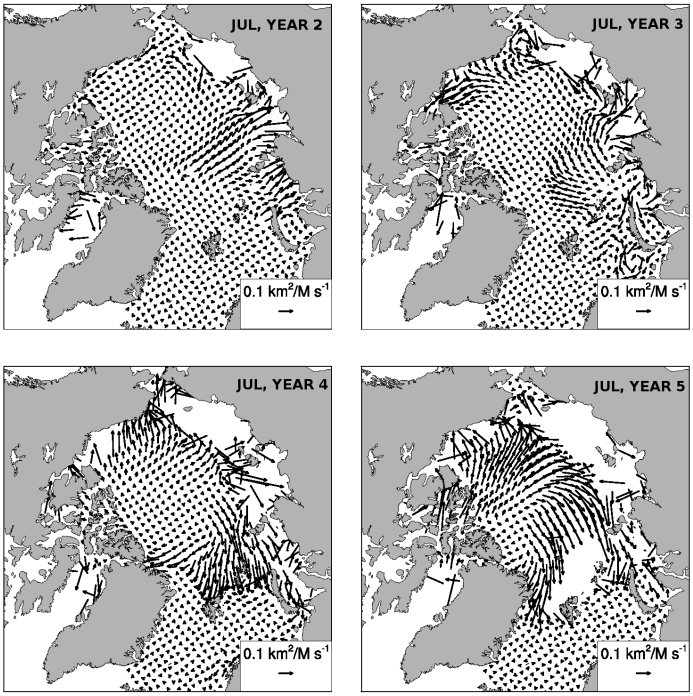

Figure 3.36— July preferable wind directions (PWD) for AREA for different years of the five-year run.

Sensitivities to wind components are stronger during July, due to increased sea ice mobility associated with a decrease in sea ice concentration, so we choose this month to show PWD for AREA and VOLUME. Figure 3.36 demonstrates PWD for AREA. The strength of the sensitivities increases from year to year, and the general tendency is that PWD favors export of the thick ice from the central parts of the Arctic Ocean towards marginal seas. There is one considerable exception during Year 3, when PWD is from the north of the Kara Sea towards the center of the

Arctic. This is probably related to the fact that July sea ice thickness during Year 3 is smallest among the years and it is better for this thin ice to stay inside the basin rather than be exported to the Kara Sea where it may be melted. Export of the thick sea ice to the seas increases the total sea ice concentration and preserves more ice for consecutive years.

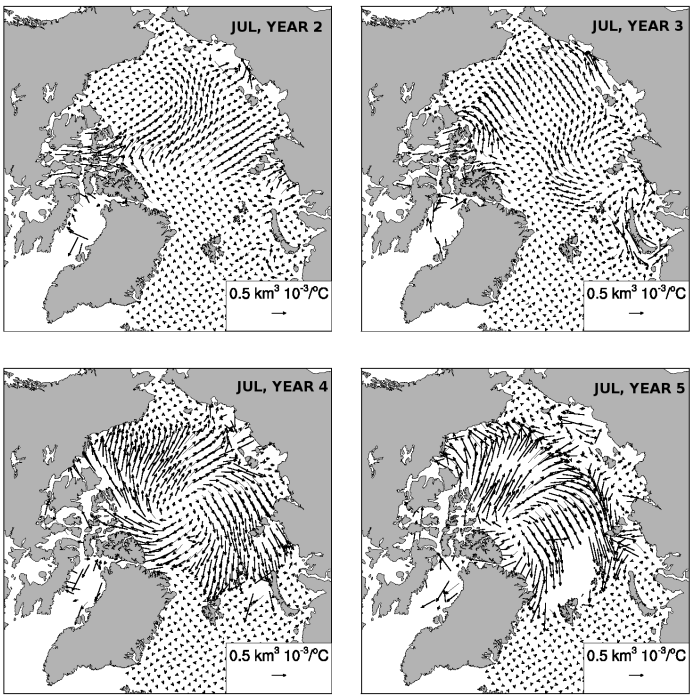

Figure 3.37— July preferable wind directions (PWD) for VOLUME for different years of the five-year run.

Figure 3.36 demonstrates PWD for the VOLUME. Surprisingly PWD for Years 2, 3, and 4 resembles more PWD for AREA, which favors sea ice transport from the central Arctic Ocean towards marginal seas. During Year 5, PWD from the center of the Arctic Ocean and from the Laptev and East Siberian seas point to some kind of the "border" where PWD has a west-east direction. So only during the "target year" do we observe PWD from the East Siberian and Laptev seas; during the preceding years there is a strong component towards these seas. Sensitivities in Years 3 and 4 are quite strong and this tells us that redistribution of the sea ice concentration and thickness several years before is important for the "target year" September sea ice VOLUME. It looks like on the shorter time scale it is better to remove the relatively thin sea ice from the seas, but on the longer time scale it is better to export thick sea ice to the edges of the Arctic Ocean. During July of the "target year", the sea ice in the marginal seas under thermodynamical forcing will become thinner and

this will have a negative effect on the VOLUME, while during preceding years this ice may grow thicker again, which will contribute positively to the "target year" VOLUME. Sensitivities to wind components are highly variable parameters which depend strongly on the background situation with sea ice concentration and thickness, so we need several other five-year runs to better explore differences between sensitivities during the "target year" and preceding years.

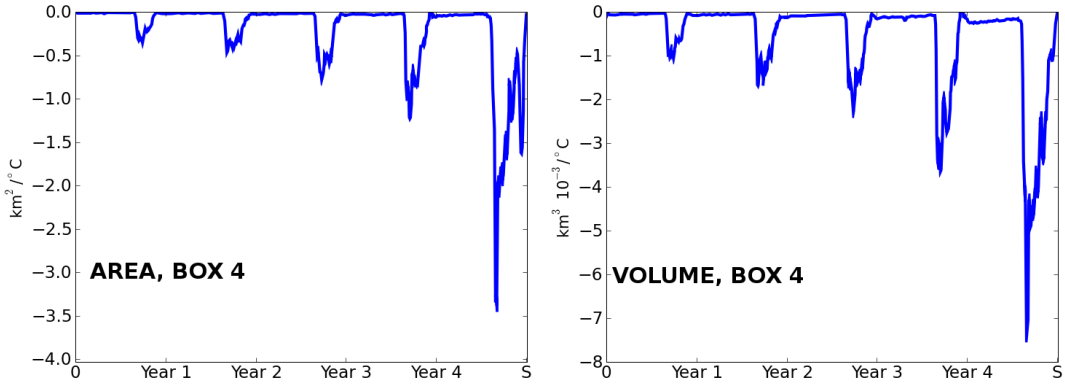

Figure 3.38— Evolution of the mean daily AREA (left) and VOLUME (right) sensitivities to surface air temperature in Box 4 for the five-year run. Every tick mark is the end of a year (30 September).

Time evolution of AREA and VOLUME sensitivities to surface atmospheric temperature in Box 4 for five years is shown in Fig. 3.38. The area to the north of the Laptev Sea has relatively high sensitivities during summer periods in all five years and seems to be very important for sea ice development. One can see close to zero sensitivities for both AREA and VOLUME during the winter seasons and strong values during the summer period. The increase in values of the sensitivities from year to year is close to exponential. For the AREA, the second, smaller peak, associated with the freezing period, can be found during every summer period, showing that this increase in sensitivities occurs not only during the "target year", but has a more general nature.

In this section we analyze results of the five-year adjoint run and show AREA and VOLUME sensitivities before the "target year". Our main findings can be summarized as follows:

- The AREA and VOLUME sensitivities to SAT and wind components are observed at least four years before the "target year". Sensitivities emerge in summer and almost completely disappear in winter. The strength of the sensitivities gradually decreases backwards in time. Relatively strong AREA sensitivities to SAT in proceeding years are associated mostly with the areas of thin ice.

- Regions of thick ice to the north of Greenland have higher VOLUME sensitivities to SAT one year before the "target year". This highlights the importance of this region as a source of the thick ice that might be later redistributed over the Arctic Ocean. To increase the resulting VOLUME, during the "target year" it is better to remove the relatively thin sea ice from the seas, but during the years preceding the "target year" it is better to export thick sea ice toward the edges of the Arctic Ocean.

- The area to the north of the Laptev Sea is of high importance for the development of the sea ice characteristics not only during the "target year", but at least four years before. Growth of the sensitivities values in this region from year to year is close to exponential.

3.9 Discussion and conclusions

In this chapter we analyze sea ice adjoint-based sensitivities to the atmospheric forcing for each year of the 1980-2007 period. We calculate sensitivities of two cost functions: mean September sea ice area (AREA) and mean September sea ice volume (VOLUME), with respect to the surface atmospheric temperature (SAT) and wind components. The adjoint method allows us to estimate sensitivities for every day and every grid point during the one-year period preceding the September for which cost functions are calculated.

To our knowledge only two attempts to use adjoint sensitivities for studying sea ice have been published in peer-reviewed literature to date. The first is Kim et al. (2006), who used adjoint sensitivities to analyze sea ice thickness (SIT) sensitivities to changes in the model parameters for the Los Alamos sea ice model CICE. They showed that adjoint sensitivities can be successfully used for tuning the model against observational data, but do not calculate sensitivities to external forcing. The second is the work of Kauker et al. (2009), who use the coupled ice-ocean model NAOSIM (North Atlantic/Arctic Ocean Sea Ice Model) for calculation of adjoint sensitivities to explore the relative contribution of different factors that led to the sea ice concentration (SIC) minimum in September 2007. As the cost function they took the sea ice area in the Arctic averaged over the period from 11 to 24 September. In this study only the period from March to September 2007 was analyzed and they found that the most important contributors to the extreme sea ice area minimum were: 2 m temperature in September, May and June wind stress, and SIT on 1 March. Our results are only in partial agreement with Kauker et al. (2009). The strongest AREA sensitivities to SAT, according to our simulations, exist in June-July, while sensitivities in September are quite small. Strong AREA sensitivities to wind components in our simulations are observed in June-September, while in May they are weak. One should remember that we analyzed monthly mean values of the sensitivities for several years, while Kauker et al. (2009) considered one summer. This, and the fact that we used different regional models of the Arctic Ocean and different cost functions, might explain the differences between our results.

Some of the mechanisms that relate atmospheric forcing and sea ice changes, suggested previously, do not find supporting evidence in our study, especially those that consider winter preconditioning as the main factor that determines the summer sea ice state. Rigor et al. (2002) proposed that winter increase in ice divergence due to increase in AO was one of the reasons for the sea ice decrease in the 1990s. In our simulations, sensitivities of AREA and VOLUME during the winter months in general have relatively large values only in regions close to the coast or to the ice edge. This shows that the impact of wind circulation is more regional, and that decreases in ice ridging and recirculation in the Beaufort Gyre do not have a large effect on summer sea ice characteristics. The only exceptions are sensitivities of VOLUME to V wind component, that during winter months showed relatively high values to the north of the Laptev Sea and over the Lomonosov ridge. This supports Rigor et al. (2002) suggestion that thin ice formed in polynyas of the Laptev Sea during winter contributes to the overall ice thinning in September.

Our results are closer to Deser et al. (2000) who showed that for the period 1979-1996, May-July SLP anomaly fields have the highest correlation with the summer ice extent, suggesting that the late spring atmosphere dynamical forcing is the most important for the summer sea ice characteristics. The AREA sensitivities to wind in our run have high values in June-September, and August showed the smallest values out of these four months. Highest values were observed in September, but due to the shift in the seasonal cycle that our model has, we should associate September strong sensitivities with the period of freezing. Therefore June and July dynamical forcing is the most important one during the melting period.

Differences in thick sea ice export from the Beaufort Sea and north of the Canadian Archipelago toward the Siberian seas determine sea ice concentration changes in the Arctic Ocean, according to Zhang et al. (2000). We also showed that sensitivities of AREA and VOLUME to wind are probably mostly related to redistribution of SIT. Export of the thicker ice toward the ice edge decreases the vulnerability of sea ice to a thermodynamic reduction of SIC. However, the source of the thick ice that helps to resist summer melting was not limited in our simulations by the Beaufort Sea and north of the Canadian Archipelago, but included the whole central Arctic where sea ice is thicker, relative to the areas closer to the ice edge. Increased sparsity of the sea ice in the 2000s also increased its mobility (Rampal et al., 2009), and this is reflected in enhanced strength of AREA and VOLUME sensitivities to the wind.

From analysis of the three different periods we can conclude that the way of thermodynamical influence of the atmosphere does not change between periods. The effect of the SAT is direct and increase in SAT over some region will lead to melting with certainly a negative effect for AREA and VOLUME. For the wind effect, it is largely dependent on the background SIT and SIC. At least for the region to the north of the Laptev and East Siberian seas in the 2000s, the effect of the onshore winds for both AREA and VOLUME changed considerably compared with the 1980s and 1990s. Dynamical forcing that led to increases in AREA and VOLUME in the 1980s and 1990s, will lead to decreases in AREA and VOLUME in the 2000s. This

might partly explain why, despite the return of the mostly negative AO conditions, we observe continued decline of the SIC (compare to Rigor and Wallace (2004)).

One of our main findings is that sea ice characteristics in late spring to the beginning of summer generally shape the way in which atmospheric forcing will affect mean September sea ice area and volume. To explore the relative importance of initial conditions and forcing we run an experiment where for initial conditions we take the model state at 1 June 2007 after a four-year spin-up and force the model for four months by the atmosphere from 1 June 1987 onwards. Then we compare monthly mean September SIC and SIT distributions in this experiment with the original run that starts from 1 June 1987 and is forced by the atmospheric conditions from this period.

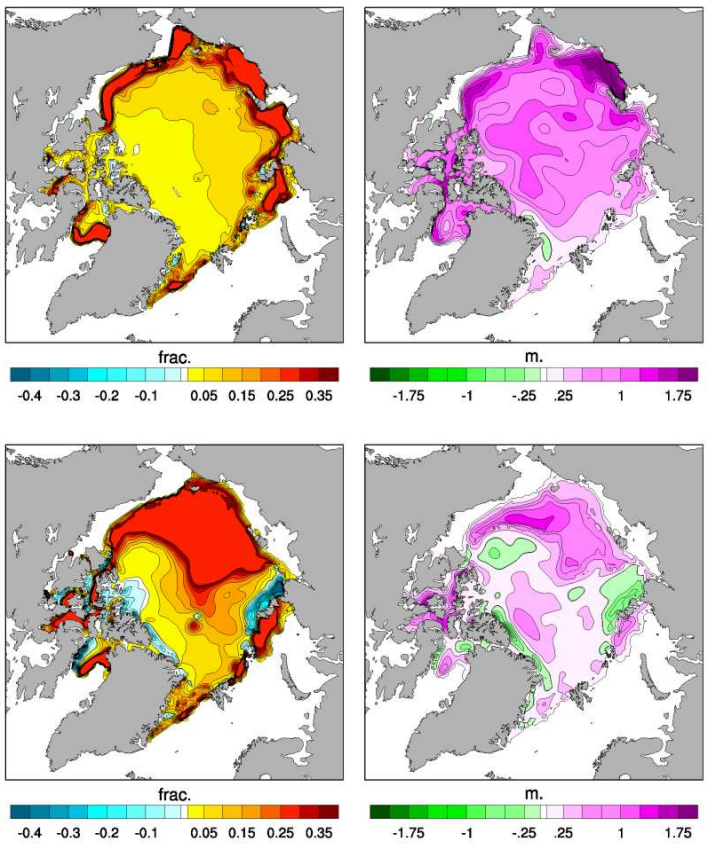

Figure 3.39— Mean September SIC and SIT difference between runs with Top: *same forcing* (four months' NCEP forcing starting at 1 June 1987) and different initial conditions (run with initial conditions from 1 June 1987 minus a run with initial conditions from 1 June 2007); bottom: *same initial conditions* (1 June 2007) and different forcing (four months' NCEP forcing starting at 1 June 1987 minus four months' NCEP forcing starting at 1 June 2007).

Differences between these two runs are shown on the top panel of Fig. 3.39. One should think of this as a difference between runs with the same forcing but different initial conditions. SIC differences do not exceed 0.05-0.1 frac. over much of the Arctic Ocean area. The biggest differences are observed near the ice edge, especially in the Siberian Shelf Seas and the Beaufort Sea. Distribution of the differences is in a good agreement with the location of the mean June-July AREA sensitivities to SAT in the 1980s, showing higher differences where the sensitivities are high and lower differences where the sensitivities are low. This means that for the run with initial conditions from 2007 it was harder to rebuild the sea ice in the areas of high sensitivities to SAT, even under the forcing from the year with high sea ice coverage.

The SIT differences are quite big and reach 1 m in the central parts of the Arctic Ocean and 1.75 m in the East Siberian Sea, demonstrating that ice thickness is probably a more conservative parameter and initial conditions here are more important for the SIT distribution. Thick enough ice cannot be formed even under favorable atmospheric conditions and some time is needed for SIT to "forget" the initially thinner mean SIT state.

The bottom panel of Fig. 3.39 shows differences between runs with the same initial conditions (1 June 2007) and different atmospheric forcing (four months' NCEP forcing starting at 1 June 1987 minus four months' NCEP forcing starting at 1 June 2007). As expected, SIC differences are mostly positive and show values of 0.05-0.2 frac. to the north of Greenland and in the Eurasian Basin and up to 0.3 frac. to the north of Siberia and Alaska. There are some negative differences as well to the north of Greenland and to the north of the Kara Sea. This figure shows that under the favorable forcing (from the year 1987), the ice recovered over large parts of the Amerasian Basin even after the initialization from 1 June 2007.

There are some positive and negative SIT differences (Fig. 3.39, lower right) in the Eurasian Basin and to the north of Greenland and the Canadian Archipelago, but they are weaker than for the runs with the same initial conditions and different forcing. Only in the region to the north of the Siberian Seas and Alaska there was no ice in the year 2007, and differences have almost the same strength as for the runs with the same initial conditions.

From these experiments we can conclude that September SIC probably depends less on June initial conditions and adapts to the atmospheric forcing very quickly with the only exception being the ice edge areas. The September SIT in contrast depends more on the initial conditions, since the growth in sea ice thickness is a slow process. We believe that "memory" of the sea ice about conditions of the previous years is carried out by SIT, and this is why we observe sensitivities several years before the "target year". One should also remember that our model is not the coupled one and the NCEP atmosphere already "remembers" where the sea ice is, having much lower temperatures there and forcing the model to form sea ice. A coupled system might react differently to a change in initial conditions.

Atmospheric forcing is the main driver of the sea ice development, but how this forcing is transformed to a particular sea ice state, where and when the effect of the

forcing will be large, and where it will be moderate or small, are still to a large degree open questions. Our study is one of the first attempts to explore these questions with the use of adjoint sensitivities. Our main findings are:

- The AREA and VOLUME sensitivities to SAT have weak values during October-May, and then experience sudden strengthening in June and gradual weakening during July-September. The AREA and VOLUME sensitivities to wind components also have the highest values in June-September, while VOLUME sensitivities in August-September are comparatively smaller.

- Despite the fact that both AREA and VOLUME depend on SIC, the spatial distributions of their sensitivities to SAT differ considerably. The AREA sensitivities have notable maximums in the marginal seas, while VOLUME sensitivities are more evenly distributed over the Arctic Ocean regions.

- According to preferable wind directions (PWD) analysis, on average, spreading of thicker sea ice from the central part of the Arctic Ocean toward marginal seas in summer increases the AREA, since it is harder to completely melt thick sea ice. At the same time, keeping thick ice away from the marginal seas increases VOLUME, since thickness of the sea ice will be reduced in those regions due to higher SAT. This is not the case for the Beaufort Sea, where sea ice movement toward the coast increases both AREA and VOLUME. Sometimes the same wind will lead to the opposite consequences for AREA and VOLUME.

- Analysis of the three different periods allows us to show how AREA and VOLUME sensitivities are related to the background distribution of SIC and SIT. The AREA sensitivities to SAT depend to a large extent on SIT showing higher values in the areas covered by 1-2 year old ice in the Eurasian Basin and 1-4 year old ice in the Amerasian Basin. The VOLUME sensitivities to SAT depend on the relation between SIT and SIC, showing higher sensitivities in regions where SIC is high and the SIT is relatively small.

- The relation between AREA and VOLUME sensitivities to wind and background sea ice characteristics is more complicated. A decrease in SIC leads to an increase in sea ice mobility, and strengthens the sensitivities. A decrease in SIT may lead to a change in PWD. In the period 2000-2007, PWD for AREA is not in agreement with the mean values, showing that due to sea ice thinning, the export of the sea ice from the central parts of the Arctic Ocean toward the Siberian seas will no longer lead to an increase in the resulting AREA.

- The mean seasonal cycle of the AREA and VOLUME sensitivities to SAT has a relatively smooth shape and differences between the three periods that we analyze are mostly in the strength of the sensitivities. In the 2000s, due to thinning of the sea ice, AREA sensitivities to SAT increase, while VOLUME sensitivities to SAT decrease. The seasonal cycle of the AREA and VOLUME sensitivities to the wind component has very high variability and mean values

for the three periods may differ considerably in strength and sign. Especially big differences were found in the 2000s, which showed a significant strengthening of sensitivities and sometimes a change in their sign.

- The AREA and VOLUME sensitivities can be found at least four years before the "target year". They show the same seasonal cycle as one-year sensitivities, with no significant values in winter and strong values in summer. The strength of the values usually decreases with time. Higher AREA sensitivities to SAT for the previous years tend to be distributed along the ice edge, while VOLUME sensitivities show more uniform distribution. VOLUME sensitivities to SAT one year before the "target year" might have stronger values than during the "target year" itself.

Chapter 4

Conclusions and outlook

4.1 Conclusions

The primary objectives of this study is to investigate how well a modern IPCC model simulates sea ice characteristics, to identify the primary forcing responsible for sea ice variability in the model, and to analyze how this forcing is distributed in time and space. In the following we will provide a summary of the main results organized according to the basic questions posted in the introduction.

1) What is the skill of IPCC AR4 model ECHAM5/MPI-OM in simulating climatological sea ice characteristics and climate variability?

To answer this question we, evaluate the twentieth century coupled ECHAM5/MPI-OM (hereafter referred to as ECHAM) run and compare its sea ice characteristics against observations of sea ice concentration (SIC), sea ice thickness (SIT) and sea ice transport for the period 1980 through 1999. The model results show a significant deficit in simulating essentially all present-day ice parameters over the Arctic Ocean. Although winter SIC distribution is relatively close to observations, summer SIC distribution has large discrepancies, especially in the regions close to the ice edge. The spatial distribution of SIT is not well represented in the model and simulated ice tend to be thicker in comparison with climatological values. Velocity of the sea ice transport in the ECHAM run is higher than observed by satellites, the center of the Beaufort Gyre is shifted toward the central Arctic Ocean, and the Transpolar Drift is shifted more toward the sea ice edge. Sea ice volume export through the Fram Strait exceeds values estimated from the observations. The standard deviation of NAO index for the ECHAM run is smaller by a factor of 1.7 than the NAO standard deviation in the NCEP forcing, consequently the interannual variability of SIC in the model is smaller than in the satellite data.

2) How does atmospheric forcing influence sea ice characteristics in this specific model, and how do uncertainties in the atmospheric model influence sea ice simulations?

To estimate the influence of the atmospheric forcing on sea ice simulations, we compare the coupled ECHAM run with a run of the ocean-ice MPI-OM model forced by the NCEP atmosphere (hereafter referred to as FNCEP). The FNCEP run produce much more realistic sea ice results, which point toward the atmosphere as the primary cause for the uncertainties in high-latitude climate parameters in the coupled ECHAM run. The results suggest that the unrealistic pressure system that centers over the North Pole in the ECHAM run and occupies the entire central Arctic, drives a quasi-permanent anticyclonic basin-scale gyre of sea ice transport. This gyre causes the buildup of thick ice in the central basin and, consequently, it lead to too high a SIC in summer. Differences in surface atmospheric temperature (SAT) between NCEP atmospheric forcing and the ECHAM run in September reach 7°C (SAT in ECHAM run is lower) and they also contribute to the deficit in SIC and SIT simulation. We conclude that a proper simulation of the mean state and variability of the atmosphere over the Arctic is necessary to improve the present-day simulations of the Arctic sea ice system.

3) How does the ocean state in the model impact the simulated sea ice distribution?

To address this question, we compare hydrographic conditions of the Arctic Ocean in the ECHAM and FNCEP runs with the Polar Hydrographic Climatology (PHC 3.0) dataset. The ECHAM run subsurface Arctic Ocean is warmer than the PHC 3.0 climatology by several degrees. However, a strong near-surface halocline suppresses heat exchange between the ocean surface and the ocean interior, and prevents strong sea ice melting from underneath. In the FNCEP run, the combination of the halocline, which is weaker than in the PHC 3.0 climatology, and higher water temperatures make penetration of heat to the ice bottom possible. Nevertheless, we seem to find no indications of Atlantic water layer heat impact on the sea ice simulated by the ECHAM and NCEP runs. This confirms that the main driver of the sea ice variability in our simulations is the atmosphere. The atmosphere is also responsible for the differences in the ocean properties between the two runs, so improvements in the atmospheric part of the coupled model will lead to a better simulation of the Arctic Ocean hydrographic characteristics.

4) Which physical processes are involved during the year in shaping mean September sea ice area and volume changes?

To answer this question we use the adjoint method to calculate sensitivities of the mean September sea ice area (hereafter referred to as AREA) and the mean September sea ice volume (hereafter referred to as VOLUME) to SAT and surface wind in a regional MITgcm model setup. Adjoint-based sensitivities are, essentially, gradients of AREA and VOLUME with respect to the atmospheric forcing for every time step and every grid point. This method allows us relatively easily track changes in sensitivities of AREA and VOLUME to SAT and surface wind through the year. The analysis covers the period from 1980 to 2007. We found the strongest influence

of atmospheric forcing on the September sea ice characteristics observed during June-September, while atmospheric forcing during October-May have a minor effect. During winter the Arctic Ocean is covered by the sea ice with a SIC close to 100 %. This suppresses sea ice movement, especially in the central parts of the Arctic during late winter, and a redistribution of the sea ice with different thickness occur only along the ice margins, and it have a weak impact on the following September's sea ice characteristics. Thermodynamic growth of the sea ice continues through the winter but its influence on AREA and VOLUME is also very small.

The rapid increase in sensitivities, observed in June, is associated with the onset of spring melting. First leads begin to form and probably serve as a "nucleus" for the following melting, enhanced by the positive ice-albedo feedback. Decreased SIC allows for a more active response of the sea ice to the wind forcing and a redistribution of the sea ice will play a major role through the whole summer.

For the AREA, thermodynamical forcing is especially important in the regions close to the ice edge in the Arctic seas, and high AREA sensitivities to SAT are associated with 1.4-2.0 m thick ice in the Eurasian Basin and 1.6-2.4 m thick ice in the Amerasian Basin. Ice that is thinner and closer to the shore at the end of the melting season will be melted completely under any realistic SAT. Ice that is thicker will survive summer, while sea ice of the above-mentioned thicknesses might or might not survive summer melting. This makes AREA very sensitive to temperature changes over that regions. In August and September the SIC and the SIT are considerably smaller than in June-July, so changes caused by thermodynamical reasons will have less effect on the resulting AREA, and sensitivities during these months also become smaller.

Positive temperatures may not melt sea ice completely, but will definitely decrease its thickness. That is why strong VOLUME sensitivities to SAT occupy larger parts of the central Arctic Ocean, and their strength depends on the relation between SIC and SIT. If, for example, both concentration and thickness are high, like in the region to the north of Greenland, sensitivities are low, since thick ice is much harder to melt due to its higher conductivity. If the SIC is still high but the thickness is small, like in the region to the north of the Laptev Sea, this high amount of thin ice, that is prone to melting, may considerably contribute to the reduction in VOLUME. Like in the case of AREA, VOLUME sensitivities to SAT become weaker in August and September due to the decrease of SIC and SIT.

Dynamical atmospheric forcing may affect the SIC and the SIT directly by moving and rigging of the sea ice and indirectly by redistribution of the sea ice with different thicknesses that will have different impacts from SAT in different regions. On average, export of thicker ice from the central parts of the Arctic Ocean to the Siberian Shelf seas leads to an increase in AREA, since it is harder to melt thick sea ice completely and thereby decrease its area. However, the same export of thick ice will decrease VOLUME, since higher temperatures over the Siberian Shelf seas make sea ice thinner. The redistribution of the thick ice from the areas to the north of Canadian Archipelago toward central parts of the Arctic Ocean and Beaufort Sea,

have a positive effect on AREA and VOLUME due to the high resistance of this ice to summer melting.

5) How do sensitivities of the mean September sea ice area and volume to atmospheric forcing change on interannual time scale, as represented here by three different periods?

We choose the periods 1980-1989, 1990-1999, and 2000-2007 for comparison. The largest differences are observed in the period 2000-2007. Due to the dramatic decline of the SIC and the SIT in the 2000s, regions that show strong AREA sensitivities to the SAT increases, so changes in the SAT causes a stronger response in AREA. The VOLUME sensitivities to SAT decrease, since melting of the thinner ice with modest SIC have a small influence on the resulting VOLUME. In contrast to the mean 1980-1989 and 1990-1999 AREA sensitivities to the wind, in 2000-2007 export of the thicker ice from the central parts of the Arctic Ocean to the Siberian Shelf seas will no longer lead to increase in AREA, since this ice is no longer thick enough to sustain summer melting. The strength of AREA and VOLUME sensitivities in 2000-2007 considerably increases due to a decrease in the SIC and associated increase in sea ice mobility. Generally, equal atmospheric forcing should cause stronger sea ice response in 2000-2007 compared to the two other periods, excluding only VOLUME response to the SAT forcing.

6) Do sensitivities in the mean September sea ice area and volume to atmospheric forcing extend further back in time for more than one year?

To answer this question we perform a five-year adjoint run from 1990 (referred to hereafter as the "target year") backwards. We find that the significant AREA and VOLUME sensitivities to the SAT and the wind can be found at least four years before, indicating that atmospheric forcing during previous years influences sea ice characteristics of the "target year" September. Strength of the sensitivities gradually increase from year to year and show the same seasonal cycle as one-year adjoint sensitivities, with no significant values in October-May and relatively strong values in June-September. Spatially, significant AREA sensitivities to the SAT in the years preceding the "target year" associated with regions with thin ice, such as Laptev and Kara seas, and increase every year. The VOLUME sensitivities to the SAT are more uniformly distributed over the Arctic Ocean and also gradually increase with time. We believe that due to its more "conservative" nature, the SIT is the primary agent that carries sea ice "memory" through the years.

4.2 Outlook

Here we would like to discuss the next steps that possibly can be taken as a continuation of the present work, in order to improve our understanding of sea ice variability in the Arctic Ocean.

In chapter 2 we show that proper atmospheric forcing is necessary in order to obtain reliable sea ice simulations. After the indication of a main source of the discrepancies, one should make one step further and find out why the atmosphere over the Arctic Ocean is so different in comparison with the NCEP data. We believe that continuous efforts in evaluation of the IPCC models against available sea ice observations are necessary. Three main sea ice characteristics are tightly connected to each other and we hope that our approach to analyze all three together will be used during evaluation of the models that participate in the upcoming IPCC report.

We show in chapter 3, that the adjoint of the MITgcm model can be used for the sensitivity analysis of the Arctic sea ice. Further use of this method with MITgcm configurations that have higher resolution and different boundary conditions, might lead to better simulation of sea ice parameters and, consequently, to a better description of sea ice sensitivities. Certainly, a switch to more realistic thermodynamical scheme is necessary, which will at least partly solve the problem with shifted sea ice seasonal cycle.

In our MITgcm experiment we use NCEP data as predefined forcing for the ocean model. This forcing already "remembers" sea ice conditions, at least in the temperature field. It would be interesting to see how different the sensitivities will be in the coupled atmosphere-ice-ocean system. It would be also interesting to analyze sea ice sensitivity to other atmospheric and ocean forcing fields, such as precipitation and sea surface temperature. In order to check how important are the initial conditions at the beginning of winter and at the end of spring for September sea ice characteristics, one could perform an analysis of the sea ice adjoint sensitivities to initial conditions.

Our conclusions about relations between background SIC and SIT conditions and sensitivities are now based mainly on a comparison of distribution of sensitivities and sea ice characteristics. In order to better understand the mechanism of the sea ice response to the atmospheric forcing we need to conduct a set of perturbation experiments, where realistic perturbations are applied to the regions with high sensitivities. The propagation of the perturbations may help us to reveal details of atmospheric influence on sea ice, especially for five-year or longer adjoint runs.

Our work is a prerequisite to quantitative sea ice data assimilation studies. From the analysis of adjoint-based sensitivities of the Arctic sea ice it is clear that both the SIC and the SIT are important for shaping sea ice characteristics in the summer months. At the present time only extensive satellite observations of the SIC are available. Without information about the SIT of high temporal and spatial resolution, we can expect only a partial improvement of Arctic sea ice representation in the model that uses data assimilation. This situation should change with the launch of the CryoSat satellite, that will provide accurate, high-resolution measurements of the thickness of floating sea ice.

Bibliography

Arzel, O., Fichefet, T., and Goosse, H.: Sea ice evolution over the 20^{th} and 21^{th} centuries as simulated by current AOGCMs, Ocean Model., 12, 401–415, doi:10.1016/j.ocemod.2005.08.002, 2006.

Bitz, C. M. and Lipscomb, W. H.: An energy-conserving thermodynamic model of sea ice, Journal of Geophysical Research, 104, doi:10.1029/1999JC900100, 1999.

Bitz, C. M., Fyfe, J. C., and Flato, G. M.: Sea ice response to wind forcing from AMIP models, J. Clim., 15, 522–536, 2002.

Bitz, C. M., Gent, P. R., Woodgate, R. A., Holland, M. M., and Lindsay, R.: The Influence of sea ice on ocean heat uptake in response to increasing CO_2, J. Clim., 19, 2437–2450, 2006.

Borodachev, B. E. and Shilnikov, V. I.: Istoriya ledovoi aviatsionnoi razvedki v Arktike i na zamerzayushchikh moryakh Rossii (1914-1993 gg) [The history of aerial ice reconnaissance in the Arctic and ice-covered seas of Russia, 1914-1993], (in Russian), Gidrometeoizdat, 2002.

Bourke, R. H. and Garrett, R. P.: Sea ice thickness distribution in the Arctic Ocean, Cold. Regions. Sci. Tech., 13, 259–280, 1987.

Boyer, T., Levitus, S., Garcia, H., Locarnini, R. A., Stephens, C., and Antonov, J.: Objective analyses of annual, seasonal, and monthly temperature and salinity for the World Ocean on a 0.25°grid, International Journal of Climatology, 25, 931–945, doi:10.1002/joc.1173, URL `http://dx.doi.org/10.1002/joc.1173`, 2005.

Budikova, D.: Role of Arctic sea ice in global atmospheric circulation: A review, Global and Planetary Change, 68, 149–163, doi:10.1016/j.gloplacha.2009.04.001, 2009.

Campin, J., Marshall, J., and Ferreira, D.: Sea ice–ocean coupling using a rescaled vertical coordinate z*, Ocean Modelling, 24, 1–14, doi:10.1016/j.ocemod.2008.05.005, 2008.

Cassano, J. J., Uotila, P., and Lynch, A.: Changes in synoptic weather patterns in the polar regions in the twentieth and twenty-first centuries, part 1: Arctic, Int. J. Climatol., 26, 1027–1049, doi:10.1002/joc.1306, 2006.

Cavalieri, D., Parkinson, C., Gloersen, P., and Zwally, H. J.: Sea ice concentrations from Nimbus-7 SMMR and DMSP SSM/I passive microwave data, Tech. rep., Boulder, Colorado USA, 1996.

Chapman, W. L. and Walsh, J. E.: Simulations of Arctic temperature and pressure by global coupled models, J. Clim., 20, 609–632, doi:10.1175/JCLI4026.1, 2007.

Comiso, J. C., Cavalieri, D. J., Parkinson, C. L., and Gloersen, P.: Passive microwave algorithms for sea ice concentration: A comparison of two techniques, Rem. Sens. Environ., 60, 1997.

Comiso, J. C., Parkinson, C. L., Gersten, R., and Stock, L.: Accelerated decline in the Arctic sea ice cover, Geophysical Research Letters, 35, L01 703+, doi:10.1029/2007GL031972, 2008.

Coon, M. D., Maykut, G. A., Pritchard, R. S., Rothrock, D. A., and Thorndike, A. S.: Modeling the pack ice as an elastic-plastic material, AIDJEX Bulletin, 24, 1–105, 1974.

Deser, C. and Teng, H.: Evolution of Arctic sea ice concentration trends and the role of atmospheric circulation forcing, 1979–2007, Geophysical Research Letters, 35, L02 504+, doi:10.1029/2007GL032023, 2008.

Deser, C., Walsh, J. E., and Timlin, M. S.: Arctic sea ice variability in the context of recent atmospheric circulation trends, Journal of Climate, 13, 617–633, 2000.

Deweaver, E. and Bitz, C. M.: Atmospheric circulation and its effect on Arctic sea ice in CCSM3 simulations at medium and high resolution, J. Clim., 19, 2415–2436, 2006.

Dickson, R., Meincke, J., Malmberg, S., and Lee, A.: The great salinity anomaly in the Northern North Atlantic 1968–1982, Progress In Oceanography, 20, 103–151, doi:10.1016/0079-6611(88)90049-3, 1988.

Dmitrenko, I. A., Polyakov, I. V., Kirillov, S. A., Timokhov, L. A., Frolov, I. E., Sokolov, V. T., Simmons, H. L., Ivanov, V. V., and Walsh, D.: Toward a warmer Arctic Ocean: Spreading of the early 21^{th} century Atlantic Water warm anomaly along the Eurasian Basin margins, Journal of Geophysical Research, 113, C05 023+, doi:10.1029/2007JC004158, 2008.

Doronin, Y. P.: On the problem of sea ice accretion (in Russian), Problems of Arctic and Antarctic, 1, 1959.

Drobot, S. D. and Maslanik, J. A.: Interannual variability in summer Beaufort sea ice conditions: Relationship to winter and summer surface and atmospheric variability, Journal of Geophysical Research, 108, doi:10.1029/2002JC001537, 2003.

Eisenman, I., Untersteiner, N., and Wettlaufer, J. S.: On the reliability of simulated Arctic sea ice in global climate models, Geophys. Res. Lett., 34, L10 501+, 2007.

Ekman, V. W.: On the influence of the earth's rotation on ocean-currents, Arkiv for Matematik, Astronomi och Fysik, 2, 1–52, 1905.

Errico, R. M.: What is an adjoint model?, Bulletin of the American Meteorological Society, 78, 2577–2591, 1997.

Flato, G. M., , and Participating: Sea-ice and its response to CO_2 forcing as simulated by global climate models, Clim. Dynam., 23, 229–241, doi:10.1007/s00382-004-0436-7, 2004.

Fowler, C.: Polar Pathfinder daily 25 km EASE-Grid sea ice motion vectors, Tech. rep., Boulder, Colorado USA, 2003.

Francis, J. A. and Hunter, E.: New insight into the disappearing Arctic sea ice, Eos, Transactions American Geophysical Union, 87, doi:10.1029/2006EO460001, 2006.

Francis, J. A. and Hunter, E.: Drivers of declining sea ice in the Arctic winter: A tale of two seas, Geophysical Research Letters, 34, L17 503+, doi:10.1029/2007GL030995, 2007.

Gent, P. R., Willebrand, J., Mcdougall, T. J., and Mcwilliams, J. C.: Parameterizing eddy-induced tracer transports in ocean circulation models, J. Phys. Oceanogr., 25, 463–474, 1995.

Gerdes, R. and Köberle, C.: Comparison of Arctic sea ice thickness variability in IPCC Climate of the 20^{th} Century experiments and in ocean – sea ice hindcasts, J. Geophys. Res., 112, C04S13+, doi:10.1029/2006JC003616, 2007.

Giering, R. and Kaminski, T.: Recipes for adjoint code construction, ACM Trans. Math. Softw., 24, 437–474, doi:10.1145/293686.293695, 1998.

Giering, R., Kaminski, T., and Slawig, T.: Generating efficient derivative code with TAF adjoint and tangent linear Euler flow around an airfoil, Future Gener. Comput. Syst., 21, 1345–1355, doi:10.1016/j.future.2004.11.003, 2005.

Graversen, R. and Wang, M.: Polar amplification in a coupled climate model with locked albedo, Climate Dynamics, 33, 629–643, doi:10.1007/s00382-009-0535-6, 2009.

Griffies, S. M.: The Gent-McWilliams skew flux, J. Phys. Oceanogr., 28, 831–841, 1998.

Haak, H.: Simulation of low-frequency climate variability in the North Atlantic Ocean and the Arctic, Ph.D. thesis, Universität Hamburg, 2004.

Haak, H., Jungclaus, J., Mikolajewicz, U., and Latif, M.: Formation and propagation of great salinity anomalies, Geophys. Res. Lett., 30, 2003.

Haas, C.: Late-summer sea ice thickness variability in the Arctic Transpolar Drift 1991–2001 derived from ground-based electromagnetic sounding, Geophysical Research Letters, 31, L09 402+, doi:10.1029/2003GL019394, 2004.

Hagemann, S. and Dümenil, L.: A parametrization of the lateral waterflow for the global scale, Clim. Dynam., 14, 17–31, 1997.

Hagemann, S. and Gates, L. D.: Improving a subgrid runoff parameterization scheme for climate models by the use of high resolution data derived from satellite observations, Clim. Dynam., 21, 349–359, 2003.

Hibler, W. D.: Dynamic thermodynamic sea ice model, J. Phys. Oceanogr., 9, 1979.

Hibler, W. D.: Modeling a variable thickness sea ice cover, Monthly Weather Review, 108, 1943–1973, 1980.

Hibler, W. D.: The role of sea ice dynamics in modeling CO_2 increases, in: Climate processes and climate sensitivity, edited by Hansen, J. E. and Takahashi, T., vol. 29 of *Geophysical Monograph*, pp. 238–253, AGU, Washington, D.C., 1984.

Holloway, G., Dupont, F., Golubeva, E., Häkkinen, S., Hunke, E., Jin, M., Karcher, M., Kauker, F., Maltrud, M., Maqueda, M. M. A., Maslowski, W., Platov, G., Stark, D., Steele, M., Suzuki, T., Wang, J., and Zhang, J.: Water properties and circulation in Arctic Ocean models, J. Geophys. Res., 112, C04S03+, doi:10.1029/2006JC003642, 2007.

Hu, Z.-Z., Kuzmina, S. I., Bengtsson, L., and Holland, D. M.: Sea-ice change and its connection with climate change in the Arctic in CMIP2 simulations, J. Geophys. Res., 109, D10 106+, doi:10.1029/2003JD004454, 2004.

Hundsdorfer, W. and Trompert, R. A.: Method of lines and direct discretization: a comparison for linear advection, Applied Numerical Mathematics, 13, 469–490, doi:10.1016/0168-9274(94)90009-4, 1994.

Hunke, E. C. and Holland, M. M.: Global atmospheric forcing data for Arctic ice-ocean modeling, J. Geophys. Res., 112, C04S14+, doi:10.1029/2006JC003640, 2007.

Jakobsson, M., Macnab, R., Mayer, L., Anderson, R., Edwards, M., Hatzky, J., Schenke, H. W., and Johnson, P.: An improved bathymetric portrayal of the Arctic Ocean: Implications for ocean modeling and geological, geophysical and oceanographic analyses, Geophysical Research Letters, 35, doi:10.1029/2008GL033520, 2008.

Johnson, M., Gaffigan, S., Hunke, E., and Gerdes, R.: A comparison of Arctic Ocean sea ice concentration among the coordinated AOMIP model experiments, J. Geophys. Res. C Oceans, 112, 2007.

Jungclaus, J. H., Keenlyside, N., Botzet, M., Haak, H., Luo, J. J., Latif, M., Marotzke, J., Mikolajewicz, U., and Roeckner, E.: Ocean circulation and tropical variability in the coupled model ECHAM5/MPI-OM, J. Clim., 19, 3952–3972, 2006.

Kalnay, E., Kanamitsu, M., Kistler, R., Collins, W., Deaven, D., Gandin, L., Iredell, M., Saha, S., White, G., Woollen, J., Zhu, Y., Leetmaa, A., Reynolds, B., Chelliah, M., Ebisuzaki, W., Higgins, W., Janowiak, J., Mo, K. C., Ropelewski, C., Wang, J., Jenne, R., and Joseph, D.: The NCEP/NCAR 40-year reanalysis project, Bull. Am. Meteorol. Soc., 77, 437–471, 1996.

Kattsov, V., Alekseev, G., Pavlova, T., Sporyshev, P., Bekryaev, R., and Govorkova, V.: Modeling the evolution of the world ocean ice cover in the 20^{th} and 21^{th} centuries, Izvestiya Atmospheric and Oceanic Physics, 43, 142–157, doi:10.1134/S0001433807020028, 2007.

Kauker, F., Kaminski, T., Karcher, M., Giering, R., Gerdes, R., and Voßbeck, M.: Adjoint analysis of the 2007 all time Arctic sea-ice minimum, Geophys. Res. Lett., 36, L03 707+, doi:10.1029/2008GL036323, 2009.

Kay, J. E., L'Ecuyer, T., Gettelman, A., Stephens, G., and O'Dell, C.: The contribution of cloud and radiation anomalies to the 2007 Arctic sea ice extent minimum, Geophysical Research Letters, 35, L08 503+, doi:10.1029/2008GL033451, 2008.

Kim, J. G., Hunke, E. C., and Lipscomb, W. H.: Sensitivity analysis and parameter tuning scheme for global sea-ice modeling, Ocean Modeling Journal, 14, 61–80, doi:doi:10.1016/j.ocemod.2006.03.003, 2006.

Köberle, C. and Gerdes, R.: Mechanisms determining the variability of Arctic sea ice conditions and export, Journal of Climate, 16, 2843–2858, 2003.

Köhl, A. and Stammer, D.: Optimal observations for variational data assimilation, Journal of Physical Oceanography, 34, 529–542, doi:10.1175/2513.1, 2004.

Köhl, A. and Stammer, D.: Variability of the meridional overturning in the North Atlantic from the 50-year GECCO state estimation, Journal of Physical Oceanography, 38, 1913–1930, doi:10.1175/2008JPO3775.1, 2008.

Kolchak, A.: Led Karskago i Sibirskago Morei (The ice of the Kara and Siberian Seas), vol. 26 of *Zapiski Imperatorskoj Akademii Nauk po Fiziko-Matematiceskomu Otdeleniju*, The Imperial Saint Petersburg Academy of Sciences, 1909.

Kolchak, A.: The arctic pack and the polynya, pp. 124–141, American Geographical Society. Special publication, no. 7, American geographical society of New York, 1928.

Kolesnikov, A. G.: On the theory of ice accretion on the sea surface (in Russian), Problems of Marine Hydrological Forecasts, Leningrad, 1946.

Konstantinov, Y. B. and Grachev, K. I.: High-latitude airborne expeditions Sever (1937, 1941-1993), Gidrometeoizdat Publishing House, St. Petersburg, Russia, 2000.

Kwok, R.: Summer sea ice motion from the 18 GHz channel of AMSR-E and the exchange of sea ice between the Pacific and Atlantic sectors, Geophys. Res. Lett., 35, L03 504+, doi:10.1029/2007GL032692, 2008.

Kwok, R. and Rothrock, D. A.: Decline in Arctic sea ice thickness from submarine and ICESat records: 1958–2008, Geophysical Research Letters, 36, L15 501+, doi:10.1029/2009GL039035, 2009.

Kwok, R., Schweiger, A., Rothrock, D. A., Pang, S., and Kottmeier, C.: Sea ice motion from satellite passive microwave imagery assessed with ERS SAR and buoy motions, J. Geophys. Res. C Oceans, 103, 8191–8214, 1998.

Kwok, R., Cunningham, G. F., and Pang, S. S.: Fram Strait sea ice outflow, J. Geophys. Res., 109, C01 009+, doi:10.1029/2003JC001785, 2004.

Laxon, S., Peacock, H., and Smith, D.: High interannual variability of sea ice thickness in the Arctic region, Nature, 425, 947–950, 2003.

Lea, D. J., Allen, M. R., and Haine, T. W. N.: Sensitivity analysis of the climate of a chaotic system, Tellus A, 52, 523–532, doi:10.1034/j.1600-0870.2000.01137.x, 2000.

Levitus, S., Boyer, T. P., Conkright, M. E., Brien, O. T., Antonov, J., Stephens, C., Stathoplos, L., Johnson, D., and Gelfeld, R.: NOAA Atlas NESDIS 18, World Ocean Database 1998: Volume 1: Introduction, U.S. Government Printing Office, Washington, D.C, 1998.

Lindsay, R. W., Zhang, J., Schweiger, A., Steele, M., and Stern, H.: Arctic sea ice retreat in 2007 follows thinning trend, J. Clim., 22, 165–176, doi:10.1175/2008JCLI2521.1, 2009.

Losch, M., Menemenlis, D., Heimbach, P., Campin, J., and Hill, C.: On the formulation of sea-ice models. Part 1: Effects of different solver implementations and parameterizations, Ocean Modelling, submitted to Ocean Modelling.

Makshtas, A., Atkinson, D., Kulakov, M., Shutilin, S., Krishfield, R., and Proshutinsky, A.: Atmospheric forcing validation for modeling the central Arctic, Geophys. Res. Lett., 34, L20 706+, doi:10.1029/2007GL031378, 2007.

Makshtas, A. P., Shoutilin, S. V., and Andreas, E. L.: Possible dynamic and thermal causes for the recent decrease in sea ice in the Arctic Basin, Journal of Geophysical Research, 108, doi:10.1029/2001JC000878, 2003.

Malmgren, F.: On the properties of sea-ice, vol. 1 of *The Norwegian North Polar expedition with the "Maud", 1918-25, Scientific results*, 1928.

Marotzke, J., Giering, R., Zhang, K. Q., Stammer, D., Hill, C., and Lee, T.: Construction of the adjoint MIT ocean general circulation model and application to Atlantic heat transport sensitivity, Journal of Geophysical Research, 104, 29 529–29 547, 1999.

Marshall, J., Adcroft, A., Hill, C., Perelman, L., and Heisey, C.: A finite-volume, incompressible Navier Stokes model for studies of the ocean on parallel computers, Journal of Geophysical Research - Oceans, 102, 5753–5766, doi: 10.1029/96JC02775, 1997a.

Marshall, J., Hill, C., Perelman, L., and Adcroft, A.: Hydrostatic, quasi-hydrostatic, and nonhydrostatic ocean modeling, Journal of Geophysical Research - Oceans, 102, null–5752, doi:10.1029/96JC02776, 1997b.

Marshall, J., Adcroft, A., Campin, J.-M., Dutkiewicz, S., Evangelinos, C., Ferreira, D., Forget, G., Fox-Kemper, B., Heimbach, P., Hill, C., Hill, E., Hill, H., Jahn, O., Losch, M., Maze, G., Menemenlis, D., and Molod, A.: MITgcm user manual, Tech. rep., MIT EAPS, 2004.

Marsland, S. J., Haak, H., Jungclaus, J. H., Latif, M., and Roske, F.: The Max-Planck-Institute global ocean/sea ice model with orthogonal curvilinear coordinates, Ocean. Model., 5, 91–127, 2003.

Martin, T. and Gerdes, R.: Sea ice drift variability in Arctic Ocean Model Intercomparison Project models and observations, J. Geophys. Res., 112, C04S10+, doi:10.1029/2006JC003617, 2007.

Martinson, D. G. and Steele, M.: Future of the Arctic sea ice cover: Implications of an Antarctic analog, Geophys. Res. Lett., 28, 307–310, doi:10.1029/2000GL011549, 2001.

Maslanik, J., Drobot, S., Fowler, C., Emery, W., and Barry, R.: On the Arctic climate paradox and the continuing role of atmospheric circulation in affecting sea ice conditions, Geophysical Research Letters, 34, L03 711+, doi: 10.1029/2006GL028269, 2007a.

Maslanik, J. A., Serreze, M. C., and Barry, R. G.: Recent decreases in Arctic summer ice cover and linkages to atmospheric circulation anomalies, Geophys. Res. Lett., 23, 1677–1680, 1996.

Maslanik, J. A., Fowler, C., Stroeve, J., Drobot, S., Zwally, J., Yi, D., and Emery, W.: A younger, thinner Arctic ice cover: Increased potential for rapid, extensive sea-ice loss, Geophys. Res. Lett., 34, L24 501+, doi:10.1029/2007GL032043, 2007b.

Maslanik, J. A., Fowler, C., Stroeve, J., Drobot, S., Zwally, J., Yi, D., and Emery, W.: A younger, thinner Arctic ice cover: Increased potential for rapid, extensive sea-ice loss, Geophysical Research Letters, 34, L24 501+, doi:10.1029/2007GL032043, 2007c.

Maykut, G. A. and Untersteiner, N.: Some results from a time-dependent thermodynamic model of sea ice, Journal of Geophysical Research, 76, doi:10.1029/JC076i006p01550, 1971.

Meier, W. N.: Comparison of passive microwave ice concentration algorithm retrievals with AVHRR imagery, in Arctic peripheral seas, IEEE Trans. Geosci. Rem. Sens., 43, 2005.

Nansen, F.: Farthest North - being the record of a voyage of exploration of the ship Fram 1893-96 and of a fifteen months' sleigh journey by Dr. Nansen and Lt. Johansen, Harper & Brothers, 1897.

Oberhuber, J. M.: Simulation of the Atlantic Circulation with a coupled sea ice-mixed layer-isopycnal general circulation model. Part I: Model description, J. Phys. Oceanogr., 23, 808–829, 1993.

Parkinson, C. L. and Cavalieri, D. J.: Arctic sea ice variability and trends, 1979-2006, J. Geophys. Res., 113, C07 003+, 2008.

Parkinson, C. L., Vinnikov, K. Y., and Cavalieri, D. J.: Evaluation of the simulation of the annual cycle of Arctic and Antarctic sea ice coverages by 11 major global climate models, J. Geophys. Res., 111, C07 012+, doi:10.1029/2005JC003408, 2006.

Perovich, D. K., Richter-Menge, J. A., Jones, K. F., and Light, B.: Sunlight, water, and ice: Extreme Arctic sea ice melt during the summer of 2007, Geophysical Research Letters, 35, L11 501+, doi:10.1029/2008GL034007, 2008.

Pinto, J., Zacharias, S., Fink, A., Leckebusch, G., and Ulbrich, U.: Factors contributing to the development of extreme North Atlantic cyclones and their relationship with the NAO, Clim. Dynam., doi:10.1007/s00382-008-0396-4, 2008.

Polyakov, I., Timokhov, L., Dmitrenko, I., Ivanov, V., Simmons, H., Beszczynska-Möller, A., Dickson, R., Fahrbach, E., Fortier, L., Gascard, J.-C., Hölemann, J., Holliday, P. N., Hansen, E., Mauritzen, C., Piechura, J., Pickart, R., Schauer, U., Steele, M., and Walczowski, W.: Observational program tracks Arctic Ocean transition to a warmer state, EOS, Trans. Am. Geophys. Union, 88, 398+, 2007.

Polyakov, I. V.: One more step toward a warmer Arctic, Geophysical Research Letters, 32, L17 605+, doi:10.1029/2005GL023740, 2005.

Polyakov, I. V., Alekseev, G. V., Bekryaev, R. V., Bhatt, U. S., Colony, R., Johnson, M. A., Karklin, V. P., Walsh, D., and Yulin, A. V.: Long-term ice variability in Arctic marginal seas, J. Clim., 16, 2078–2085, 2003.

Proshutinsky, A. and Kowalik, Z.: Preface to special section on Arctic Ocean Model Intercomparison Project (AOMIP) studies and results, J. Geophys. Res., 112, C04S01+, doi:10.1029/2006JC004017, 2007.

Rampal, P., Weiss, J., and Marsan, D.: Positive trend in the mean speed and deformation rate of Arctic sea ice, 1979–2007, Journal of Geophysical Research - Oceans, 114, C05 013+, doi:10.1029/2008JC005066, 2009.

Redi, M. H.: Oceanic isopycnal mixing by coordinate rotation, J. Phys. Oceanogr., 12, 1154–1158, 1982.

Rigor, I. G. and Wallace, J. M.: Variations in the age of Arctic sea-ice and summer sea-ice extent, Geophys. Res. Lett., 31, L09 401+, doi:10.1029/2004GL019492, 2004.

Rigor, I. G., Colony, R. L., and Martin, S.: Variations in surface air temperature observations in the Arctic, 1979–1997, Journal of Climate, 13, 896–914, 2000.

Rigor, I. G., Wallace, J. M., and Colony, R. L.: Response of sea ice to the Arctic Oscillation, Journal of Climate, 15, 2648–2663, 2002.

Roe, P. L.: Some contributions to the modelling of discontinuous flows, in: Large-Scale Computations in Fluid Mechanics, edited by Engquist, B. E., Osher, S., and Somerville, R. C. J., vol. 22 of *Lectures in Applied Mathematics*, pp. 163–193, American Mathematical Society, Providence, RI, 1985.

Roeckner, E., Bauml, G., Bonaventura, L., Brokopf, R., Esch, M., Giorgetta, M., Hagemann, S., Kirchner, Kornblueh, L., Manzini, E., Rhodin, A., Schlese, U., Schulzweida, U., and Tompkins, A.: The atmospheric general circulation model ECHAM 5. PART I: model description., MPI-M Tech. Rep. 349, MPI-M, 2003.

Romanov, I. P.: Atlas of ice and snow of the Arctic Basin and Siberian Shelf seas, Backbone Publishing Company, second edn., 1995.

Rothrock, D. A. and Zhang, J.: Arctic Ocean sea ice volume: What explains its recent depletion?, J. Geophys. Res. C Oceans, 110, 1–10, doi:10.1029/2004JC002282, 2005.

Rothrock, D. A., Percival, D. B., and Wensnahan, M.: The decline in Arctic sea-ice thickness: Separating the spatial, annual, and interannual variability in a quarter century of submarine data, J. Geophys. Res., 113, C05 003+, doi:10.1029/2007JC004252, 2008.

Schweiger, A. J., Zhang, J., Lindsay, R. W., and Steele, M.: Did unusually sunny skies help drive the record sea ice minimum of 2007?, Geophysical Research Letters, 35, L10 503+, doi:10.1029/2008GL033463, 2008.

Semtner, A. J.: A model for the thermodynamic growth of sea ice in numerical investigations of climate, J. Phys. Oceanogr., 6, 379–389, 1976.

Semtner, A. J.: On modelling the seasonal thermodynamic cycle of sea ice in studies of climatic change, Climatic Change, 6, 27–37, doi:10.1007/BF00141666, 1984.

Serreze, M. C., Maslanik, J. A., Key, J. R., Kokaly, R. F., and Robinson, D. A.: Diagnosis of the record minimum in Arctic sea ice area during 1990 and associated snow cover extremes, Geophysical Research Letters, 22, 2183–2186, doi:10.1029/95GL02068, 1995.

Serreze, M. C., Holland, M. M., and Stroeve, J.: Perspectives on the Arctic's shrinking sea-ice cover, Science, 315, 1533–1536, 2007.

Shuleikin, V. V.: The drift of ice-fields (in Russian), Doklady Akademii Nauk SSSR, 19, 587–592, 1938.

Smith, T. M., Reynolds, R. W., Peterson, T. C., and Lawrimore, J.: Improvements to NOAA's historical merged land-ocean surface temperature analysis (1880-2006), Journal of Climate, 21, 2283–2296, doi:10.1175/2007JCLI2100.1, 2008.

Spreen, G.: Satellite-based estimates of sea ice volume flux: Applications to the Fram Strait region, Ph.D. thesis, Inst. of Oceanogr., Univ. of Hamburg, Hamburg, Germany, 2008.

Stammer, D., Wunsch, C., Giering, R., Eckert, C., Heimbach, P., Marotzke, J., Adcroft, A., Hill, C. N., and Marshall, J.: Global ocean circulation during 1992-1997, estimated from ocean observations and a general circulation model, Journal of Geophysical Research (Oceans), 107, 1, doi:10.1029/2001JC000888, 2002.

Stammer, D., Park, S., Köhl, A., Lukas, R., and Santiago-Mandujano, F.: Causes for large-scale hydrographic changes at the Hawaii ocean time series station, Journal of Physical Oceanography, 38, 1931–1948, doi:10.1175/2008JPO3751.1, 2008.

Steele, M. and Boyd, T.: Retreat of the cold halocline layer in the Arctic Ocean, J. Geophys. Res., 103, 10 419–10 435, doi:10.1029/98JC00580, 1998.

Steele, M., Morley, R., and Ermold, W.: PHC: A global ocean hydrography with a high-quality Arctic Ocean, J. Clim., 14, 2079–2087, 2001.

Steele, M., Ermold, W., and Zhang, J.: Arctic Ocean surface warming trends over the past 100 years, Geophysical Research Letters, 35, L02 614+, doi:10.1029/2007GL031651, 2008.

Stefan, J.: Ueber die Theorie der Eisbildung, insbesondere über die Eisbildung im Polarmeere (in German), Annalen der Physik, 278, 269–286, doi:10.1002/andp.18912780206, 1891.

Stössel, A. and Owens, W. B.: The Hamburg sea-ice model, Tech. Rep. 3, German Climate Computer Center (DKRZ), Hamburg, Germany, 1992.

Stroeve, J., Holland, M. M., Meier, W., Scambos, T., and Serreze, M.: Arctic sea ice decline: Faster than forecast, Geophys. Res. Lett., 34, 2007.

Stroeve, J., Serreze, M., Drobot, S., Gearheard, S., Holland, M., Maslanik, J., Meier, W., and Scambos, T.: Arctic sea ice extent plummets in 2007, EOS, Trans. Am. Geophys. Union, 89, 2008.

Sverdrup, H. U.: The wind-drift of the ice on the North Siberian Shelf, vol. 4 of *The Norwegian North Polar Expedition with the "Maud" 1918-1925, scientific results*, pp. 1–46, 1928.

Valcke, S., Caubel, A., Declat, D., and Terray, L.: OASIS Ocean Atmosphere Sea Ice Soil users guide, Tech. rep., Cent. Eur. Formation Avancee Calcul Sci., Toulouse, France, 2003.

Vinje, T., Nordlund, N., and Kvambekk, Å.: Monitoring ice thickness in Fram Strait, J. Geophys. Res., 103, 10 437–10 449, 1998.

Walsh, J. E. and Crane, R. G.: A comparison of GCM simulations of Arctic climate, Geophys. Res. Lett., 19, 29–32, doi:10.1029/91GL03004, 1992.

Walsh, J. E., Chapman, W. L., and Shy, T. L.: Recent decrease of sea level pressure in the central Arctic, Journal of Climate, 9, 480–486, 1996.

Winton, M.: Amplified Arctic climate change: What does surface albedo feedback have to do with it?, Geophysical Research Letters, 33, L03 701+, doi:10.1029/2005GL025244, 2006.

Zhang, J. and Hibler, W. D.: On an efficient numerical method for modeling sea ice dynamics, Journal of Geophysical Research - Oceans, 102, null+, doi:10.1029/96JC03744, 1997.

Zhang, J., Hibler, W. D., Steele, M., and Rothrock, D. A.: Arctic ice-ocean modeling with and without climate restoring, Journal of Physical Oceanography, 28, 191–217, 1998.

Zhang, J., Rothrock, D., and Steele, M.: Recent changes in Arctic sea ice: The interplay between ice dynamics and thermodynamics, Journal of Climate, 13, 3099–3114, 2000.

Zhang, J., Lindsay, R., Steele, M., and Schweiger, A.: What drove the dramatic retreat of Arctic sea ice during summer 2007?, Geophys. Res. Lett., 35, L11 505+, doi:10.1029/2008GL034005, 2008.

Zhang, X. and Walsh, J. E.: Toward a seasonally ice-covered Arctic Ocean: Scenarios from the IPCC AR4 model simulations, J. Clim., 19, 1730–1747, 2006.

Zubov, N. N.: Arctic ice, (in Russian), Izdatelstvo Glavsevmorputi, Moscow, 1945.

Zubov, N. N. and Somov, M. M.: Ice drift in the northern Arctic Basin (in Russian), Problems of Arctic, 2, 51–68, 1940.

Die gesamten Veröffentlichungen in der Publikationsreihe des MPI-M
„Berichte zur Erdsystemforschung“,
„Reports on Earth System Science“,
ISSN 1614-1199

sind über die Internetseiten des Max-Planck-Instituts für Meteorologie erhältlich:

http://www.mpimet.mpg.de/wissenschaft/publikationen.html



ISSN 1614-1199